DOE/ER/40335--13

DE92 019286

THEORETICAL NUCLEAR PHYSICS

Progress Report
for Period October 1, 1991 - August 1, 1992

Ernest Rost and James R. Shephard

The Regents of the University of Colorado
Boulder, Colorado 80309-0019

August 1992

Prepared for

THE U.S. DEPARTMENT OF ENERGY
AGREEMENT NO. DE-FG02-87ER40335

CONTENTS

A. 1992 PROGRESS REPORT – October 1, 1991 to August 1, 1992

1. Exact 1-Loop Vacuum Polarization Effects in 1+1 Dimensional QHD T. C. Ferrée, C. E. Price and J. R. Shepard

Vacuum polarization effects in QHD (at the 1-fermion-loop level) have typically been included via the local density approximation (LDA) or its extension, the derivative expansion (DE),[1,2] but it is difficult to assess the accuracy of these procedures. Furthermore, they are clearly valid only for relatively smooth systems as are typical in QHD, but not for the strongly nonuniform systems that are common to soliton models of the nucleon. Therefore, extending QHD vacuum techniques to other problems may require a more direct treatment of the vacuum.

To address this need , we have developed a spectral method for computing *exactly* 1-loop vacuum polarization contributions based on a Fourier expansion of the exact wavefunctions. This method allows us to determine fully self-consistent QHD-I nuclear ground states in 1+1 dimensions with negligible uncertainties in the 1-loop contributions (extensions to 1+3 dimensions are straightforward, although tedious, and are discussed in subsequent sections). A spectral approach is in some ways more desirable than a nonspectral approach because one calculates single-particle eigenstates and their energies directly and carries out a state-by-state renormalization which allows much more physical insight than a nonspectral formulation. Also, spectral approaches allow an unambiguous counting of states so that portions of the spectrum treated in discrete and continuous representations can be easily joined with no possibility for double counting.

Integration methods have been used widely for solving differential equations like the Dirac equation, so much so that they have become accepted by many as a standard numerical method for solving such equations, and subsequently have occasionally been applied to problems where they may not be particularly well-suited to the task. In calculating a few bound states, a Numerov or Runge-Kutta integration scheme on a uniform spatial grid is entirely adequate, and the results are insensitive to the details of the boundary conditions being imposed outside the nucleus. This computational approach is well suited for solving for exact eigenfunctions, but has severe limitations when attempting to calculate very many states in an infinite complete set and sum over renormalized density contributions from each. In such circumstances, a Numerov or Runge-Kutta integration scheme is clearly inadequate on its own, since the maximum number of nodes in any obtainable wavefunction is restricted by the number of grid points chosen for the integration. In fact, the number of grid points must be at roughly an order of magnitude greater than the number of nodes of the deepest state considered, or the high-energy part of the spectrum will be unacceptably sensitive to the grid parameters. On the other hand, one cannot choose an arbitrarily fine grid because of machine error and constraints in computing time. We have investigated this approach thoroughly in QHD-I, and have found that while one may be able to reach reasonable convergence with integration methods in scalar-only systems, the presence of a vector potential slows convergence in the Dirac sea so greatly that it is essentially impossible to reach convergence in the Dirac sea by integration methods alone. More specifically, we have seen that the total renormalized vacuum baryon density arising from a large number of low-lying states calculated by Numerov integration is negative outside

the nucleus, and can be equal to a substantial fraction of its value inside the nucleus. This gives rise to an appreciable attractive vector potential outside the nucleus which is sufficient to cause severe instability. Furthermore, one finds that the total densities converge very slowly as the number of states included in the sum is increased. Thus integration methods alone are extremely cumbersome (if not entirely inappropriate) when computing vacuum polarization densities in models including a vector potential.

This point is illustrated in Figures 1 and 2 which show the renormalized baryon and scalar densities for several values of the number of sea states included (for illustration purposed this number was kept very small but the qualitative features of these figures are essentially unchanged even for arbitrarily large values of the cutoff). Since the nucleus occupies the region inside roughly 4 fm, it is clear that these vacuum densities have large contributions from the region outside the nucleus where its affect should be zero. We have traced this problem to the loss of completeness that comes from the uncontrolled truncation of the vacuum spectrum that is implied by placing the problem of a spatial grid. Since the vacuum densities are renormalized they must integrate to zero, yet due to the potentials there are a few bound vacuum states that are completely localized in the region of the nucleus. Therefore, the net effect on the remainder of the vacuum states must be an antilocalization that exactly compensates for the bound states. So, by arbitrarily truncating the basis, this matching of localized and anitlocalized states is lost with the result that there are substantial densities outside the nucleus.

In our spectral approach, we write our basis in terms of free parity eigenstates:

$$\varphi_{n+}(x) = \sqrt{\frac{N_n}{a}\frac{E_n+m}{2E_n}}\begin{pmatrix}\cos(k_n x)\\ +i\sqrt{\frac{E-M}{E+M}}\sin(k_n x)\end{pmatrix}$$

$$\varphi_{n-}(x) = \sqrt{\frac{N_n}{a}\frac{E_n+m}{2E_n}}\begin{pmatrix}\sin(k_n x)\\ -i\sqrt{\frac{E-M}{E+M}}\cos(k_n x)\end{pmatrix} \qquad (01)$$

and we obtain the exact states by diagonalizing a matrix. Since the matrix contains all information on the mixing of a limited set of basis states, the corresponding exact states will incorporate a psuedo-completeness (which can be traced to the 'completeness' property of the sines and cosines, *i.e.* $\sin^2(kx)+\cos^2(kx)=1$). By this I mean that any localization found in one part of the exact spectrum will be exactly compensated by an antilocalization elsewhere in the basis. This is demonstrated in Figures 1 and 2. The various curve compare the Numerov and exact results for the vacuum densities including 20, 25 and 30 basis states. Notice that the two methods give very similar results for the lower number of basis states, but the two methods disagree near the end of the basis. Furthermore, when the basis is exhausted (at 30 states) the exact spectral method finds densities that are well behaved outside of the nucleus. So, even with very small basis sizes our exact method preserves the crucial aspects of completeness, and any remaining truncation sensitivity reflects the true effects of considering only a portion of the vacuum (We have observed that the results converge quite quickly with increasing basis size, and that the convergence can be speeded by adding an LDA or DE for the deep states in the sea beyond our truncated basis).

In comparing different theoretical models for computing vacuum polarization effects in finite nuclei, it is especially useful to consider observable quantities which describe the overall properties of the nuclear system, such as the self-consistent rms nuclear size $x_{\rm rms}$, and the average binding energy per nucleon BE/N. An important parameter in these QHD models which facilitates a systematic study of the various vacuum models is the scalar mass, which has drastic effects on the many-body solution. In fact, in 3+1 dimensional calculations, the scalar mass is adjusted to tune the nuclear rms size to match experimental data. We have studied the scalar mass dependence of our self-consistent solutions on primarily two properties of the nucleus: the rms size $x_{\rm rms}$, and the average binding energy per nucleon BE/N. We will see that for very high scalar masses, where our ground state solutions become increasingly nonuniform, the various vacuum models begin to differ slightly. However, these differences are seen to be essentially negligible for the systems studied here, and we conclude that the DE provides an adequate approximation for the calculation of vacuum polarization effects in 1+1 dimensional QHD.

Figure 3 shows the rms size of self-consistent nuclear solutions with three closed shells as a function of the scalar mass parameter. The first feature one notices is that the MFT solutions have the least dependence on m_s, and are clearly distinct from all of the models which include vacuum polarization. Next, the rms sizes of LDA and DE solutions are undistinguishable at low m_s, but start to differ slightly at very high scalar mass, with the DE solutions tending surprisingly *closer* to the MFT solutions. (This might seem surprising at first because the DE is an expansion in derivatives of the potentials which has the LDA as its first term, so one might expect that the LDA solutions would lie between the MFT and DE solutions. On the contrary, the inclusion of meson field derivatives in the vacuum polarization densities pushes the DE solutions slightly *closer* to the MFT solutions. We must keep in mind, however, that the coupling constants in MFT and RHA models are very different, so a strong statement about this observation is not possible.) Similarly, the FDE solutions differ slightly from both the LDA and DE solutions at very high scalar mass, also tending yet more toward the MFT solutions. Although these differences are thought to be due to how these different models account for meson field derivatives, we see that the differences are minimal.

Figure 4 shows the average binding energy per nucleon BE/N of our nuclear solutions as a function of the scalar mass. Again, the first feature one notices is that the MFT solutions are distinct from the RHA solutions and the MFT model is much less dependent upon m_s than the RHA solutions. In contrast to the behavior of the rms size, we see here that the LDA and DE models are not distinct at high scalar mass on the scale of this plot, and the FDE solutions exhibit almost imperceivable differences with the DE solutions for all scalar masses, although the difference are *slightly* enhanced at higher scalar masses, also. The BE/N is much less sensitive to the derivative terms appearing in the vacuum polarization densities, and does not reflect the subtle differences in these models as clearly as the rms size. Also, we see that when the basis size N is increased by several factors, the FDE results in Figures 3 and 4 tend very precisely toward the DE results for all scalar masses, although slightly less quickly at very high scalar masses. In Figures 3 and 4 above, solutions in all models were calculated with $N = 30$. If N is increased we see the FDE solutions tend more toward the DE solutions for all scalar masses. However, the tiny scale of these differences together with the slow convergence of these slowly disintegrating solutions at high scalar mass makes it difficult, if not impossible, to ascertain if these differences are reflective of the theoretical models themselves, or of the convergence properties of these theoretical models in our numerical codes. A simple extrapolation to infinite basis size N based on calculations carried out for many different finite N seems to show that the FDE results converge to the DE more precisely than at high scalar mass, but in both cases the agreement is so close that it suffices to say that the DE is clearly adequate for the description of vacuum polarization in these systems.

While this work has demonstrated that approximate treatments of the vacuum are adequate in 1+1 dimensional QHD, it is not clear that the same will be true 3+1 dimensional QHD or in other field theoretic models. It is certain, however, that direct calculations of the vacuum in any system require great care in order to preserve the crucial completeness properties of the vacuum. An article describing the details of this work has been submitted to Phys. Rev. **C**.

1. C.J. Horowitz and B.D. Serot, Nucl. Phys. **A368**, 503 (1981).
2. R.J. Perry, Phys. Lett. B **182**, 269 (1986).

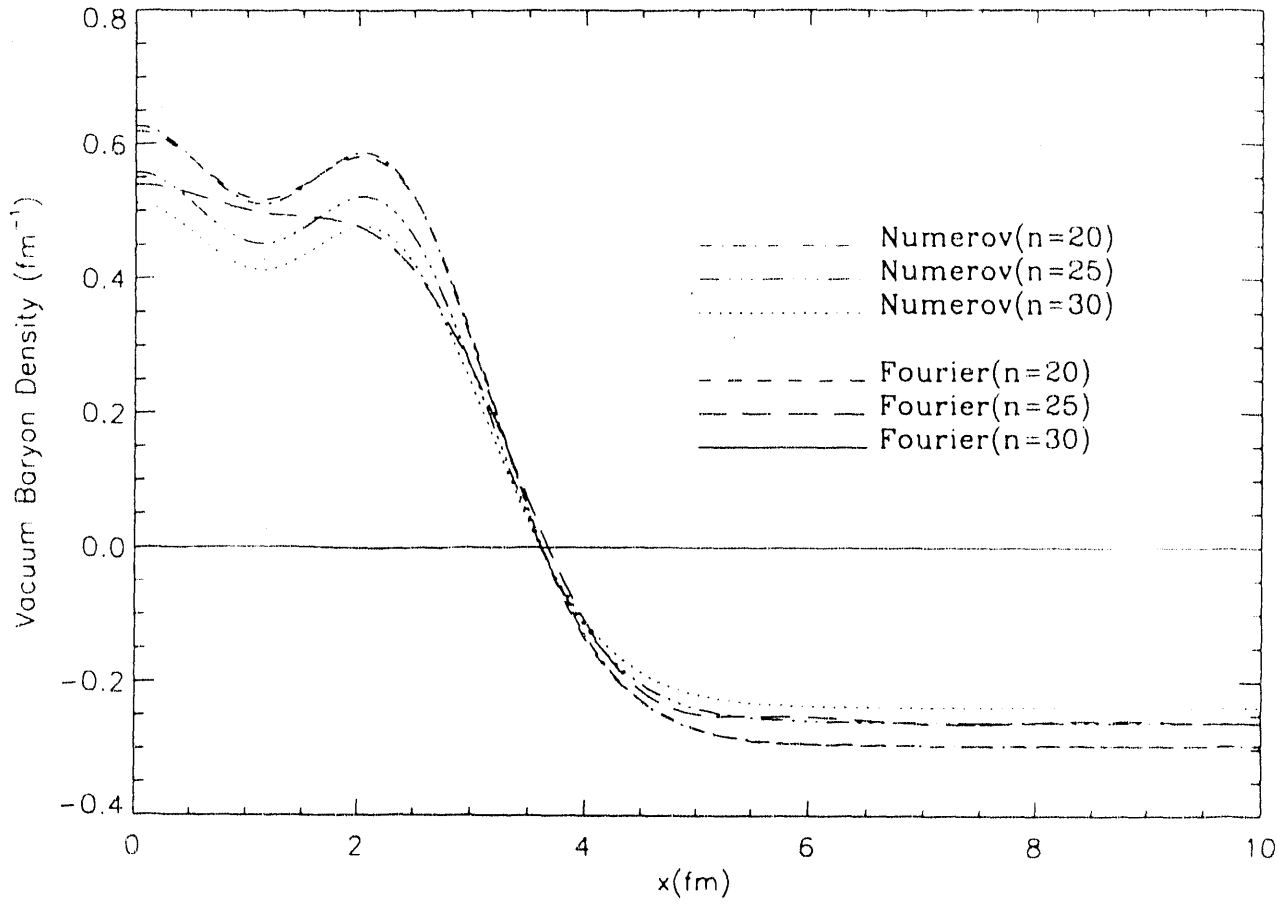

Fig. 1. Convergence of vacuum baryon density near the end of the truncated basis computed in F(N=30).

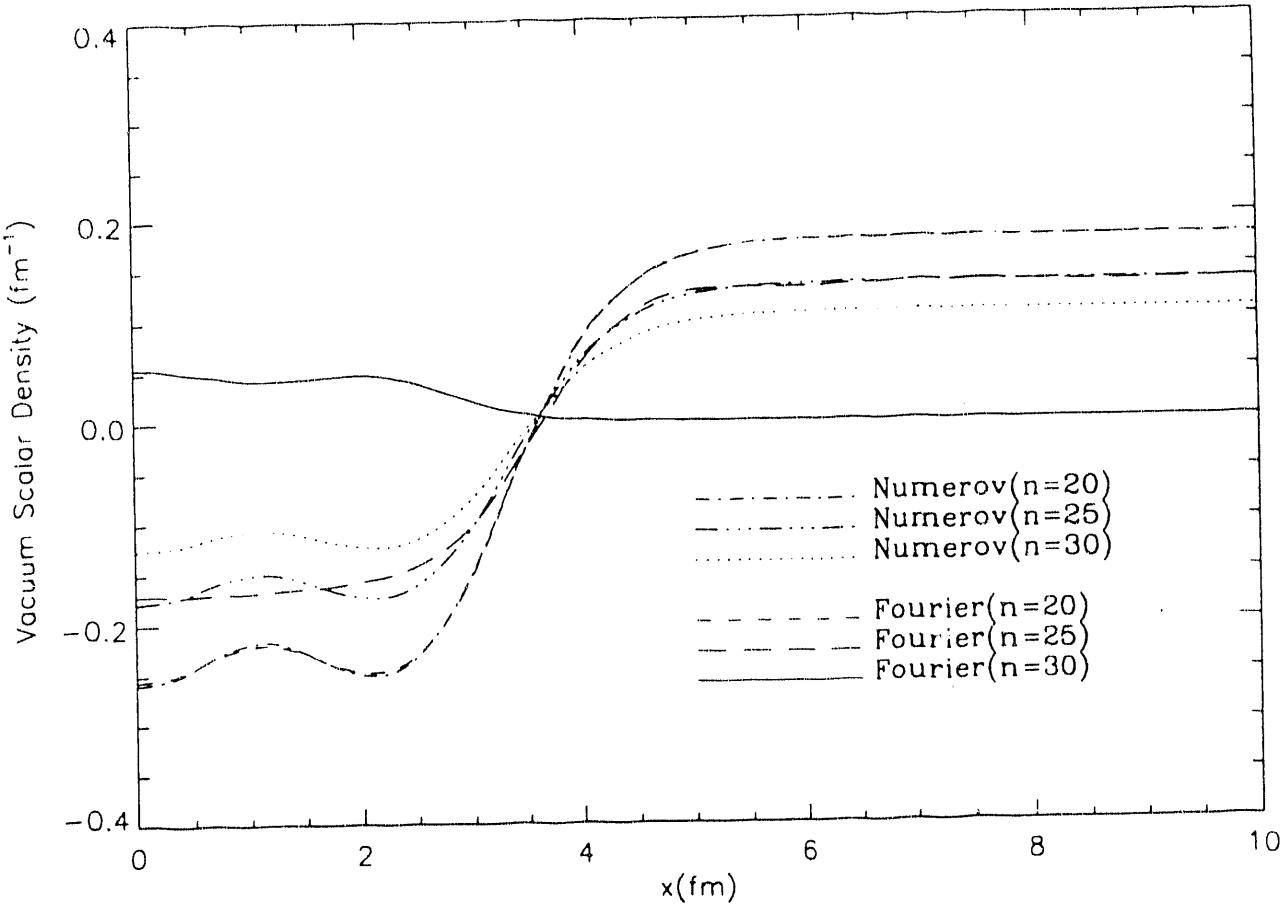

Fig. 2. Convergence of vacuum scalar density near the end of the truncated basis computed in F(N=30).

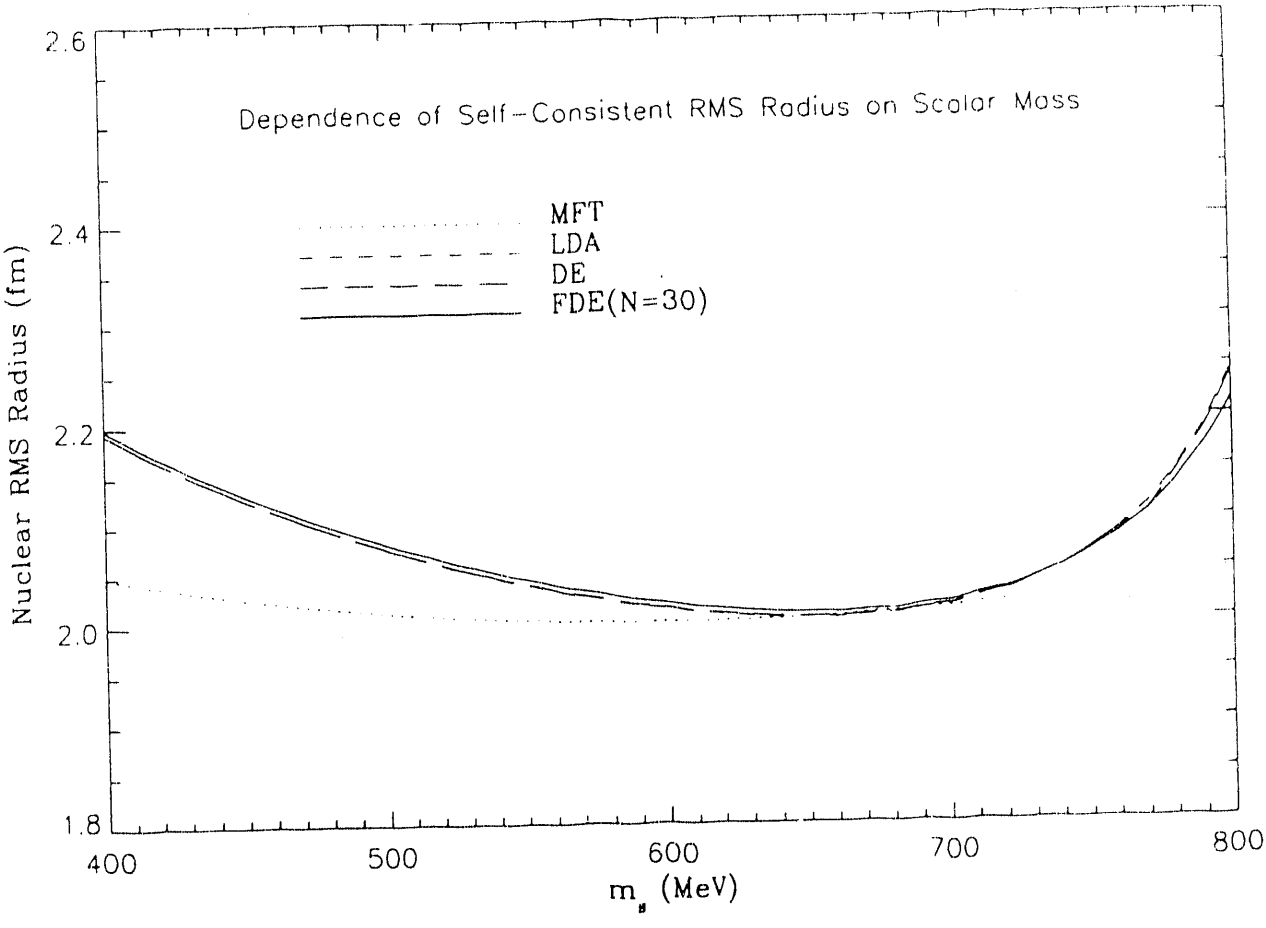

Fig. 3. Nuclear rms size versus scalar meson mass in self-consistent MFT, LDA, DE and FDE (fourier with derivative expansion extension) models.

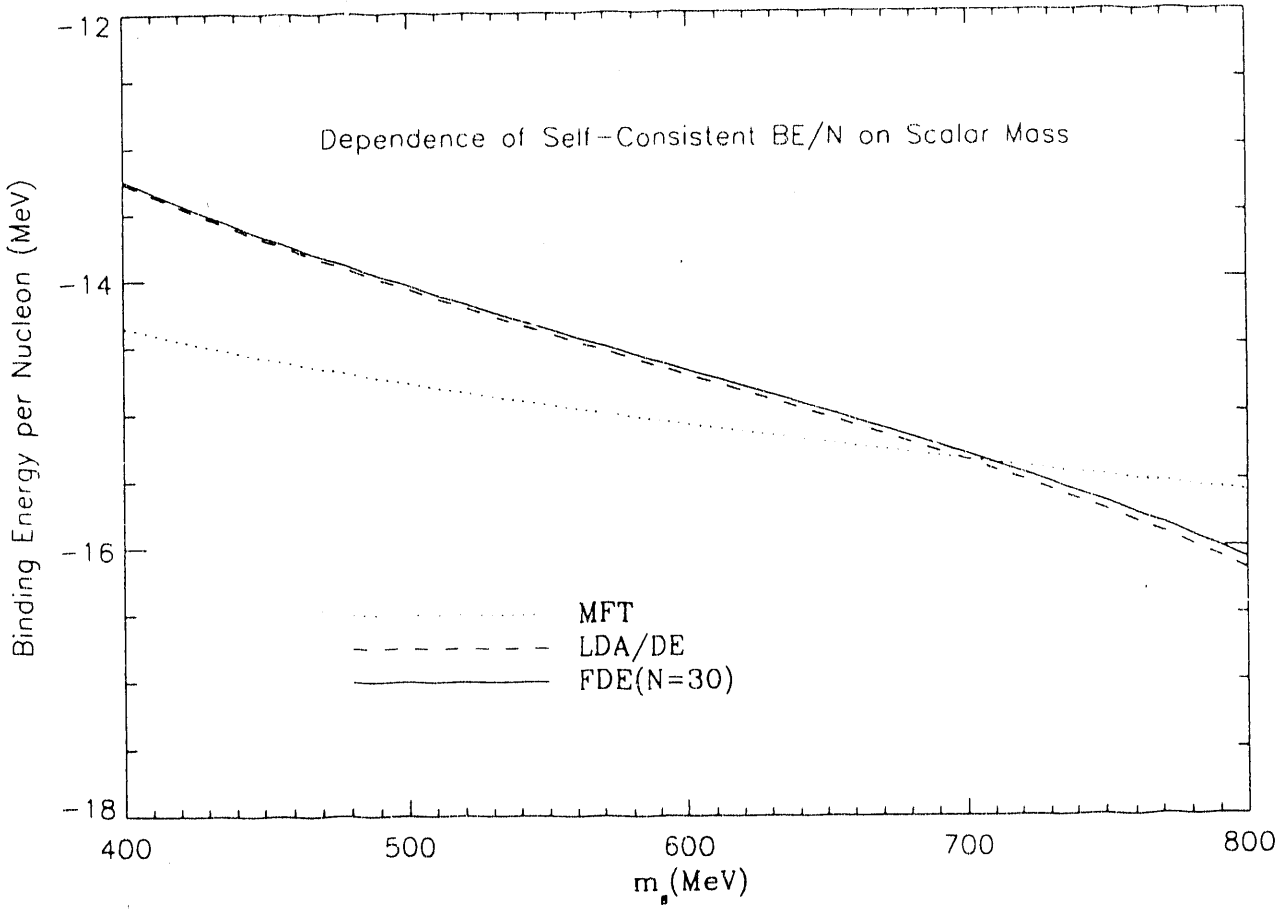

Fig. 4. Average nuclear binding energy versus scalar meson mass in self-consistent MFT, DE and FDE models. The LDA and DE results are indistinguishable on this scale.

2. Exact 1-Fermion Loop Contributions in 1+1 Dimensional Solitons J. R. Shepard, C. E. Price and T. C. Ferrée

In Section 1 of this document we report calculations of *exact* 1-fermion loop contributions in 1+1 dimensional quantum hadrodynamics (QHD). One of the conclusions of that work is that, for a wide range of QHD problems, the familiar derivative expansion (DE) is an adequate approximation to the exact treatment. Partly to see how our exact approach fares in a more demanding context but more importantly because of interesting physics issues to be addressed, we have computed exact 1-fermion loop contributions in solitons in a 1+1 dimensional discrete chiral model. This model is, of course, a simplification of the linear sigma model[1-5] which has been studied for three decades because of its conceptual simplicity, dynamical richness and "built-in" chiral symmetry. One of the more intriguing features of the model is the existence of solutions – at least in the classical limit for the scalar field – for which the fermions are strongly confined to a finite region where the scalar field vanishes. These solutions – often referred to as "kink solutions" – have been examined in detail by, *e.g.*, the SLAC Bag Collaboration[6] in an effort to describe hadronic structure and by a variety of others (see, *e.g.*, Refs. 7 and 8) to study "abnormal phases" of nuclear matter.

Almost from the very beginning of these studies, there has been speculation about the persistence of such solutions when vacuum contributions are included.[4,7] Indeed, there is current interest[9,10,11] in this question. Such analyses are complicated by the fact that the kink or deep-bag solutions are of course non-uniform and therefore the treatment of vacuum contributions is considerably harder than for uniform systems. A number of workers have developed exact treaments of 1-fermion loop effects in such systems. For example, Campbell and Liao[4] presented early calculations of 1-fermion loop contributions to the kink energy in 1+1 dimensions. However, their treatment was restricted to a single special set of coupling constants. Li, Perry and Wilets[12] and, more recently, Wasson[13] have reported similar exact calculations. Wasson has furthermore presented results for a variety of couplings and for which the 1-fermion loop contributions are treated in a fully self-consistent manner. While some of these authors have focussed exclusively on calculational aspects of the problem, others[4,11] have concluded that 1-fermion loop contributions render the kink solution either absolutely unstable or metastable with respect to other (*e.g.*, shallow bag) solutions. In what follows, we outline our calculational method and sketch some of our findings. A manuscript detailing these studies has been prepared and submitted to Physical Review **D**. The interested reader is referred there for a more thorough discussion than will appear here.

We assume the following Lagrangian in 1+1 dimensions:

$$\mathcal{L} = \bar{\psi} i\gamma \cdot \partial\psi + g\phi\bar{\psi}\psi + \frac{1}{2}\partial\phi \cdot \partial\phi - U(\phi) + \mathcal{L}_{ctc} \tag{01}$$

where ψ is the fermion field, ϕ is the scalar field and where $\mathcal{L}_{ctc}$ is the counter-term Lagrangian whose exact form will be specified below. The scalar potential is

$$U(\phi) = \frac{\lambda}{4}(\phi^2 - f^2)^2. \tag{02}$$

This is of course the Lagrangian of the linear sigma model without the pseudoscalar field and it thus possesses discrete rather than continuous chiral symmetry. For a uniform system, in the absence of coupling to the fermion field ($g = 0$), the classical scalar field satisfies

$$\phi^2 = f^2. \tag{03}$$

There also exists a higher energy non-uniform "kink" solution

$$\phi(x) = f \tanh\left(\sqrt{\frac{\lambda}{2}} f \; x\right) \tag{04}$$

which "interpolates" between the two uniform solutions, namely $\phi = \pm f$. In general, the classical field dynamically generates both fermion and scalar masses. Standard manipulations of the Lagrangian produce coupled equations of motion for the *expectation value* of the scalar field, ϕ_0 and the fermion spectrum. The Dirac equation is solved using techniques identical to those employed in 1+1 QHD as described in Section 1.

The fermion energy density is of course divergent and must be renormalized. Renormalization of the energy density will also show how to treat the scalar density. With the fermion basis truncated at momentum Λ, the unrenormalized energy density due to the sea is, *for a uniform system with* $\phi^2 = f^2$ (or, equivalently, for $S = 0$),

$$\mathcal{E}_V^{(0)}(x) = -\int_{-\Lambda}^{+\Lambda} \frac{dk}{2\pi} \, E_k^0 \tag{05}$$

where $E_k^0 \equiv +\sqrt{k^2 + (gf)^2} = \sqrt{k^2 + m^2}$. Upon discretizing,

$$\mathcal{E}_V^{(0)} \to \frac{1}{a} \sum_{i=-N+1}^{N} (-E_i^0) \tag{06}$$

where $E_i^0 \equiv \sqrt{k_i^2 + (gf)^2}$ and $k_i \equiv (2i-1)\pi/a$. The *shift* in this energy density due to $S(x) \neq 0$ is, schematically,

$$\mathcal{E}_V(x) - \mathcal{E}_V^{(0)}(x) = \sum_{n=1}^{\infty} \frac{1}{n} \mathrm{Tr}\left[SG_0\right]^n \tag{07}$$

where G_0 is the "free" fermion propagator. Examination of the first four terms of this expansion provide the detailed form of the renormalization counter-terms. They are constructed with care to maintain consistency with the truncated finite basis in which the equations of motion – especially the Dirac equation – are solved. While the derivations are straightforward, they and the expressions they yield are somewhat lengthy and will not be reproduced here.

In addition to applying our new method for treatment of 1-fermion loop effects, we also examine a renormalization scheme which differs from that typically used in such studies. Specifically, we make one more chiral subtraction than, *e.g.*, Wasson[13] in addition to making a derivative counter-term subtraction. We refer to the two renormalization procedures as "full" and "minimal", respectively. Both schemes ensure that the renormalized energy and scalar density vanish at the renormalization point defined by $\phi^2 = f^2$ and $q^2 = 0$. Examination of their differences begins by observing that, in the absence of coupling to fermions, or, more generally, in the classical limit,

$$\left.\frac{\partial^2 U}{\partial \phi^2}\right|_{\phi^2=f^2} = 2\lambda f^2 = \mu_0^2 \tag{08}$$

where μ_0 is the spontaneously generated classical scalar mass. This implies we may interpret

$$\left.\frac{\partial^2 \mathcal{E}_{loop}}{\partial \phi^2}\right|_{\phi^2=f^2} \rightarrow g^2 \left.\frac{\partial^2 \mathcal{E}_{loop}}{\partial S^2}\right|_{S=0} = \delta\mu_0^2 \tag{09}$$

where $\mathcal{E}_{loop}$ is the *renormalized* loop energy density as the correction to the scalar mass due to 1-fermion loop effects. Using our "full" renormalization method, $\delta\mu_0^2 = 0$ at the renormalization point. In the "minimal" scheme, going to the infinite-cutoff, continuum limit, $\delta\mu_0^2 \rightarrow g^2/\pi$ at the same point. Hence, while the "full" dressed scalar meson mass for $\phi^2 = f^2$ and $q^2 = 0$ is the *classical* mass, $\mu_0 = \sqrt{2\lambda} f$, the "minimal" result is

$$\mu^2 = \mu_0^2 + g^2/\pi. \tag{010}$$

Our derivative counter term contribution ensures that, at the renormalization point,

$$\left.\frac{\partial}{\partial q_\mu^2}\Delta^{-1}(q_\mu^2)\right|_{q_\mu^2=0} = 1 \tag{011}$$

where $\Delta(q_\mu^2)$ is the scalar propagator dressed by 1-fermion loop contributions. This relation is of course satisfied by the classical scalar propagator, $\Delta_0(q_\mu^2) = (q_\mu^2 - \mu_0^2)^{-1}$. Finally, additional terms in the full chiral renormalization generally imply more suppression of loop contributions than for the minimal case.

We test the numerics of our calculations by comparing with the published results of Campbell and Liao[4] and of Wasson,[13] both of which employ minimal renormalization. For this renormalization scheme, kink solutions with $\lambda/g^2 = 2$ constitute a special case in that the 1-fermion loop contribution to the scalar density vanishes when $\phi(x)$ is given by the classical kink solution, Eqn. (04). Hence, this kink solution is also *self-consistent* (with or without any fermions in the lowest positive energy level). Campbell and Liao treat only this case and find an analytic expression for the total kink energy, namely, their Eqn. 4.15. Their result implies $E_{loop} = g/\pi \simeq 0.318310g$. We agree well with Campbell and Liao. In fact, a calculation with a basis size given by $N_{order} = 100$ differs from the analytic result by less than 0.004% . Wasson[13] presents non-iterated (or perturbative) as well as self-consistent results for various values of λ/g^2 and we agree with him in all cases.

Table 1 presents results utilizing our full renormalization scheme. We note that the loop energies are roughly two-thirds of those found with the minimal scheme. It also appears that the classical kink solution is self-consistent in the full calculations for $\lambda/g^2 = 0.5$ rather than $\lambda/g^2 = 2$ as before. Among other things, we see that DE contributions from outside the basis are roughly two orders of magnitude smaller when computed with full rather than minmal renormalization. It is thus apparent that the full chiral renormalization – in effect – *cuts off* 1 loop contributions from the fermion sea at quite small values of momentum For example, we see (Table 1) that, for $\lambda/g^2 = 2$, less than 1/2 % of the loop energy is due to levels in the sea with momentum greater than $\sim 2g$, *i.e.*, $\sim 2\times$ the asymptotic fermion mass, $m = -gf$. Such a drastic (effective) cutoff is surprising in light of the huge changes in the fermion effective mass implied by the kink solution, namely

$$0 \leq \left(\frac{m^*}{m}\right)^2 = \left(\frac{\phi}{f}\right)^2 \leq 1.$$

Put another way, fermions whose mass-squared is g^2 far from the kink are subject to interactions so strong that their mass *vanishes* at the center of the kink. Such interactions could be expected to polarize the negative energy sea very significantly and would seem to suggest much larger 1 loop contributions from deep in the sea than are observed, especially with full renormalization. (We note in this regard that, for the uniform system, the 1 fermion loop energy density possesses a logarithmic singularity at $m^* = 0$.)

We also make comparisons between "kink" and "shallow bag" solutions. It is assumed in *both* cases that the lowest positive energy fermion level is fully occupied, *i.e.*, this state contains N_{sea} fermions where N_{sea} is the fermion multiplicity owing to, *e.g.*, color, flavor, etc. (Note that $N_{sea} = 1$ was assumed throughout the preceeding discussion in order to compare with Wasson.) For the kink solutions the lowest positive energy state (*and* the highest negative energy state) has zero total energy and yields a vanishing scalar density. Hence occupancy of this state has *no effect* on either the loop energy or the scalar field configuration. In contrast, the positive energy fermions are *essential* for the shallow bag solutions since the associated scalar fields would decay to the trivial uniform configuration ($\phi^2 = f^2$) in their absence.

Properties of these solutions obtained using minimal (full) renormalization are displayed in Table 2 (3). Also, Figure 1 (2) shows vector and scalar fermion densities as well as fermion scalar potentials for self-consistent minimal (full) kink and shallow bag solutions with $\lambda/g^2 = 0.5$ and $N_{sea} = 6$. Figure 3 (4) presents the same quantities but for $N_{sea} = 18$. Because of the symmetries built into our free basis which ensure, for example, that all densities are symmetric about $x = 0$, "kinks" occur in pairs located symmetrically about the origin. (See Figures 1-4.) Furthermore, the vector (*i.e.*, probability) density for the lowest positive energy fermion state associated with the kinks is strongly localized at the center of each kink where $S(x) = -g$ and m^* vanishes. Hence, each kink contains $N_{sea}/2$ fermions. In contrast, the shallow bag solutions are localized near the origin and each contains N_{sea} fermions. For this reason, we compare quantities for *two* kinks with results for one shallow bag in Tables 2 and 3. We note also (Figures 2 and 4) that the fully renormalized kink scalar densities for $\lambda/g^2 = 0.5$ *vanish*; in fact, the valence and sea contributions vanish separately. The same phenomenon is, of course, observed for $\lambda/g^2 = 2$ with minimal renormalization.

Armed with analytic results for $\lambda/g^2 = 2$, Campbell and Liao[4] determined that, in this special case, shallow bags are more bound than kinks for $N_{sea} < 4\pi$ while for $N_{sea} > 4\pi$, the situation is reversed. Our numerical results are consistent with this finding since, as revealed in Table 2, shallow bag total energies are less than kink energies *except* for $N_{sea} = 18$. Here our shallow bag solution evolves (slowly!) toward the kink and the <0.002% energy difference appearing in Table 2 is simply an artifact of incomplete convergence after starting the iterations with a shallow bag configuration. It thus appears that, for $N_{sea} < 4\pi$, self-consistent kink solutions can be found which are *metastable* with respect to the shallow bag while, for $N_{sea} > 4\pi$, the shallow bag is *unstable* and only the kink can be self-consistent. As λ/g^2 is reduced from the special value of 2, the value of N_{sea} for which kinks and shallow bags become degenerate appears to increase from 4π. This conclusion is suggested by the fact that, for $\lambda/g^2 = 0.5$ and 1, the shallow bag is more bound for all values of N_{sea} appearing in Table 2. It is interesting, however, to inspect the shallow bag vector densities for $N_{sea} = 6$ (Figure 1) and 18 (Figure 3) and to see that, even for $\lambda/g^2 = 0.5$ when the shallow bag is always more bound, larger values of N_{sea} result in shallow bags which look increasingly like slightly overlapping kinks. This suggests that, when kinks and shallow bags become degenerate, the two solutions are no longer distinct. It also leads to the intriguing notion that the shallow bag can – for large values of N_{sea} but where the shallow bag is still energetically favored – be viewed as a weakly bound pair of kinks.

Table 3 presents properties of kink and shallow bag solutions employing *full* renormalization and reveals that the shallow bag results are more bound for all values of λ/g^2 and N_{sea} presented, including $\lambda/g^2 = 2$ and $N_{sea} = 18$. We have done additional calculations for $N_{sea} = 18$ which suggest that, for this multiplicity, kink *versus* shallow bag degeneracy occurs for some value of λ/g^2 between 3 and 4. Another view of this situation is that, for a given value of λ/g^2, larger values of N_{sea} are required for degeneracy when using full rather than minimal renormalization. It also appears that, as before, distinct self-consistent kink *and* shallow bag solutions exist for small values of N_{sea} and that – above some critical value – only the kink is self-consistent. Also, because "full" renormalization *reduces* the repulsive 1-fermion loop contributions, these solutions are always more bound than their "minimal" counterparts. (See Table 3.) Greater binding is also reflected in the potentials presented in Figures 1–4 which are always "steeper" functions of x with full renormalization.

Although the principal aim of the present paper is (1) to demonstrate the utility of our calculational method and (2) to examine difference between minimal and full chiral renormalization schemes, it seems of interest to examine kink and shallow bag solutions for "baryons" consisting of *three* fermions in the lowest positive energy state with $N_{sea} = 6$. The kink solutions whose properties are summarized in Tables 2 and 3 are of course just *two* such baryons. Further, the kink densities shown in Figures 1 and 2 represent *one* kink baryon. New shallow bag solutions are required. Properties of these shallow bag baryons are displayed in Table 4 and the associated densities and scalar potentials are displayed in Figure 5. For $\lambda/g^2 = 2$ and minimal renormalization, the shallow bag solutions are more bound than the kink configurations. However, as λ/g^2 is reduced and the relative scalar-fermion coupling goes up, the situation is reversed. With $\lambda/g^2 = 0.5$ and minimal renormalization, the binding energy/fermion for the kink is more than twice that of the shallow bag. When using the full renormalization, *the kink binding is always greater than that of the shallow bag.* Comparison of the kink vector densities shown in Figures 1 and 2 with the shallow bag vector densities of Figure 5 show that the former have widths which are roughly 1/2 those of the latter as might be expected from the binding energy differences. For relatively strong scalar-fermion coupling, the binding energies of both

solutions roughly double with full renormalization and the kink values are again more than twice the shallow bag results. For the most strongly bound fully renormalized kink solution, the binding energy/fermion is nearly 1/3 the asymptotic fermion mass. We have made no effort to factor out center-of-mass effects[4,5] from our solitonic solutions and are therefore at some remove from ascribing physical significance to them even after extrapolating to 1+3 dimensions. However, we *can* conclude that the *details* of the renormalization procedure – *e.g.*, the difference between minimal and full prescriptions – can be critical in establishing properties of kink *versus* shallow bag solutions *including their relative stabilities.*[11]

1. J.Schwinger, Ann.Phys.(N.Y.)**2**,407 (1959).
2. M.Gell-Mann and M.Levy, Nuovo Cimento**16**,706 (1960).
3. B.W.Lee, Chiral Dynamics, Gordon and Breach, N.Y. (1972).
4. D.Campbell and Y.-T.Liao, Phys.Rev.**D14**,2093 (1976).
5. S.Coleman, "Classical Lumps and Their Quantum Descendents," in Aspects of Symmetry, Cambridge University Press, Cambridge (1985).
6. W.A.Bardeen,M.S.Chanowitz,S.D.Drell,M.Weinstein and T.-N.Yan, Phys.Rev.**D11**,1094 (1975).
7. T.D.Lee and G.C.Wick, Phys.Rev.**D9**,2291 (1974).
8. See, *e.g.*, J.Boguta, Nucl.Phys.**A501**,637 (1989).
9. G.W.Anderson,L.J.Hall and S.D.H.Hsu, Phys.Lett. **B249**, 505 (1990).
10. S.Dimopolous,B.W.Lynn,S.Selipsky and N.Tetradis, Phys.Lett. **B253**, 237 (1991).
11. J.A.Bagger and S.G.Naculich, Phys.Rev.Let.**67**,2252 (1991).
12. M.Li, R.J.Perry and L.Wilets, Phys.Rev.**D36**,596 (1987); see also: M.Li and R.J.Perry, Phys.Rev.**D37**,1670 (1988) ; M.Li, L.Wilets and R.J.Perry, Jour.Comp.Phys.**85**,457 (1989).
13. D.A.Wasson, Nucl.Phys.**A535**,456 (1991); see also: D.A.Wasson and S.Koonin, Phys.Rev.**D43**,3400 (1991).

λ/g^2	N_{order}	Λ/g	N_{iter}	E_{loop}/g	% DE
0.5	8	1.98	1	0.2335	0.09
	25	6.47	1	0.2330	0.00
			10	0.2330	0.00
	50	13.07	1	0.2330	0.00
			10	0.2330	0.00
	100	26.28	1	0.2330	0.00
2.0	8	1.98	1	0.2466	0.18
	15	3.83	1	0.2477	0.008
			4	0.2469	0.008
			15	0.2468	0.008
	25	6.47	1	0.2476	0.00
			15	0.2467	0.00
	50	13.07	1	0.2476	0.00
			15	0.2467	0.00

Table 1. Properties of "sea-only" kink solutions with full renormalization scheme. Assumes $N_{sea} = 1$, $f^2 = 1$. E_{loop} is the renormalized energy contribution due to the sea, i.e., $\tilde{E}_V$ plus DE contributions from outside the basis. Also shown is the DE percentage of the loop energy.

N_{sea}	λ/g^2	E_{meson}	E_{loop}	E_{val}	E_{tot}	BE/fermion	$S(0)$
Kink Solution							
3	2.0	2.6667	1.9090	0	4.5766	+0.5256	
	1.0	1.8932	1.9306	0	3.8240	+0.2756	
	0.5	1.3734	1.9780	0	3.3516	+0.1172	
6	2.0	2.6667	3.8198	0	6.4866	+0.0811	
	1.0	1.9043	3.8461	0	5.7505	-0.0416	
	0.5	1.4158	3.8965	0	5.3125	-0.1146	
18	2.0	2.6667	11.4594	0	14.1265	-0.2152	
	1.0	1.9346	11.4842	0	13.4195	-0.2545	
	0.5	1.5090	11.5224	0	13.0320	-0.2760	
Shallow Bag Solution							
3	2.0	0.0861	0.0214	2.8445	2.9520	-0.0160	-0.1045
	1.0	0.2004	0.1029	2.5579	2.8613	-0.0462	-0.2786
	0.5	0.2944	0.2956	2.1238	2.7138	-0.0954	-0.5089
6	2.0	0.4740	0.2615	4.9618	5.6973	-0.0505	-0.3461
	1.0	0.7565	0.8960	3.6653	5.3204	-0.1133	-0.7223
	0.5	0.6858	1.4689	2.8162	4.9708	-0.1715	-0.9347
18	2.0	2.6649	11.0840	0.3783	14.1268	-0.2152	-1.9582
	1.0	1.8959	10.3681	1.1435	13.4075	-0.2551	-1.8366
	0.5	1.3286	9.0000	2.6562	12.9848	-0.2786	-1.6217

Table 2. Kink *versus* Shallow Bag Solutions with minimal renormalization. Assumes lowest positive energy fermion level filled and $f^2 = 1$. E_{loop} is the same as for Table 1. E_{meson} is the energy due to the scalar field and E_{val} is that for the positive energy fermions. BE/fermion= $(E_{tot} - N_{val}\, g)/N_{val}$ where N_{val} is the number of positive energy fermions. $S(0)$ is the shallow bag scalar potential at $x = 0$.

N_{sea}	λ/g^2	E_{meson}	E_{loop}	E_{val}	E_{tot}	BE/fermion	$S(0)$
Kink Solution							
3	2.0	2.6741	1.4699	0	4.1442	+0.3814	
	1.0	1.8892	1.4160	0	3.3054	+0.1018	
	0.5	1.3333	1.3977	0	2.8377	-0.0896	
6	2.0	2.6919	2.9152	0	5.6072	-0.0655	
	1.0	1.8962	2.8222	0	4.7188	-0.2315	
	0.5	1.3333	2.7954	0	4.1292	-0.3118	
18	2.0	2.8026	8.5657	0	11.3691	-0.3684	
w	1.0	1.9253	8.4173	0	10.3438	-0.4254	
	0.5	1.3333	8.3862	0	9.7210	-0.4599	
Shallow Bag Solution							
3	2.0	0.1636	0.0035	2.7570	2.9241	-0.0253	-0.1606
	1.0	0.5181	0.0758	2.1243	2.7182	-0.0939	-0.5146
	0.5	0.6586	0.3157	1.3990	2.3732	-0.2089	-0.8463
6	2.0	1.4170	0.3683	3.5307	5.3159	-0.1140	-0.7810
	1.0	1.4045	1.0961	1.9963	4.4969	-0.2505	-1.1395
	0.5	0.9871	1.4204	1.5137	3.9212	-0.3465	-1.2051
18	2.0	2.7619	6.6004	1.9628	11.3250	-0.3708	-1.6553
	1.0	1.7976	6.2340	2.2075	10.2391	-0.4312	-1.5307
	0.5	1.1781	6.2803	2.1361	9.5945	-0.4670	-1.4884

Table 3. Same as Table 2 but with full renormalization.

Solution	λ/g^2	E_{meson}	E_{loop}	E_{val}	E_{tot}	BE/fermion
Minimal Renormalization						
Shallow Bag	2.0	0.0506	0.0249	2.8928	2.9683	-0.0106
	1.0	0.0788	0.0779	2.7681	2.9247	-0.0251
	0.5	0.0878	0.1660	2.6173	2.8711	-0.0430
Kink	2.0	1.3333	1.9099	0	3.2433	+0.0811
	1.0	0.9521	1.9230	0	2.8753	-0.0416
	0.5	0.7079	1.9482	0	2.6562	-0.1146
Full Renormalization						
Shallow Bag	2.0	0.1473	0.0058	2.7742	2.9273	-0.0242
	1.0	0.3371	0.0699	2.3615	2.7685	-0.0772
	0.5	0.3633	0.2136	1.9746	2.5515	-0.1495
Kink	2.0	1.3459	1.4576	0	2.8036	-0.0655
	1.0	0.9481	1.4111	0	2.3594	-0.2135
	0.5	0.6666	1.3977	0	2.0646	-0.3118

Table 4. Same as for Tables 2 and 3 but for 3-fermion "baryons". See text for discussion.

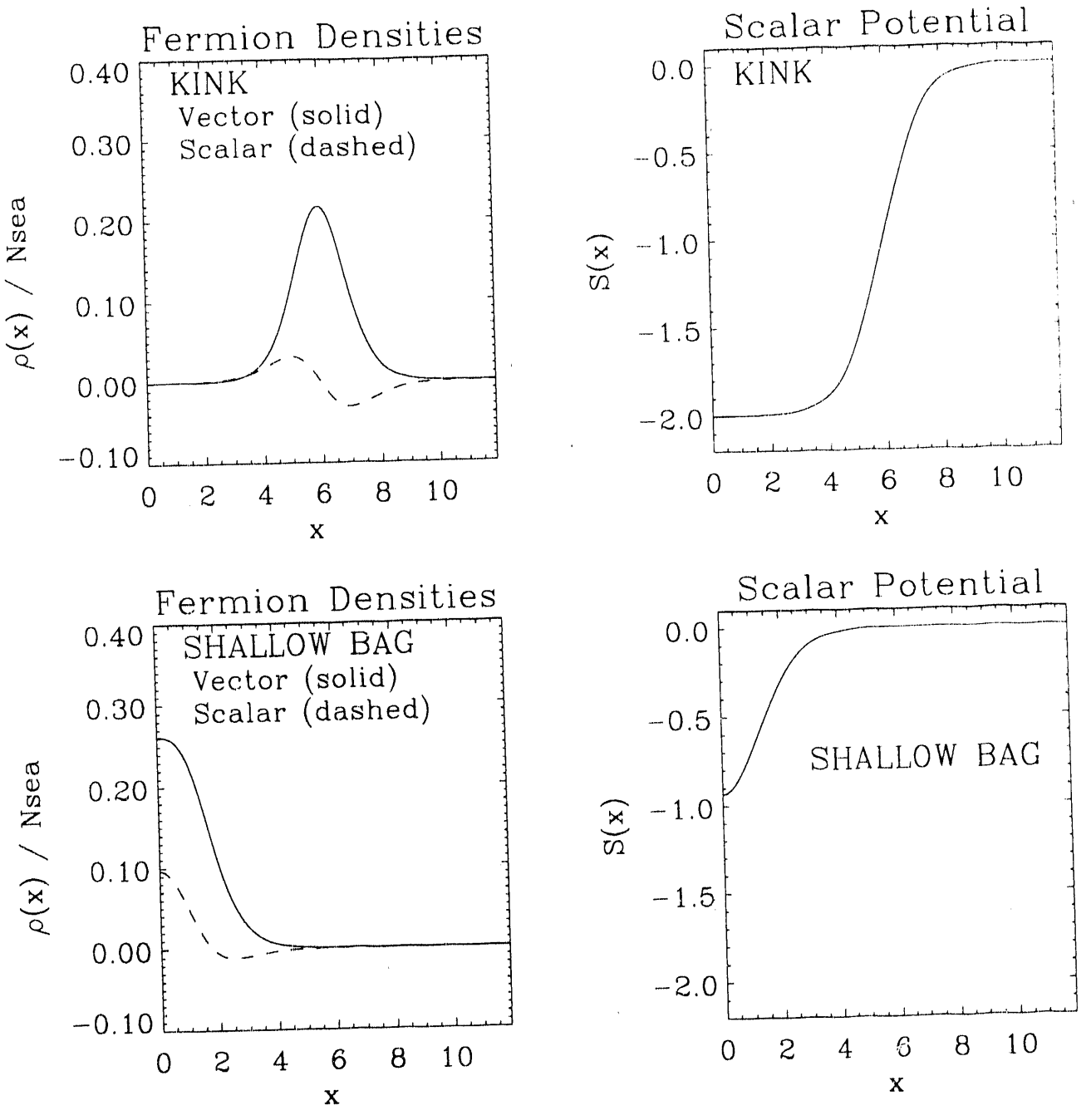

Figure 1. Densities and scalar potentials for the $\lambda/g^2 = 0.5$, $N_{sea} = 6$ kink and shallow bag solutions of Table 2, *i.e.*, minimal renormalization is employed. Lengths are in units of $1/g$ while densities and energies are in units of g. All quantities displayed are *even* functions of x.

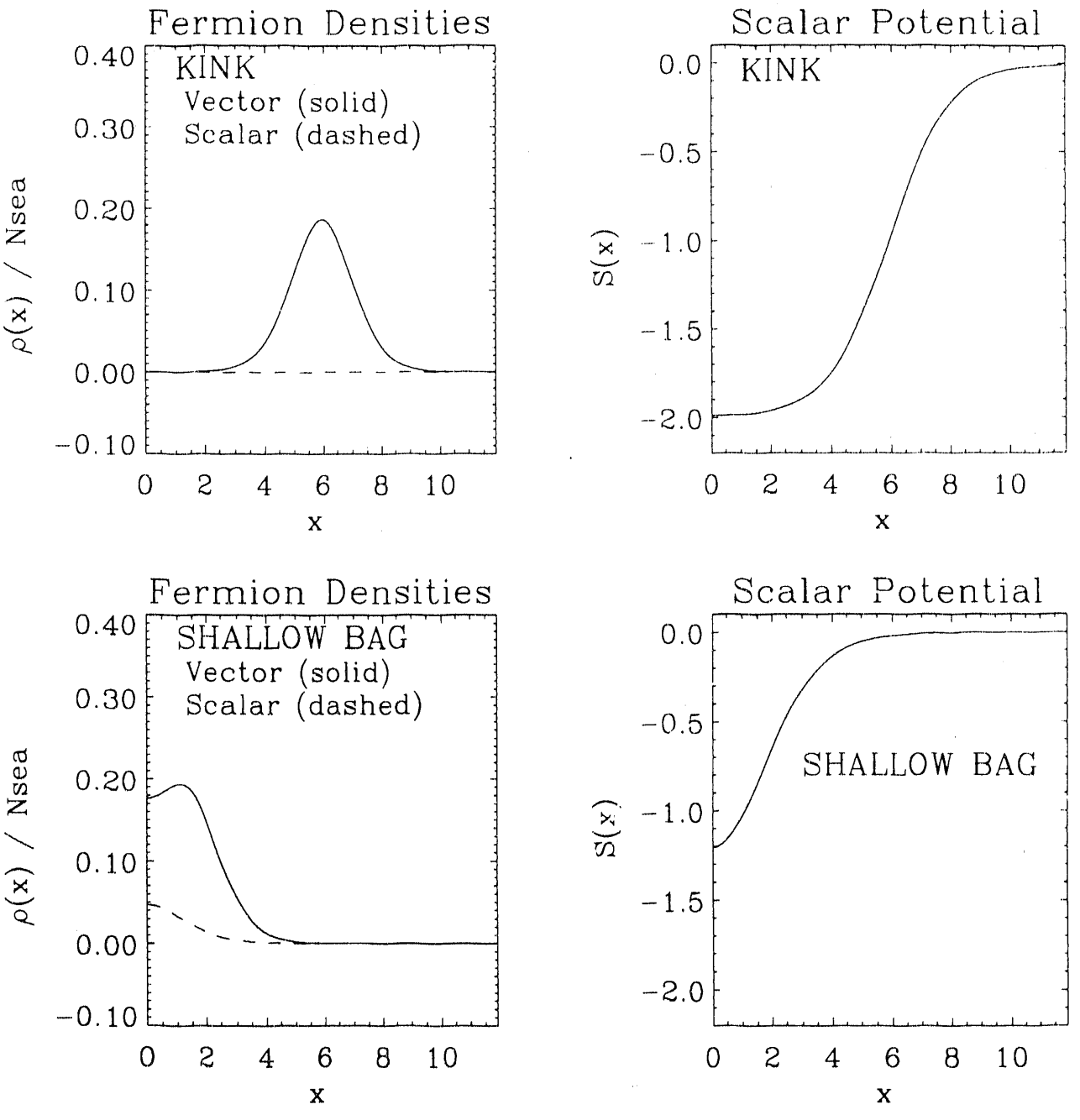

Figure 2. Same as Fig. 1 but with full renormalization.

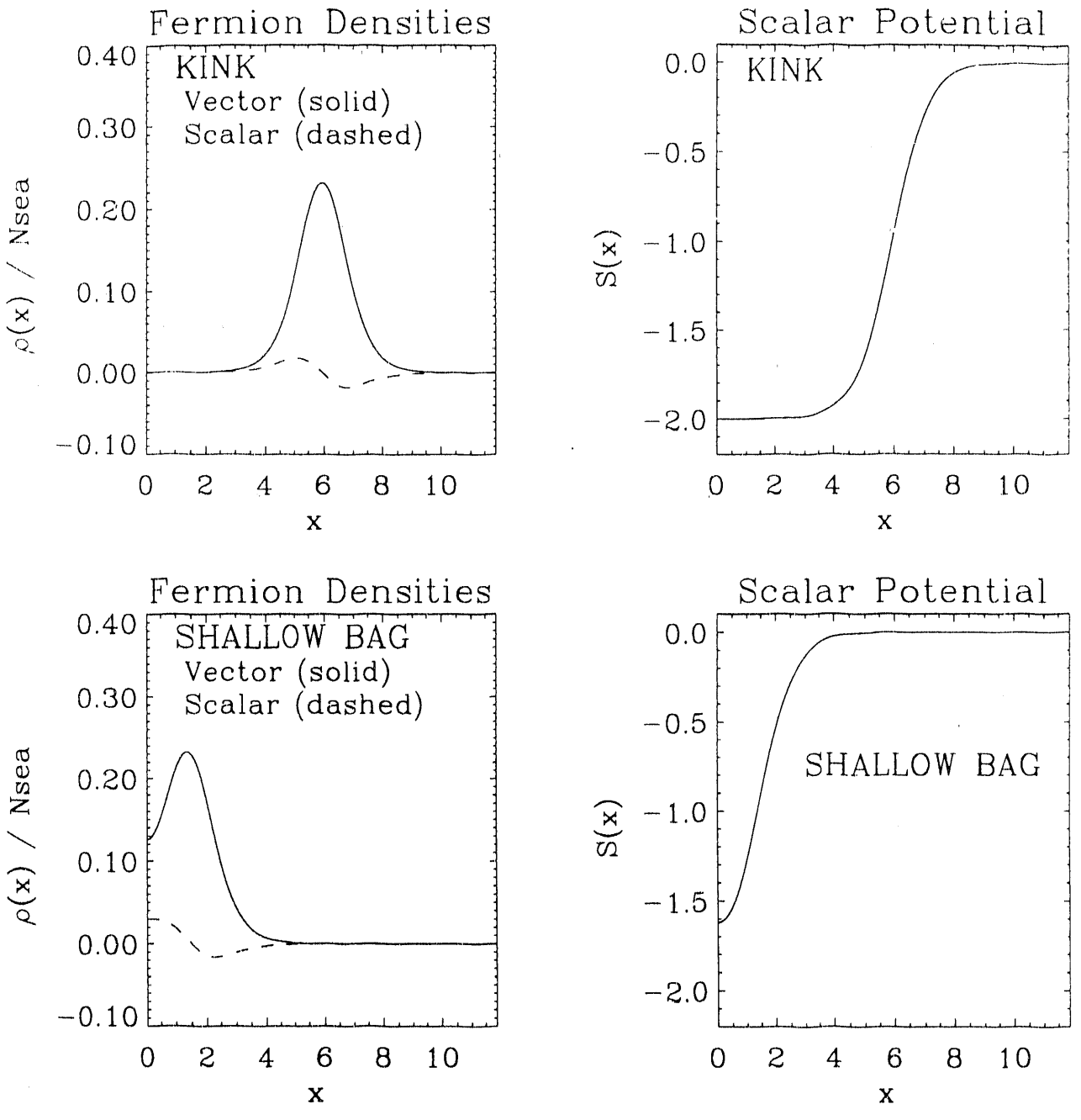

Figure 3. Same as Fig. 1 but with $N_{sea} = 18$.

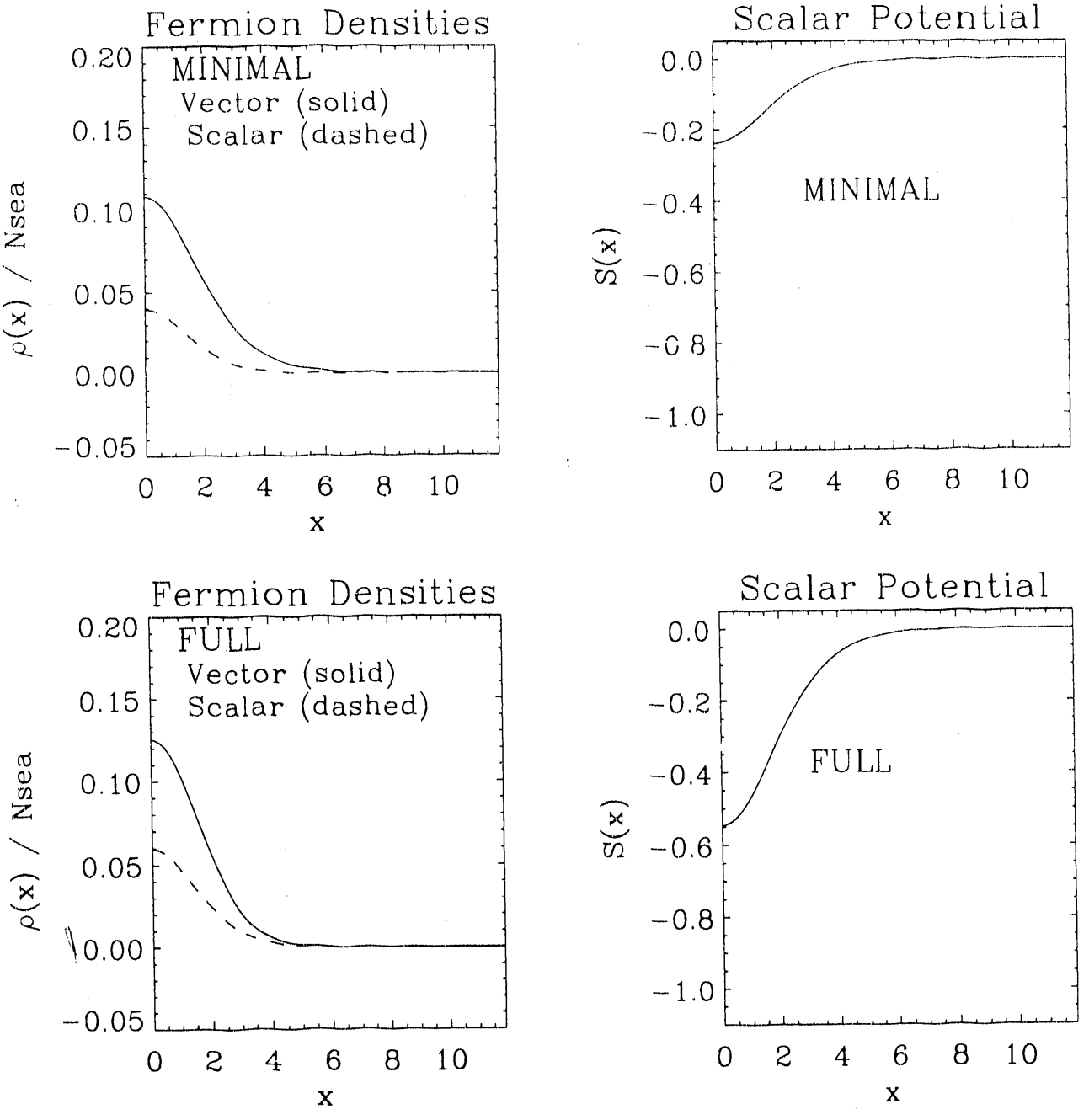

Figure 4. Same as Fig. 2 but with $N_{sea} = 18$.

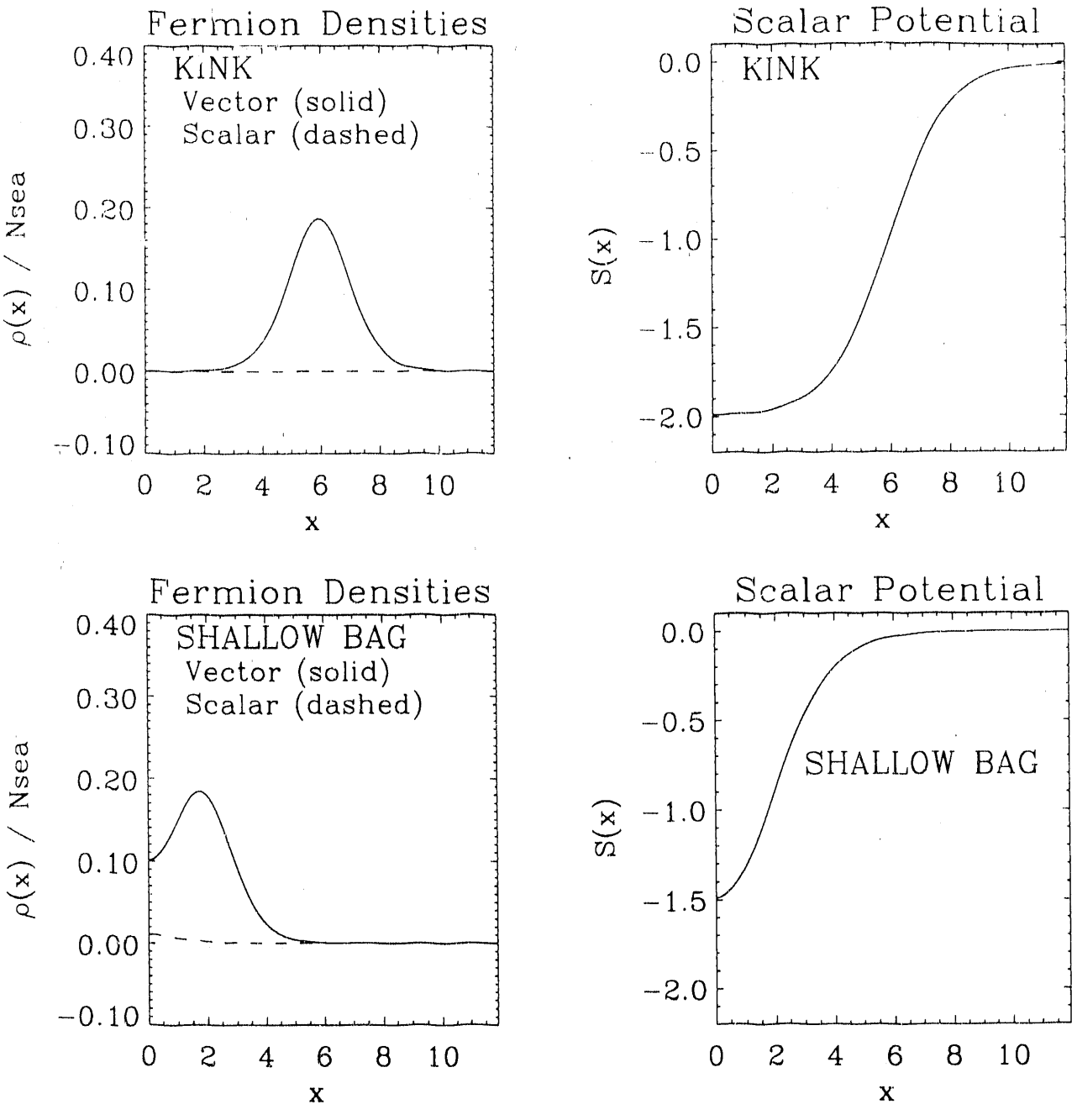

Figure 5. Densities and scalar potentials for shallow bag "baryons" whose properties are presented along with kink counterparts in Table 4. Units are the same as in Figures 1--4 but note that the scales are expanded by a factor of 2 here. The corresponding kink "baryons" appear in Figures 1 and 2. See text for discussion.

3. **Exact Scalar 1-loop Contributions in 1+3 Dimensions** J. R. Shepard, C. E. Price and J. F. Garten

As discussed sections 1 and 2 of this report, we have developed a new method for exactly evaluating 1-loop contributions in relativistic quantum field theories in 1+1 dimensions. Two papers addressing 1-*fermion* loop effects in quantum hadrodynamics (QHD) and in discrete chiral solitons have been prepared and submitted to The Physical Review. Preliminary calculations of 1-*scalar* loop quantities in the discrete chiral model show that our method accurately and efficiently reproduces previously published results, *e.g.*, those of Wasson and Koonin.[1] While these accomplishments are gratifying, they must ultimately be considered as preliminaries to calculations in 1+3 dimensions. In this section, we report our initial efforts at extending our method to 1+3.

Our treatment in 1+1 dimensions depends on scrupulously maintaining consistency between the free basis in which the equations of motion are solved by matrix diagonalization and the counter-term subtractions required for renormalization. By imposing periodic boundary conditions, one naturally arrives at a discretized basis consisting of sines and cosines. One element of such a basis is

$$\varphi(x) = \sqrt{\frac{2}{a}} \cos k_n x, \quad k_n = \frac{2n\pi}{a} \tag{01}$$

where a is the "box length." This basis has a number of desirable features, a crucial one being that it is straightforward to express the *product* of two elements of the basis as the *sum* of single elements. Here, this feature follows from simple trigonometric identities, *e.g.*,

$$\cos k_m x + \cos k_n x = \frac{1}{2}\big[\cos(k_m - k_n)x + \cos(k_m + k_n)x\big]. \tag{02}$$

Extending our method to 1+3 dimensions depends on finding a 3D basis with similar properties. Standard basis choices are not satisfactory in this regard. For example, a spherical Fourier-Bessel basis consists of states of the following form:

$$\varphi_{nLM}(\vec{r}) \propto j_L(k_{nL}\, r)\; Y_{LM}(\theta, \phi) \tag{03}$$

where $k_{nL} = x_{Ln}/R$ and where x_{Ln} is the n-th zero of $j_L(x)$ and R is the radius of a spherical box and is the 3D analogue of the 1D box length. While the *angular* functions in the basis of course satisfy

$$Y^*_{LM}(\Omega)\; Y_{L'M'}(\Omega) = \sum_{\mathcal{L}\mathcal{M}} (LL'00|\mathcal{L}0)(LLMM'|\mathcal{L}\mathcal{M}) \sqrt{\frac{(2L+1)(2L'+1)}{4\pi(2\mathcal{L}+1)}}\, Y_{\mathcal{L}\mathcal{M}}(\Omega), \tag{04}$$

no such relation exists for the $j_L(k_{nL}\, r)$.[2]

To illustrate the philosophy behind our method in 1+3, we briefly consider a method for solving the free wave equation in 1+2 dimensions which employs the Y_{LM}'s referred to above. In 1+2, the time-independent wave equation in cylindrical coordinates is, of course,

$$(\nabla^2 + k^2)\varphi(\rho,\theta) = \left[\frac{1}{\rho}\frac{\partial}{\partial\rho}(\rho\frac{\partial}{\partial\rho}) + \frac{1}{\rho^2}\frac{\partial^2}{\partial\theta^2} + k^2\right]\varphi(\rho,\theta) = 0 \qquad (05)$$

and, via the standard separation of variables, *i.e.*, assuming

$$\varphi(\rho,\theta) \rightarrow P(\rho)\ \Theta(\theta) \rightarrow P(\rho)\ e^{iM\theta},$$

the radial DE is

$$\left[\frac{1}{\rho}\frac{d}{d\rho}(\rho\frac{d}{d\rho}) + (k^2 - \frac{M^2}{\rho^2})\right] P(\rho) = 0 \qquad (06)$$

which has as its regular solution

$$P(\rho) \rightarrow J_M(k\rho). \qquad (07)$$

Let us now reexamine the solution to the free wave equation in 1+3 appearing in Eq. (03). The wave equation in spherical coordinates is

$$\left[\frac{1}{r^2}\frac{\partial}{\partial r^2}(r^2\frac{\partial}{\partial r^2}) + \frac{1}{r^2\sin\theta}\frac{\partial}{\partial\theta}(\sin\theta\frac{\partial}{\partial\theta}) + \frac{1}{r^2\sin^2\theta}\frac{\partial^2}{\partial\phi^2} + k^2\right]\varphi(r,\theta,\phi) = 0 \qquad (08)$$

and separation of variables yields the standard angular DE which can be written as

$$\frac{1}{r^2}\left[\frac{1}{\sin\theta}\frac{d}{d\theta}(\sin\theta\frac{d}{d\theta}) - \frac{M^2}{\sin^2\theta} + k_L^2 r^2\right]\Theta(\theta) = 0 \qquad (09)$$

where we have again assumed the azimuthal dependence has the form $\Phi(\phi) \rightarrow e^{iM\phi}$. Of course, the regular solution is

$$\Theta(\theta) \rightarrow P_L^M(\cos\theta)$$

with $k_L \rightarrow \sqrt{L(L+1)}/r$. We now reexpress the DE in Eq. (09) in terms of $\rho \equiv r\theta$ and furthermore assume $\theta << 1$ or, equivalently, $\rho << r$. The result is

$$\left[\frac{1}{\rho}\frac{d}{d\rho}(\rho\frac{d}{d\rho}) + (k_L^2 - \frac{m^2}{\rho^2})\right]\ \Theta(\rho/r) = 0 \qquad (010)$$

which we have already seen has the solution $J_M(k_L\ \rho)$. Hence, for $\rho << r$,

$$P_L^M[\cos(\rho/r)] \propto J_M\left(\frac{\sqrt{L(L+1)}}{r}\rho\right) \qquad (011)$$

which is known as the Hilb formula[4,3] . The point of this exercise is that, provided we are treating 2D systems *localized near the "north pole" of a sphere of radius r*; i.e., systems

whose radial extent ρ_0 satisfies $\rho_0 << r$, we may assume solutions to the free wave equation are

$$\varphi(\rho,\theta) \propto P_L^M[\cos(\rho/r)]\; e^{iM\theta} \propto Y_{LM}(\rho/r,\theta). \tag{012}$$

Note that the wavenumbers are discrete and are given by $k \rightarrow k_L = \sqrt{L(L+1)}/r$. We may now use the solutions as a basis in which to solve the wave equation by matrix diagonalization when interactions localized near the north pole are present. The advantage of this basis is that Eq. (04) is satisfied while no such relation exists for the $J_M(k\rho)$. In consequence, provided that expansions of the interactions in the basis exist, *e.g.*, for a radially symmetric interaction,

$$V(\rho) = \sum_L V_L\; Y_{L,0}(\rho/r), \tag{013}$$

all matrix elements required for diagonalization may be *exactly* evaluated *analytically*. Furthermore, expansion coefficients of *powers* of V may also be found analytically in terms of the original coefficients, the V_L's. Beyond this, if self-consistent solutions are sought, the expansion coefficients of any densities bilinear in the basis states can also be evaluated analytically. These features are all crucial to our method for numerical renormalization.

The method of extension to problems in 1+3 dimensions is now apparent. We first find solutions to the free wave equation in spherical coordinates in 1+4 dimensions. We then define a hypersphere of fixed radius R in 1+4 and, using methods analogous to those presented above, show that, near the "north pole" of the hypersphere, the angular functions of our free solution approach the standard 3D solution given in Eq. (03). These new solutions will presumably satisfy relations similar to that given in Eq. (04) for the Y_{LM}'s and thus will be suitable for numerical renormalization in 3 spatial dimensions. We now sketch a derivation of the required solutions beginning with the free wave equation:

$$\left\{ \frac{1}{R^3}\frac{\partial}{\partial R}\left(R^3\frac{\partial}{\partial R}\right) + \frac{1}{R^2\sin^2\theta_1}\frac{\partial}{\partial\theta_1}\left(\sin^2\theta_1\frac{\partial}{\partial\theta_1}\right) + \frac{1}{R^2\sin^2\theta_1}\left[\frac{1}{\sin\theta_2}\frac{\partial}{\partial\theta_2}\left(\sin\theta_2\frac{\partial}{\partial\theta_2}\right) + \frac{1}{\sin^2\theta_2}\frac{\partial^2}{\partial\phi^2}\right] + k^2 \right\}\varphi(R,\theta_1,\theta_2,\phi) = 0 \tag{014}$$

The desired solution is

$$\varphi(R,\theta_1,\theta_2,\phi) \rightarrow \varphi_{NLM}(R,\theta_1,\theta_2,\phi) \;\propto\; \frac{J_{N+1}(kR)}{kR}\; T_{NL}(\cos\theta_1)\; Y_{LM}(\theta_2,\phi) \tag{015}$$

where the T_{NL} are related to the ultraspherical or Gegenbauer polynomials[3] and satisfy

$$\left[(1-x^2)\frac{d^2}{dx^2} - 3x\frac{d}{dx} + N(N+2) - \frac{L(L+1)}{1-x^2}\right]\; T_{NL}(x) = 0 \tag{016}$$

and require $L \leq N$. On the hypersphere and for $r \equiv R\,\theta_1 << R$, approximate solutions

to the free wave equation in 1+3 are given by

$$\begin{aligned}\varphi(r,\theta_2,\phi) \to \varphi_{NLM}(r,\theta_2,\phi) &\simeq T_{NL}(\cos r/R)\; Y_{LM}(\theta_2,\phi) \\ &\simeq j_L(k_N R) Y_{LM}(\theta_2,\phi)\end{aligned} \tag{017}$$

with

$$k \to k_N = \frac{\sqrt{N(N+2)}}{R}. \tag{018}$$

A valuable discussion of the T_{NL} is given by Bander and Itzykson[5] and beginning with the representation of T_{NL} appearing immediately after their Eq. A7, it is straightforward to derive

$$T^*_{NL}(x)\; T_{N'L'}(x) \propto \sum_{\mathcal{J}=|J-J'|}^{J+J'} (-)^{J+J'+L+\mathcal{J}} \sqrt{(2J+1)(2J'+1)} \begin{Bmatrix} J & J & L \\ J' & J' & \mathcal{J} \end{Bmatrix} T_{\mathcal{N},0}(x) \tag{019}$$

where $\begin{Bmatrix} J & J & L \\ J' & J' & \mathcal{J} \end{Bmatrix}$ is the usual six-j symbol and where $2J = N, 2J' = N', 2\mathcal{J} = \mathcal{N}$ and where the proportionality factor depends on details of the normalization of the T_{NL}. Eq. (019) is the desired analogue to Eqs. (02) and (04) and again ensures exact analytic expressions for matrix elements, etc.

Our first application of the 1+3 method just outlined is to a scalar-only field theory with the following Lagrangian:

$$\mathcal{L} = \frac{1}{2}\partial\phi \cdot \partial\phi \; - \; U(\phi) + g\rho\phi \tag{020}$$

where $U(\phi) = \frac{\lambda}{4}(\phi^2 - f^2)^2$ and where ρ is a fixed external source. Upon decomposing the scalar field according to $\phi = \phi_0 + \sigma$ and expanding in powers of σ, the Lagrangian becomes

$$\begin{aligned}\mathcal{L} =& \frac{1}{2}\partial\phi_0 \cdot \partial\phi_0 - U(\phi_0) + g\rho\phi_0 \\ &+ \partial\phi_0 \cdot \partial\sigma - U'(\phi_0)\sigma \\ &+ \frac{1}{2}[\partial\sigma \cdot \partial\sigma - U''(\phi_0)\sigma^2] \\ &- \frac{1}{3!}U'''(\phi_0)\sigma^3 - \frac{1}{4!}U''''(\phi_0)\sigma^4.\end{aligned} \tag{021}$$

Assuming ϕ_0 satisfies

$$\Box\,\phi_0 + U'(\phi_0) = g\rho, \tag{022}$$

terms linear in σ vanish. The loop expansion through 1-loop order is found by dropping terms of order σ^3 and σ^4. Further assuming ϕ_0 to be static, the energy of the system is,

to this order,

$$E = E_0 + E_{loop}$$

where

$$E_0 = \int d^3r \left[\frac{1}{2}\left(\vec{\nabla}\phi_0(\vec{r})\right)^2 + U\left(\phi_0(\vec{r})\right) - g\rho(\vec{r})\phi_0(\vec{r})\right] \tag{023}$$

and

$$E_{loop} = \frac{1}{2}\sum_n E_n \tag{024}$$

where E_n is the eigenenergy of the n-th mode, $\sigma_n(\vec{r})$, satisfying

$$\left[-\nabla^2 + U''\left(\phi_0(\vec{r})\right)\right]\sigma_n(\vec{r}) = E_n^2\ \sigma_n(\vec{r}). \tag{025}$$

Of course E_{loop} is divergent and must be renormalized. In the present calculations, we make an initial guess for $\phi_0(\vec{r})$, namely

$$\phi_0(\vec{r}) = f\ \tanh\left[\sqrt{\frac{\lambda}{2}} f\ (r - r_0)\right] \tag{026}$$

which, in 1+1, would be the "kink solution" for the classical field (See Section 2 of this report.) Note that the external source, $\rho(\vec{r})$, is required in 1+3 to sustain the kink solution since it is not stable by itself. The kink is then expanded via

$$\phi_0(\vec{r}) \rightarrow \phi_0(r) = \sum_{N=0}^{N_{max}} \phi_N\ T_{N,0}(\cos r/R) \tag{027}$$

and, with a similar expansion for the external source which is also assumed to be a function of r only, the equation of motion for $\phi_0(r)$, Eq. (022), may readily be solved by iteration (specifically, one solves separately for each of the expansion coefficients, ϕ_N). Using Eq. (019) then allows expansion coefficients of $U''\left(\phi_0(\vec{r})\right)$ to be found analytically. Expressing the mode eigenfunctions in terms of the basis states, *i.e.*,

$$\begin{aligned}\sigma_n(\vec{r}) \rightarrow & \sigma_{nLM}(r, \theta_2, \phi) \rightarrow \sigma_{nLM}(R\theta_1, \theta_2, \phi) \\ & = \sum_{N=L}^{N_{max}} a_{NL}^{(n)}\ T_{NL}(\cos\theta_1)\ Y_{LM}(\theta_2, \phi),\end{aligned} \tag{028}$$

the corresponding equation of motion, Eq. (025), is easily solved by matrix diagonalization since the required matrix elements, namely

$$< T_{NL}\ Y_{LM} | U''\left(\phi_0(r)\right) | T_{N'L'}\ Y_{L'M'} > \tag{029}$$

can again be evaluated analytically using Eq. (019). The counter-term subtractions required to renormalize E_{loop} are simple to determine using procedures analogous to those

employed in 1+1 (See Section 2). The renormalized 1-loop energy is, upon choosing the uniform $\rho = 0$ vacuum with $\phi_0^2 = f^2$ as the renormalization point,

$$E_{loop} = \sum_{L=0}^{N_{max}} \sum_{N=L}^{N_{max}} (2L+1) \left[E_N - (E_N^{(0)} + \frac{1}{2E_N^{(0)}} V_0^{(1)} - \frac{1}{8E_N^{(0)}} V_0^{(2)} + \Delta E_{N,D}^{(0)}) \right] \tag{030}$$

where $E_N^{(0)} = \sqrt{N(N+2)/R^2 + 2\lambda f^2}$ and where, with $V(r) \equiv U''(\phi_0(r)) - 2\lambda f^2$, expansions of powers of V are defined via

$$V^n(r) = \sum_{N=0}^{N_{max}} V_N^{(n)} \, T_{N,0}(\cos r/R). \tag{031}$$

Finally, $\Delta E_{N,D}^{(0)}$ is a derivative counter-term contribution of a somewhat complicated form.

We now present a sample calculation assuming $f = -93$ MeV, $\lambda = g = 20$ and where the external source is

$$\rho(r) = \rho_0 \, e^{-(r-r_0)^2/2r_1^2} \tag{032}$$

and is normalized so that its integral over the hypersphere is 4π. We have chosen $r_0 = 1$ fm and $r_1 = 0.2$ fm while the radius of the hypersphere is $R = 20/2\pi$ fm $\simeq 3.18$ fm. The basis size is determined by $N_{max} = 60$. We then find the total energy of the configuration to be 964.5 MeV consisting of 2273.9 MeV from ϕ_0, -1304.3 MeV from the interaction term, $g\rho\phi_0$, and $E_{loop} = -5.25$ MeV. We note that the *unrenormalized* loop energy of Eq. (024) is 8.33×10^6 MeV implying that, after counter-term subtractions, only about 1 part in 1,500,000 of the unrenormalized loop energy survives. The stability of the loop energy against changes in basis size (N_{max}) and hypersphere radius (R) which we observe demonstrates that numerical convergence has been achieved.

We are in the process of finding *self-consistent* 1-scalar loop kink-like solutions. By applying standard path integral techniques[6] generalized to account for the non-uniformity of the system, equations of motion for ϕ_0 and for the modes, σ_n, which are self-consistent through 1-loop in the loop expansion are readily obtained. Preliminary results indicate that it is very difficult to find stable solutions in this approximation and we intend to examine alternative expansion schemes, including for example those of Refs. 7 and 8. Of course, we also plan to incorporate the new method of solution of the Dirac equation in 1+3 as outlined in Section 4 of this report so as to find self-consistent solutions for, *e.g.*, chiral models including *both* meson and fermion 1-loop contributions.

1. D.A.Wasson and S.Koonin, Phys.Rev.**D43**,3400 (1991)
2. G.N.Watson, Theory of Bessel Functions, Cambridge University Press, 1962.
3. M.Abramowitz and I.A.Stegun, Handbook of Mathematical Functions, National Bureau of Standards Applied Mathematics Series • 55 (1964)
4. E.Hilb,Math.Z.**5**,17 (1919)
5. M.Bander and C.Itzykson, Rev.Mod.Phys.**38**,330 (1966)
6. see, *e.g.*, B.D.Serot and J.D.Walecka, Adv. in Nucl.Phys., J.W.Negele and E.Vogt,eds., Plenum, N.Y.,1986,Vol. 8
7. T.D.Lee and M.Margulies, Phys.Rev.**D11**,1591 (1975)
8. K.Tanaka and W.Bentz, Nucl.Phys.**A540**,383 (1992)

4. **Exact Vacuum Calculations in a Hyper-Spherical Basis** C. E. Price, J.R. Shepard and J. F. Garten

As reported in Section ???, we have successfully developed an efficient numerical procedure for exactly renormalizing one-loop vacuum contributions to the ground states of finite nuclei in a version of QHD for one spatial dimension. As is well-known, extension of one-dimensional techniques to three spatial dimensions is highly non-trivial. In the present case, for example, the crucial "completeness" relation exploited in one dimension which emerges because the free basis consists of sines and cosines cannot be readily duplicated in three dimensions using the usual free basis constructed from spherical Bessel functions (and the relativistic spin-angle functions).

In order to find an appropriate basis in three dimensions we have examined solutions to the Dirac equation in *four* Euclidean dimensions. The fundamental idea behind this approach is that the angular (3 angles) part of this basis should possess the required completeness properties and should be a reasonable approximation to the desired three-D solutions in the vicinity of the "north pole" of the four dimensional hypersphere.

The first step in determining the basis is to specify the representation of the gamma matrices in four dimensions. We have chosen to use a four by four representation that preserves the usual description of the spin:

$$\gamma_0 = \begin{pmatrix} 1 & 0 \\ 0 & -1 \end{pmatrix} \qquad \vec{\gamma} = \begin{pmatrix} 0 & \vec{\sigma} \\ -\vec{\sigma} & 0 \end{pmatrix} \qquad \gamma_4 = \begin{pmatrix} 0 & \imath \\ \imath & 0 \end{pmatrix}$$

where γ_4 is the new matrix corresponding to the additional spatial dimension. The dirac equation now takes the form:

$$(\gamma_0 E - M + \imath\vec{\gamma}\cdot\vec{\nabla} - \nabla_4)\psi(\vec{r}_4) = 0$$

where $\vec{\nabla}$ and ∇_4 are the components of the gradient in four dimensions. Then writing the Dirac spinor ψ in terms of upper (G) and lower (F) components leads to:

$$\Big[E^2 - M^2 + \frac{1}{{r_4}^3}\frac{\partial}{\partial r_4}{r_4}^3\frac{\partial}{\partial r_4} + \frac{1}{{r_4}^2\sin^2\rho}\frac{\partial}{\partial\rho}\sin^2\rho\frac{\partial}{\partial\rho} + \frac{1}{{r_4}^2\sin^2\rho\sin\theta}\frac{\partial}{\partial\theta}\sin\theta\frac{\partial}{\partial\theta} + \frac{1}{{r_4}^2\sin^2\rho\sin^2\theta}\frac{\partial}{\partial\phi}\frac{\partial}{\partial\phi}\Big]G(\vec{r}_4) = 0 \tag{01}$$

with

$$F(\vec{r}_4) = \frac{1}{E+M}[-\imath\vec{\gamma}\cdot\vec{\nabla} - \nabla_4]G(\vec{r}_4).$$

It is simple to show that in the limit $r_4 \to R$ (where R is a constant) these equations reduce to the usual three dimensional equation in the region where $\sin\rho \approx \rho$.

The solutions to equation (01) on the hypersphere are of the form:

$$G(\rho,\Omega) \propto \frac{1}{R} T_{nl}(\rho)\Phi_{jlm}(\Omega)$$

where the T_{nl} are hyper-spherical polynomials[1] and the Φ_{jlm} are the usual spin-angle functions[2] and $E^2 = (n+1)^2/R^2 + M^2$. Notice that the lower components will not have a definite parity but will involve some mixture of spin-angle functions of both parities. Since we are ultimately interested in the behavior of these solution near the pole, we choose a linear combination of degenerate solutions to equation (01) which approximates the usual three dimensional solutions in the vicinity of the pole. One such choice is:

$$G_{\pm}(\rho,\Omega) = \sqrt{\frac{E+M}{2E\pi R^3}}\left[\left(\sqrt{\frac{n+l+2}{n+1}}T_{n,l} \pm \sqrt{\frac{n-l+1}{n+2}}T_{n+1,l}\right)\Phi_{jlm} - \imath\left(\sqrt{\frac{n-l}{n+1}}T_{n,l'} \mp \sqrt{\frac{n+l+3}{n+2}}T_{n+1,l'}\right)\Phi_{jl'm}\right]$$

$$F_{\pm}(\rho,\Omega) = \sqrt{\frac{E-M}{2E\pi R^3}}\left[\left(\sqrt{\frac{n-l+1}{n+2}}T_{n+1,l} \mp \sqrt{\frac{n+l+2}{n+1}}T_{n,l}\right)\Phi_{jlm} - \imath\left(\sqrt{\frac{n+l+3}{n+2}}T_{n+1,l'} \pm \sqrt{\frac{n-l}{n+1}}T_{n,l'}\right)\Phi_{jl'm}\right]$$

where the $\pm$ subscript differentiates between states with $l = j \pm 1/2$ ($l' = j \mp 1/2$) near the pole.

In addition to preserving the correct three dimensional behavior near the north pole of the hypersphere, this free basis has several remarkable properties (which can be traced directly to the properties of ultra-spherical polynomials and spherical harmonics). First, both the baryon and scalar densities that arise from this basis are uniform when all degenerate eigenstates are included (this implies summing over l and m at fixed n). This allows for the sort of simple treatment of nuclear matter that is common in plane wave bases but very difficult in any other spherical basis, and allows for a natural energy cutoff (which amounts to a cutoff in the quantum number n) for the vacuum contributions. Secondly, by expanding any required potentials in the form:

$$V(\rho) = \sum_n V_n T_{n,0}(\rho)$$

it is simple to show that this basis is closed. By this we mean that the product of the potential and any state in the basis can be uniquely analytically expanded it terms of other elements of the basis. These two properties do not exist for a standard three dimensional basis using Bessel functions, and greatly simplify the calculation of vacuum polarization effects.

We have successfully demonstrated that this basis can be used to reproduce the usual mean field results for finite nuclei provided the radius of the hypersphere is large enough so that all of the physics (the entire nucleus) takes place in the region near the north pole where $\sin\rho \approx \rho$. Calculations including an exactly renormalized vacuum (that makes no use of the local density approximation or the derivative expansion) are in progress.

1. M. Bander and C. Itzykson, Rev. Mod. Phys. **38** 330 (1966)
2. J. D. Bjorken and S. D. Drell, *Relativistic Quantum Mechanics* (McGraw-Hill, New York)

5. Relativistic Nuclear Matter with Self-Consistent Correlation Energy C. E. Price, J. R. Shepard and J. A. McNeil (Colorado School of Mines)

One of the more appealing features of QHD is its elegant saturation mechanism, namely the relativistic quenching of the scalar attraction at high densities. However, attempts to include vacuum effects beyond the Hartree (one-loop) level have proved difficult. The loop expansion appears not to converge as the self-consistent 2-loop solutions are radically different from their one-loop cousins (even in terms of the physics of saturation).[1] In a preliminary effort to examine alternative organization schemes we have calculated the correlation energy in the ring sum approximation based on the mean field (no-vacuum) basis. Using mean field parameters we confirm the earlier calculation by Ji[2] which showed a large correlation energy, -33 MeV per nucleon. Thus, the correlation energy is large compared to the mean field energy and may not be treated as a perturbation. In this work we include the correlation energy self-consistently in fixing the model parameters, and compare to the standard mean field results.

The role of the vacuum in relativistic nuclear models based on meson-nucleon degrees of freedom is controversial.[3] We know that nucleons have substructure on the scale of ~ 1 GeV. For QHD-I at the one-loop level energy scales beyond this are significant, but do not dominate the physics at least as regards the saturation mechanism and the low energy phenomenology. The relativistic Hartree results are qualitatively the same and quantitatively similar to the mean field results. Beyond one-loop the high energy sector completely dominates the physics in an uncontrolled manner. Prakash, et al.[4] argue that the subnucleon structure implies a cutoff on scales of 1 GeV. They calculated the two-loop contributions including vertex cutoffs on this scale and found that the two-loop terms were small. To mimic the softening of the vertices in the ring energy due to the onset of subnucleonic degrees of freedom which are beyond the scope of the present model, we have calculated the vacuum polarized correlation energy using renormalized vacuum polarizations with vertices regularized by vertex form-factors. In this way we retain the "low-lying" effects of the vacuum. The price we pay is that the results are quantitatively sensitive to the choice of cutoff parameter in the vertex form factor. Nevertheless, we know that the scale of such effects is about 1 GeV, and we find that the qualitative features of the results are similar for any cut-off on this scale. Using this regularization scheme, we self-consistently fit the model parameters including the correlation energy.

Starting from the QHD-I Lagrangian, we focus our attention on the ring-sum polarization energy density given by

$$\mathcal{E}_{ring}(k_F, M^*) = -\frac{i}{2}\int \frac{d^4q}{(2\pi)^4}\{\mathrm{Tr}(D\Pi_0) + \ln[\det(1 - D\Pi_0)]\}$$

where Π_0 is the mixed scalar-vector polarization insertion which can be represented by a 3x3 scalar-vector matrix and a 2x2 (diagonal) transverse vector matrix:[5]

$$\Pi_{sv} = \begin{pmatrix} q^2\Pi_l & wq\Pi_l & \Pi_m \\ -wq\Pi_l & -w^2\Pi_l & -w/q\Pi_m \\ \Pi_m & w/q\Pi_m & \Pi_s \end{pmatrix}$$

$$\Pi_{trans} = \begin{pmatrix} \Pi_T & 0 \\ 0 & \Pi_T \end{pmatrix}$$

where the 4-momentum transfer is $q^\mu = (\omega, \vec{q})$. Kurasawa and Suzuki's[6] analytic forms for the various polarizations greatly reduce the computing time.

The analytic structure of the integrand allows a Wick rotation. Defining $\omega = iq_0$, we have

$$q_\mu^2 = \omega^2 - q^2 = -(q_0^2 + q^2) = -q_E^2$$

where q_E is the Euclidean 4-momentum. The integrals then become

$$\mathcal{E}_{ring}(k_F, M^*) = \frac{1}{(2\pi)^3} \int_0^\infty dq_E q_E^3 \int_0^{2\pi} d\theta_E \cos^2(\theta_E)\{Tr(D\Pi_0) + \ln[\det(1 - D\Pi_0)]\}$$

where $q_0 = q_E \sin(\theta_E), q = q_E \cos(\theta_E)$. The remaining two integrals are performed numerically. For mean field parameters we find convergence at an upper limit for $q_E \sim 10k_F$. Using the mean field parameters given in Table I, we find a large ring energy of -33 MeV per nucleon as did Ji.[2] It is therefore clear that within this model the ring-sum correlation energy is not a small effect being twice the magnitude of the MFT binding energy.

Model	g_s^2	g_v^2	M^*/M	κ (MeV)	E_{ring}(MeV)	Λ (GeV)
MFT(w/o fit)	109	189	.54	450	-33	–
MFT(w/ fit)	43.1	100.3	.853	178	-46	–
RHA-1	48.9	75.9	.839	298	-1.93	1.0
RHA-2	48.9	80.7	.835	313	-6.98	2.0

Table I. Parameters for relativistic nuclear matter fit to saturation density (k_F=1.42 fm^{-1}) and binding energy per nucleon (-15.75 MeV). The meson masses were fixed at m_v=783 MeV and m_s=500 MeV.

We sought to include the ring-sum correlation energy in the total nuclear matter energy density and refit the coupling parameters to saturation density and binding energy per nucleon (with meson masses fixed at $m_v = 783$ MeV and $m_s = 500$ MeV). The total energy density is given by

$$\mathcal{E} = \mathcal{E}_{mesons} + \mathcal{E}_F + \mathcal{E}_{ring} + \mathcal{E}_{vac}$$

where

$$\mathcal{E}_F = \frac{\gamma}{16\pi^2}[2k_F E_F^3 - M^{*2} k_F E_F - M^{*4} \ln(\frac{k_F + E_F}{M^*})],$$

$$\mathcal{E}_{mesons} = \frac{1}{2}\frac{g_v^2}{m_v^2}\rho_B^2 + \frac{1}{2}\frac{g_s^2}{m_s^2}\rho_s^2,$$

$$\mathcal{E}_{vac} = -\frac{\gamma}{16\pi^2}[M^{*4}\ln(\frac{M^*}{M}) - \frac{25}{12}M^{*4} + 4M^{*3}M - 3M^{*2}M^2 + \frac{4}{3}M^*M^3 - \frac{1}{4}M^4].$$

We fix the saturation density appropriate to $k_F = 1.42$ fm^{-1}. The saturation condition is

$$\left.\frac{\partial\mathcal{E}}{\partial k_F}\right|_{k_f=1.42fm^{-1}} = 0.$$

At each step of the fitting procedure the self-consistency condition,

$$M^* = M - \frac{g_s^2}{m_s^2}\rho_s,$$

is maintained.

The scalar density in turn can be found from the energy density through the minimization condition,

$$\left.\frac{\partial\mathcal{E}}{\partial M^*}\right|_{k_f=1.42fm^{-1}} = 0,$$

which gives

$$\rho_s = \frac{\partial(\mathcal{E}_F + \mathcal{E}_{vac} + \mathcal{E}_{ring})}{\partial M^*}.$$

As usual the Fermi sea contribution to the scalar density is

$${\rho_s}^F = \frac{\partial\mathcal{E}_F}{\partial M^*} = \frac{\gamma}{4\pi^2}M^*[k_F E_F - M^*\ln(\frac{k_F + E_F}{M^*})]$$

and the ring contribution is calculated numerically.

The coupling constants were varied until a self-consistent solution was obtained. Once the coupling parameters were found, the equation of state was generated by finding the self-consistent total energy at various values of k_F near the saturation value keeping the coupling parameters fixed. Three models were considered: the mean field model and the relativistic Hartree model with vertex cutoffs of 1 GeV and 2 GeV. The resulting coupling constants and bulk properties are given in Table I.

The resulting equation of state for the mean field model is shown in Fig. 1. We found a compressibility of 179 MeV which is significantly smaller than the standard MFT result of around 400 - 500 MeV, and is near the values derived from analyses of the breathing modes of heavy nuclei. Also shown in Fig. 1 are the separate contributions from the MFT-terms and the correlation energy. We see that the saturation curve is a sensitive cancellation of the large repulsive MFT terms with the large attractive ring-sum energy. (At the saturation point the ring energy is -46 MeV !). The saturation mechanism is therefore quite different than the usual one of relativistic quenching of the scalar attraction with higher density. Here the attractive ring energy dominates at moderate densities with the repulsive vector-MFT term dominating at high densities. It is an open question whether this saturation mechanism is realistic in that it is consistent with other low energy finite nuclear phenomenology. Given the relatively large value of the M^*/M one suspects that the spin-orbit splitting in finite nuclei will be too small. This issue will be explored in subsequent work.

The corresponding ring-sum energy when the vacuum is included is divergent even when the polarizations themselves have been renormalized. Since the theory is renormalizable, the new divergences may be rendered finite; however this prescription is not realistic in that the high energy sector of QHD does not incorporate the physically correct internal nucleon degrees of freedom. There are other ways of moderating the high energy sector within QHD. We have crudely incorporated the internal nucleon degrees of freedom using a vertex form-factor of the standard dipole form:

$$f(q_\mu^2, \Lambda) = \frac{1}{(1 + q_\mu^2/\Lambda^2)^2}$$

where Λ is chosen to be of the order of 1 GeV. Over this scale ($1 \rightarrow 2$ GeV) the results are quantitatively sensitive to Λ.

In Fig. 2 we show the equation of state for $\Lambda = 1$ GeV and in Fig. 3 the corresponding curve for $\Lambda = 2$ GeV. For $\Lambda = 1$ GeV the standard relativistic Hartree energy dominates. At the saturation density the ring energy is just -1.93 MeV per nucleon. The self-consistent coupling parameters are given in Table I. The compressibility is 298 MeV which is significantly smaller than the usual RHA result of around 450 MeV. However, as in the previous MFT case the ratio, M^*/M, is 0.839 which is larger than the usual RHA result and will probably imply a spin-orbit splitting in finite nuclei which is too small. While these quantitative values are not meaningful due to their sensitivity to the cutoff, we find that the fundamental saturation mechanism of the underlying RHA is preserved and the correlation energy is a relatively small correction comparable to that found in non-relativistic nuclear structure models. For $\Lambda = 2$ GeV the correlation energy is naturally larger. At saturation density the ring energy is -6.98 MeV. The coupling parameters for this case are also found in Table I. The compressibility is 313 MeV while the ratio M^*/M is 0.835. Thus we see that these bulk quantities are relatively insensitive to the cutoff in the region of 1-2 GeV. Comparing Figures 2 and 3 one can see the trend in the increasing importance of the ring energy as Λ is increased. The attraction from the σ meson plays a smaller role as the correlation energy begins to dominate the energy in the equation of state near saturation.

We have also solved (but not shown) the self-consistent relativistic Hartree model for a sigma mass of 600 MeV. We found that the qualitative features remain similar, but that the compressibility increases dramatically to around 450-600 MeV while the M^*/M-ratio drops to around 0.72. The higher compressibility results from a more rapid change in

the ring energy with respect to k_F near the saturation point for this value of the sigma mass as compared to the previous case. The smaller M^*/M should give about the correct spin-orbit splitting in finite nuclei. There appears to be a correlation between the larger compressibility and the smaller M^*/M. This correlation was shown in previous work by Furnstahl, Price, and Walker[7] in the context of non-linear QHD models, and may be a universal feature of non-linear self-consistent relativistic models of nuclear matter.

The lesson learned from this study is that relativistic nuclear models, such as QHD, based only on hadronic degrees of freedom are capable of realizing a credible (i.e. successful and convergent) phenomenology if the high energy sector is moderated at scales beyond 1-2 GeV. It remains for quark-nucleon models to provide a quantitative understanding of the nature and scale of such modifications. However, given the phenomenological nucleon form factors, one would expect any successful quark model of nucleons to result in effective vertex form factors with cutoffs on the scale of 1 GeV where, as we have shown here, models based on meson-nucleon degrees of freedom preserve the simple relativistic saturation mechanism when ring energy contributions are included. It remains to investigate whether other low energy phenomena can be consistently described in this extended model.

1. R. J. Furnstahl, R. J. Perry, B. D. Serot, Phys. Rev. **106** 372 (1989)
2. X. Ji, Caltech preprint (unpublished)
3. T. Cohen, in Workshop Proceedings: From Fundamental Fields to Nuclear Phenomena, p. 18, eds. J. A. McNeil and C. E. Price, World Scientific, Singapore (1991)
4. T. D. Cohen, Phys. Rev. Lett. **62** 3027 (1989)
5. S. A. Chin, Ann. of Phys. (N.Y.)**108** 301 (1977)
6. Kurasawa and Suzuki, Nucl. Phys. **B122** 219 (1988)
7. R. J. Furnstahl, C. E. Price and G. E. Walker, Phys. Rev. **C36** 2590 (1987)

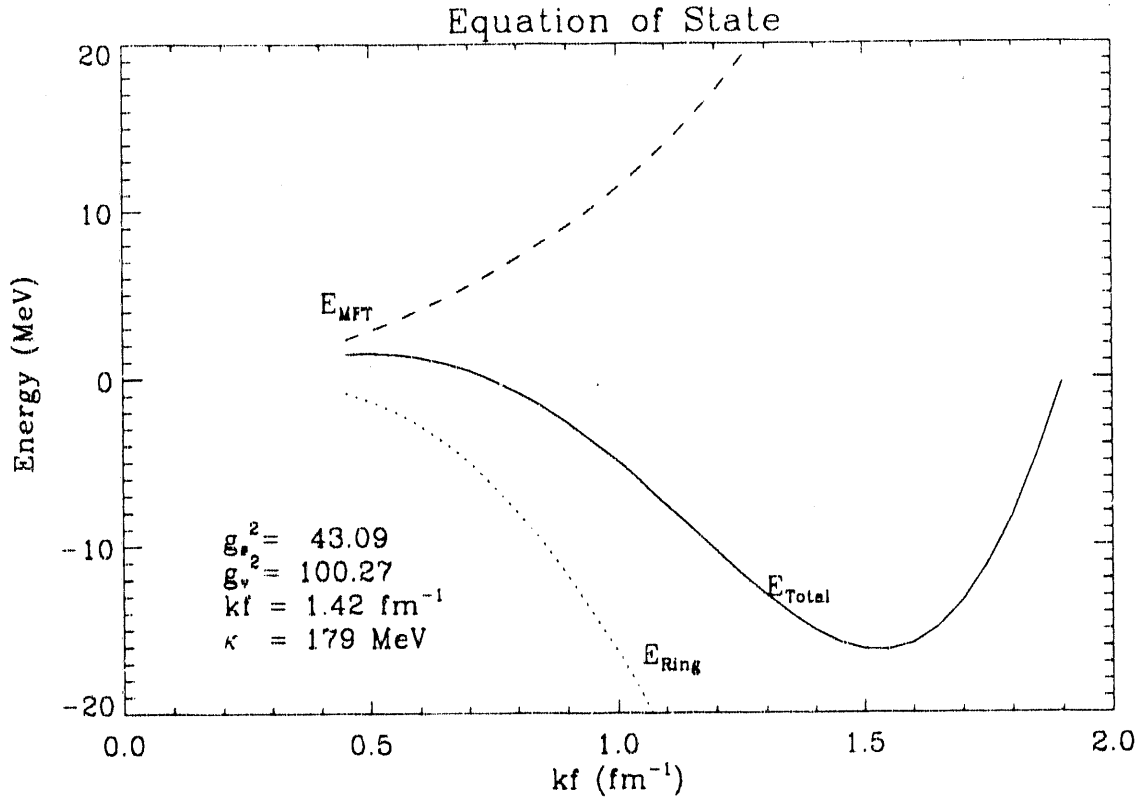

Fig. 1. Equation of state for mean field theory with ring-sum correlations.

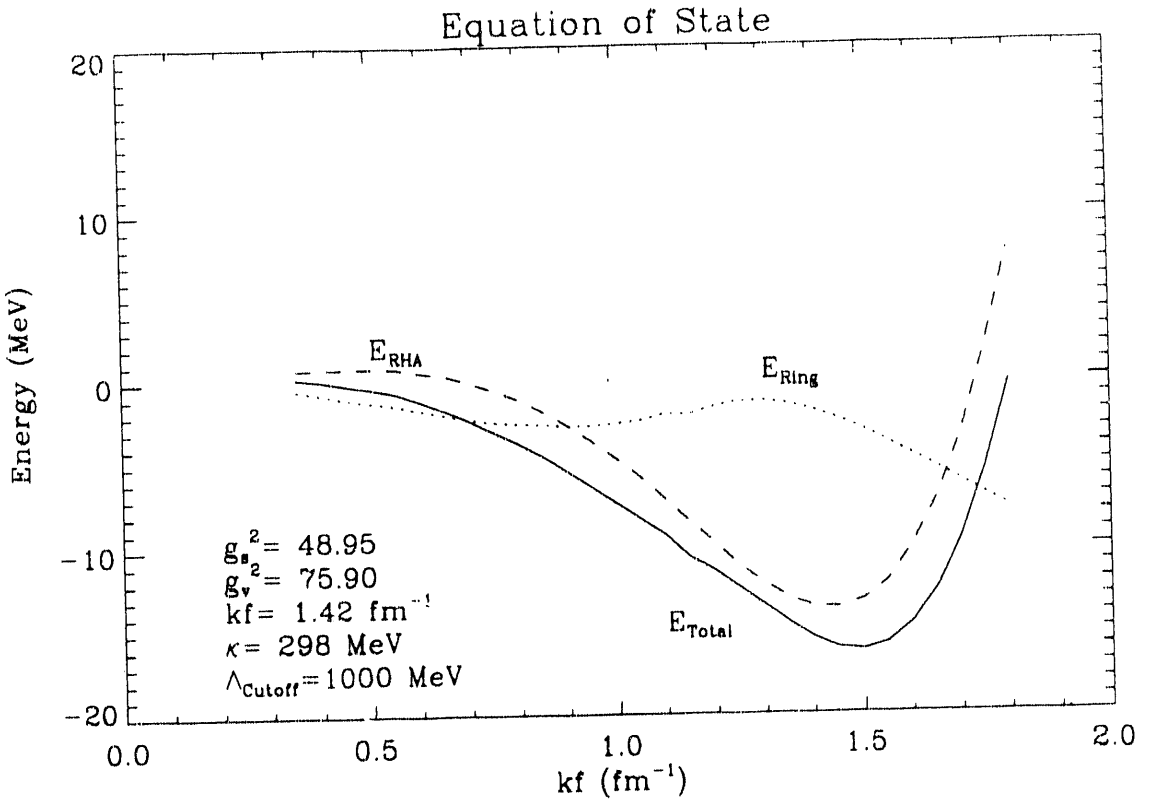

Fig. 2. Equation of state for relativistic Hartree theory with ring-sum correlations with vertex cutoff of 1 GeV.

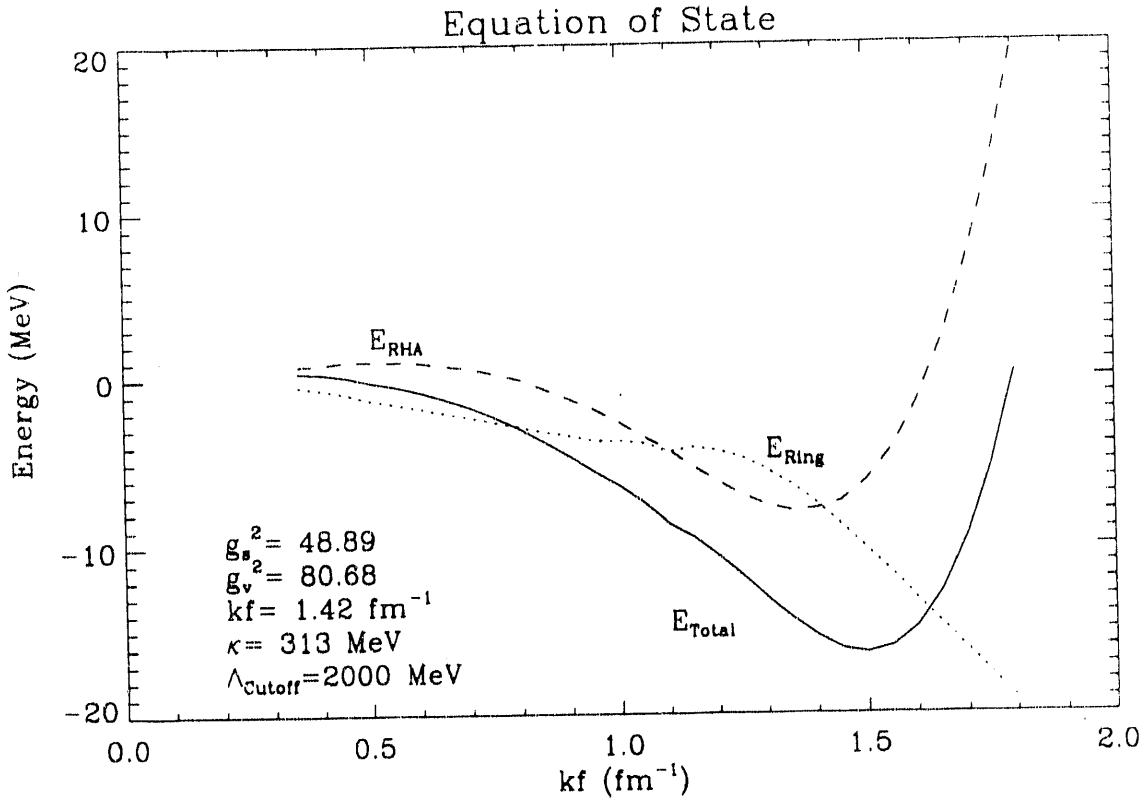

Fig. 3. Equation of state for relativistic Hartree theory with ring-sum correlations with vertex cutoff of 2 GeV.

6. Consistent RHA-RPA for Finite Nuclei C. E. Price, E. Rost, J. R. Shepard and J. A. McNeil (Colorado School of Mines)

We have formulated a consistent RPA based on the relativistic Hartree approximation (RHA) to finite nuclear ground states.[1] In the standard approach, degrees of freedom associated with the negative energy Dirac sea of nucleons are described via the derivative expansion of the 1-loop effective action. A consistent RPA is obtained by expanding the vacuum-dressed σ- and ω-propagators and retaining only those terms also found in the derivative expansion used for the RHA.

We have also examined the influence of 3-momentum cutoffs (or "sideways form-factors") in the Dirac sea on our RHA-RPA calculations. We view such cutoffs as a crude way of suppressing contributions involving small length scales where the finite size of the nucleon almost certainly implies such contributions are unphysical. We find that, when QHD parameters are adjusted to reproduce the saturation point of nuclear matter, the strength of the resulting spin orbit potential for finite nuclei depends strongly on the cutoff momentum. Specifically, a cutoff of *zero* - implying no vacuum contributions – yields the strongest spin orbit interaction while an infinite cutoff corresponding to the standard RHA gives the weakest. A physically plausible 3-momentum cutoff equaling $2M_{proton}$ provides a good description of, *e.g.*, the $0d_{5/2}$ versus $0d_{3/2}$ splitting in ^{40}Ca.

Our RPA results show the importance of the consistency mentioned above. For example, the calculated (e,e') Coulomb form factors for the lowest 3^- levels in ^{16}O and ^{40}Ca display the high degree of collectivity seen in the data only in the consistent calculations. Using a simple local density approximation in the RHA ground state and the full σ- and ω-propagators in the RPA diminish the peak values of the form factors by at least a factor of two.

For the quasielastic (e,e') Coulomb response, consistency *per se* is not so important as it is for the low-lying collective excitations. However, as also noted by, *e.g.*, Horowitz and Piekarewicz,[2] inclusion of vacuum contributions appreciably improves the agreement between theory and experiment for ^{12}C and ^{40}Ca at $\mid \vec{q} \mid$=400 and 550 MeV/c.

1. C. E. Price, E. Rost, J. R. Shepard and J. A. McNeil, Phys. Rev. **C45** 1[illegible] (1992); J. R. Shepard in "From Fundamental Fields to Nuclear Phenome[illegible], C. E. Price and J. A. McNeil, eds., (World Scientific, Singapore) 1991, pp. 190-211
2. C. J. Horowitz and J. Piekarewicz, Nucl. Phys. **A511** 461 (1990)

7. Transverse Response Functions in the Δ-Resonance Region, E. Rost, C. E. Price and J. R. Shepard

In recent years several measurements[1-3] of separated (e,e′) response functions, S_L and S_T, have been performed at high momentum transfer ($|\mathbf{q}| \gtrsim 400$ MeV/c). The longitudinal response function, S_L, has been useful in studying nuclear properties such as the Coulomb sum rule[4], RPA correlations[5] and vacuum fluctuation[6] effects. Nuclear many-body theories agree with the data at the $\sim 20\%$ level and the study of various effects via comparison with experiment is meaningful. On the other hand the measured transverse response functions, S_T, increase at large excitation energies while nucleon-only theories yield decreasing transverse response with energy. It has long been suspected that this effect is a result of Δ excitation (see *e.g.* Ref 7). We have calculated the excitation of the Δ using a relativistic Hartree approximation (RHA) in configuration space. While previous works have emphasized the $\gamma N\Delta$ vertex at the expense of the nuclear structure part of the calculation, we have chosen to treat the nuclear structure carefully and to make some approximations in treating the vertex. This permits us to employ the successful RHA description of nuclear properties in a straightforward way.

The response functions are calculated in terms of a Feynman propagator (or Green function) which, for nucleon excitation, satisfies a Dirac equation

$$[\omega\gamma^0 + i\gamma\cdot\nabla - M - \Sigma_H(\mathbf{x})]G_F(\mathbf{x},\mathbf{y};\omega) = \delta(\mathbf{x}-\mathbf{y}), \tag{1}$$

in the presence of the self-consistent Hartree field, Σ_H, and with the appropriate boundary conditions.[8-11]

We generalize the excited state spectrum to include excitation of the 3-3 nucleon resonance taken to be a Δ particle of mass M_Δ=1232 MeV/c^2 and decay width Γ=110 MeV. The Feynman propagator, G_F in Eq. (1), will then involve Δ states while the hole states will remain of nucleon character so that we need to evaluate a $\gamma N\Delta$ transition amplitude written symbolically as $\langle\Delta|J^\mu|N\rangle$. The conventional choice yields[12,13]

$$\langle\Delta|J^\mu|N\rangle = \Psi^{\Delta\beta}(k)\ F(q^2)\ \Gamma^\mu_\beta(q)\Psi(p), \tag{2}$$

with

$$\Gamma^\mu_\beta(q) = (-q_\beta g^{\mu\lambda} + q^\lambda g^\mu_\beta)M_\Delta\gamma_\lambda\gamma_5 + (q_\beta k^\mu - q^\nu k_\nu g^\mu_\beta)\gamma_5. \tag{3}$$

and

$$F(q^2) = \frac{-3.0(M_\Delta + M_N)}{M_N((M_\Delta+M_N)^2 - q^2)}\sqrt{3/2}\Big(1 - \frac{q^2}{0.71GeV^2}\Big)^{-2}\Big(1 - \frac{q^2}{3.5GeV^2}\Big)^{-1/2}. \tag{4}$$

Here k is the outgoing 4-momentum of the Δ, p is the incoming 4-momentum of the nucleon, $q = k - p$, Ψ is a nucleon spinor, and $\Psi^{\Delta\beta}$ is a Δ spinor with an index β.

The operator in Eq. (3) is too complicated to be readily treated in configuration space. In order to reduce its complexity, we note that the second term should be smaller than the

first by roughly the ratio of the momentum k to M_Δ. Also the first term involves diagonal coupling in the Dirac spinors while the second term couples upper and lower components (so again the first term should dominate). We also note that for the cases considered here, the space-like part of the 4-momentum, $\mathbf{q}$, is larger than the time-like part ω. Hence we take Eq. (3) to be of the form

$$\Gamma^\mu_\beta(q) \longrightarrow \alpha_0 \; M_\Delta \; |\mathbf{q}| \gamma_5 \gamma^\mu, \tag{5}$$

leading to

$$\langle \Delta | J^\mu | N \rangle \simeq \alpha(|\mathbf{q}|) \; \Psi^\Delta(k) \, \gamma_5 \gamma^\mu \, \Psi(p), \tag{6}$$

with

$$\alpha(|\mathbf{q}|) \equiv \alpha_0 \; F(q^2) \; M_\Delta \; |\mathbf{q}|. \tag{7}$$

This form preserves the πN character of the Δ with its γ_5 term and preserves the 4-vector character of the amplitude (via the γ^μ) but the Δ is now effectively treated as a spin-1/2 spinor. A constant factor α_0 has been inserted since the simplification in Eq. (5) is severe. Surprisingly, we find that $\alpha_0 = 1.0$ is adequate for all cases that we studied. We also find that the value of $\alpha(|\mathbf{q}|)$ varies slowly for the cases considered in this work (e.g., for the ^{12}C dip region it varies from ~ 0.60 to ~ 0.75.)

We also generalize the propagator of Eq. (1) to satisfy

$$[(\omega + i\Gamma/2)\gamma^0 + i\gamma \cdot \nabla - M_\Delta - \Sigma_H(\mathbf{x})] G_F(\mathbf{x}, \mathbf{y}; \omega) = \delta(\mathbf{x} - \mathbf{y}), \tag{8}$$

i.e., an imaginary term is added to the energy and the Δ mass is used. The $i\Gamma/2$ addition to the energy in Eq. (8) is non-vanishing S_T below the Δ threshold.

In Fig. 1 we show the transverse response for ^{12}C as a function of energy loss at a three-momentum transfer $|\mathbf{q}|$=550 MeV/c calculated using the mean-field parameters of ref. 9 (g_s^2=109.626, m_s=520, g_v^2=190.431, m_v=783.) The dotted line shows the calculated response involving nucleon excitation alone and is identical to the corresponding curve in ref. 10. The dashed curve presents the calculation using *only* Δ excitation as outlined above and the solid curve is the incoherent sum of the two. The agreement with the data is surprisingly good and may be fortuitous. Indeed we expected that the severe approximation involved in the simplification of Eq. (5) might require an effective normalization constant, α_0, for which we have found the value of unity to be adequate.

We note that the Delta is propagated in our model with its *free* width Γ. This ignores medium effects of Δ propagation such as Pauli blocking and pion absorption. Such effects have been calculated (see, e.g., ref. 14) in a momentum-space Δ-hole formalism. A subsequent paper[15] observed that most of these effects could be roughly accounted for by a simple shift ($-30 - i40$) MeV in the position of the Delta (the -30 MeV real shift corresponds to a simplified self-energy Σ in our notation.)

In Fig. 2 we show the effect of various alternate prescriptions for the the Delta parameters in Eq. (7) as applied to the Δ-excitation part of Fig. 1. The dot-dashed line was calculated using a Delta width reduced by 40 MeV as suggested in Ref. 15. The dotted

curve modified this 40 MeV reduction by a factor $\rho(r)/\rho(0)$ as is more reasonable since Pauli blocking decreases as the density $\rho(r)$ decreases. Finally the short dashed curve is calculated with the extreme assumption of setting Σ_H to 0. It is interesting that the difference between the dashed curves is about equal to a constant -30 MeV shift as suggested by Chen and Lee.[15].

The significance of the curves in Fig. 2 is that they have similar shapes and thus would all give comparable results in the dip region with a small modification of α_0. The falloff in the dip region, say from 300 MeV to 200 MeV, is about a factor 4. The Gaussian folding prescription of Ref. 13 leads to a falloff factor of about 8 over the same range and the results of Δ-hole momentum space calculations[16] also produce a Delta "line shape" which falls off sharply with energy below threshold. This different rate of falloff is the reason that our calculations are able to reproduce the experimental data in the dip region.

Although we are not able at present to improve on the vertex simplification in Eq. (5), we can make some assessment of its importance by performing the calculations with an even simpler prescription obtained by removing all lower components from the calculations so that the vertex is essentially the operator σ taken between non-relativistic wavefunctions. The effect of this truncation is a very minor ($\sim$ 1 to 2 %) change in S_T which would be indistinguishable from the dashed curve in Fig. 2. Our relativistic formulation is used mainly for its convenience in computing nuclear structure realistically with a minimal number of parameters. *We believe that our results for S_T in the dip region are dominated by our employment of a configuration space calculation which treats the nuclear radius, surface and binding energies accurately.*

Figures 3–5 present RHA calculations at $|\mathbf{q}|$=400 MeV/c for ^{12}C, and at $|\mathbf{q}|$=550 MeV/c for ^{40}Ca and ^{56}Fe (treated approximately by assuming ^{56}Fe is equivalent to a closed-shell ^{56}Ni nucleus.) The agreement with data in the Delta-excitation and the dip region is surprisingly good considering that all employ the $\alpha_0 = 1$ normalization of the simplified $\gamma N\delta$ vertex.

1. P. Barreau *et al.*, Nucl. Phys. **A402** (1983) 515
2. Z.E. Meziani *et al.*, Phys Rev. Lett. **54** (1985) 1233
3. J.P. Chen *et al.*, Phys. Rev. Lett. **66** (1991) 1283
4. J.D. Walecka, Nucl. Phys. **A399** (1983) 387
5. J.R. Shepard, From Fundamental Fields to Nuclear Phenomena, ed. J.A. McNeil and C.E. Price (World Scientific, New York, 1991) p. 190
6. C.J. Horowitz and J. Piekarewicz, Phys. Rev. Lett. **62** (1989) 391
7. E.J. Moniz, Phys. Rev. **184** (1969) 1154
8. J.R. Shepard, E. Rost, C.-Y. Cheung and J.A. McNeil, Phys. Rev. **C37** (1988) 1130
9. C.J. Horowitz and J. Piekarewicz, Nucl. Phys. **A511** (1990) 461
10. C.J. Horowitz and B.D. Serot, Nucl. Phys. **A368** (1981) 503
11. J.R. Shepard, E. Rost and J.A. McNeil, Phys. Rev. **C40** (1989) 2320
12. H.F. Jones and M.D. Scadron, Ann. of Phys. **81** (1973) 1
13. K. Wehrberger, C. Bedau and F. Beck, Nucl. Phys. **A504** (1989) 797
14. J.H. Koch and N. Ohtsuka, Nucl. Phys. **A435** (1985) 765
15. C.R. Chen and T.-S.H. Lee, Phys. Rev. **C38** (1988) 2187
16. J.H. Koch, E.J. Moniz and N. Ohtsuka, Ann. of Phys. **154** (1984) 99

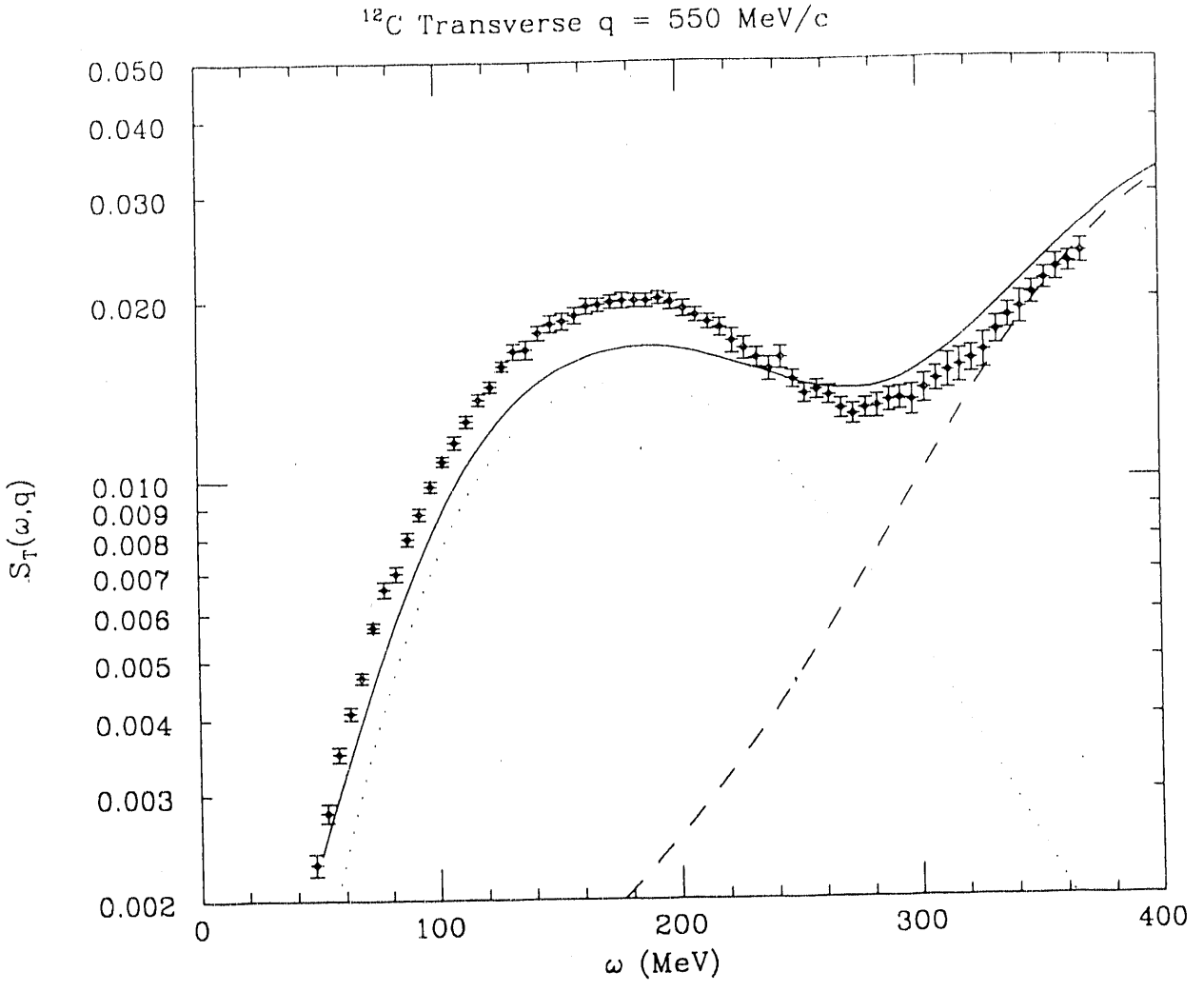

Fig. 1. Transverse response functions for ^{12}C at $|\mathbf{q}|$=550 MeV/c. The dotted curve is the RHA result using only nucleon excitation. The dashed curve is the RHA result with only Δ excitation as described in the text. The solid curve is the sum of the dotted and dashed curves.

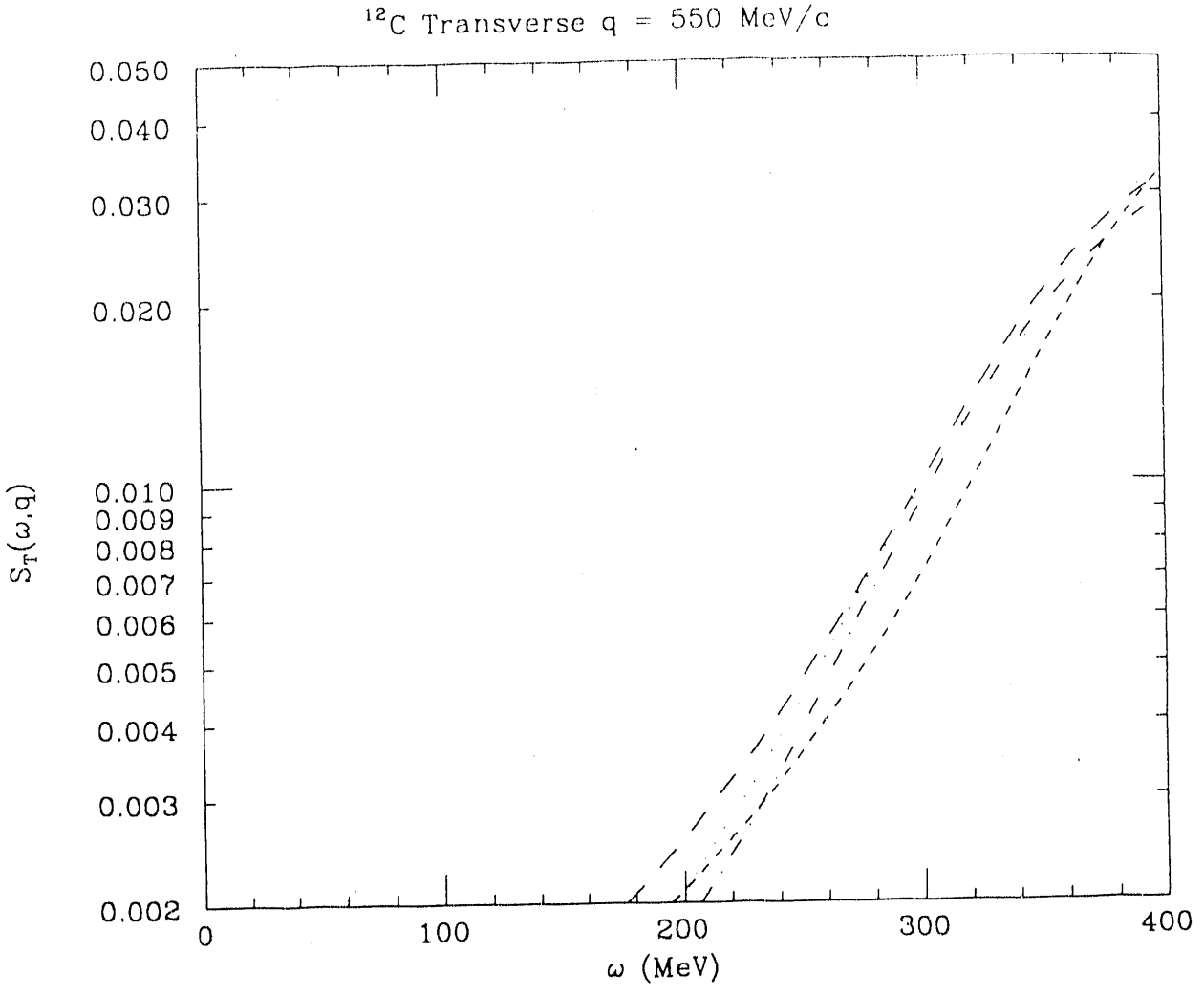

Fig. 2. Transverse response function for ^{12}C at $|\mathbf{q}|$=550 MeV/c with only Δ excitation. The dashed curve represents our "standard" RHA calculation as in Fig 1. The dot-dashed curve is calculated with a shift of the Δ width by -40 MeV whereas the dotted curve modifies this shift by a density ratio factor as discussed in the text. The short dashed curve is calculated using a zero self-energy Σ.

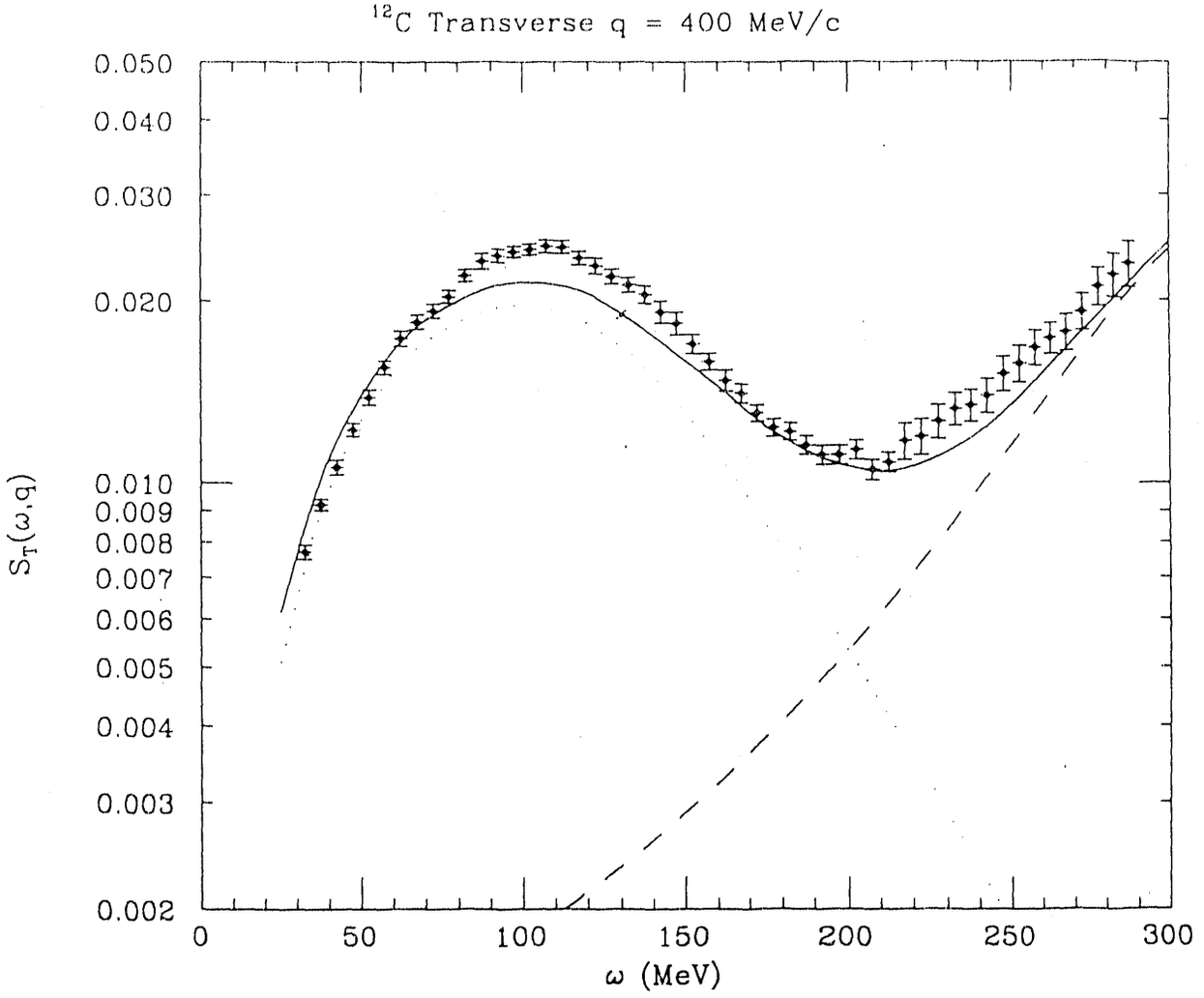

Fig. 3. Transverse response functions for ^{12}C at $|\mathbf{q}|$=400 MeV/c. The curves are described in the caption to Fig. 1.

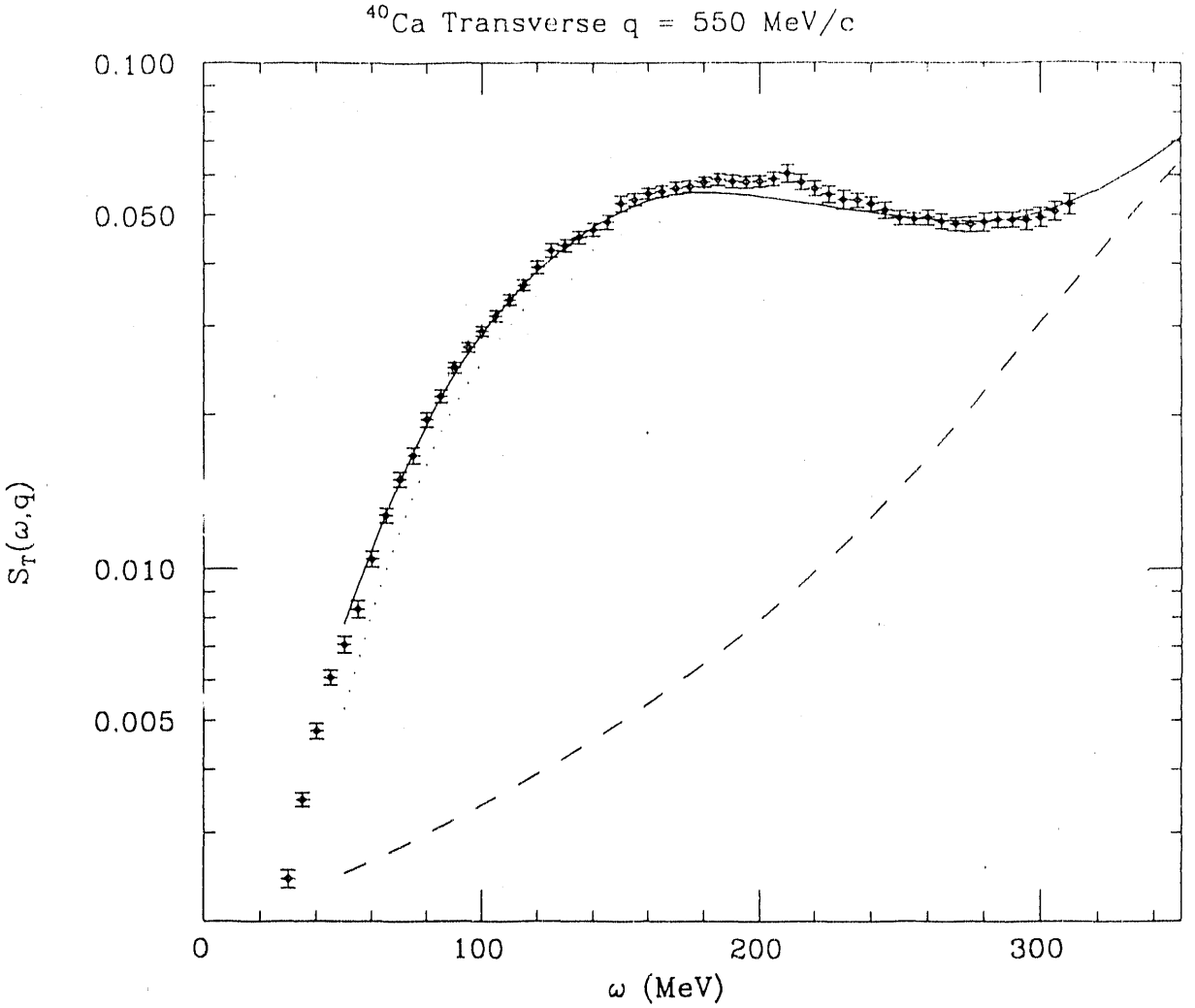

Fig. 4. Transverse response functions for ^{40}Ca at $|\mathbf{q}|$=550 MeV/c. The curves are described in the caption to Fig. 1.

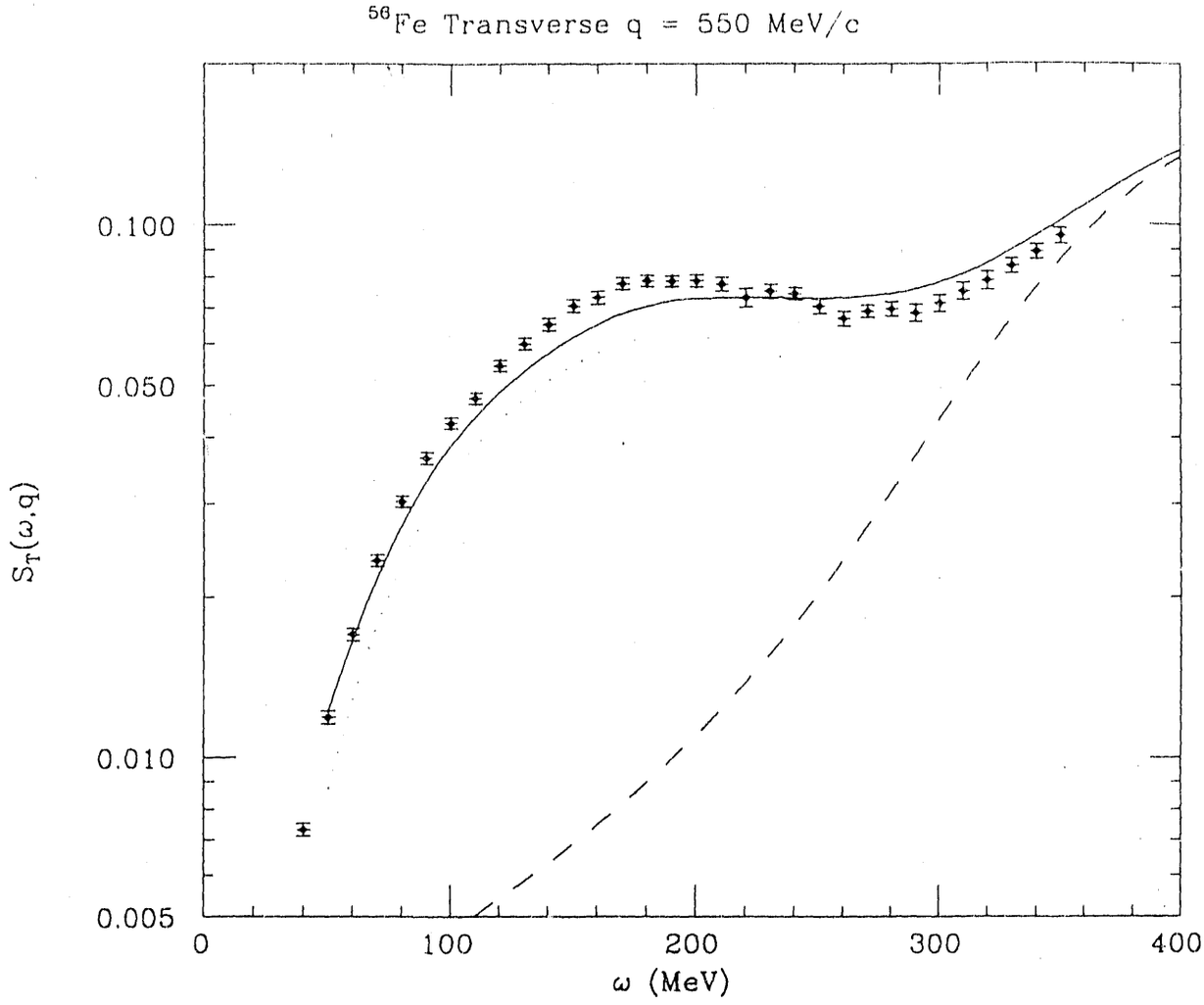

Fig. 5. Transverse response functions for ^{56}Fe at $|\mathbf{q}|$=550 MeV/c. The curves are described in the caption to Fig. 1.

8. **Hadronic Matter in a Nontopological Soliton Model** J. R. Shepard and J. Piekarewicz (Supercomputer Computations Research Institute, Florida State University)

Quantum chromodynamics (QCD) is widely believed to be the correct theory of the strong interactions. Unfortunately, remarkably little progress has been made in solving the theory in the low-energy region relevant to nuclear physics. In spite of some impressive achievements in lattice QCD, it is unrealistic to expect any major contribution from this field to nuclear physics in the foreseeable future. Consequently, one is left with the difficult task of formulating phenomenological models that, while being computationally tractable, capture the essence of QCD. One such is the standard σ-model of Gell-Mann and Levy[1] in which the small empirical values of the pion mass and of the pion-nucleon s-wave amplitude are a direct consequence of chiral symmetry. Furthermore, a self-consistent mean-field calculation gives saturation of nuclear matter and guarantees that the pion remains a Goldstone boson in the nuclear medium.[2,3] The σ-model has also been used to study an "abnormal" phase of nuclear matter that is characterized, in particular, by the presence of massless nucleons.[4] In fact, it was this model which inspired Friedberg and Lee to conceive the nontopological soliton model.[5] In the high density limit of this model, Lee and Wick found that the uniform solution with massless fermions yielded, at least at the mean-field level, a global minimum in the energy of the system. The low-density limit of the many-quark system is, however, more subtle. At low density, one expects that most ground-state properties of the system will still be dominated by its symmetry-broken vacuum phase. It is not clear, however, that a spatially-uniform quark distribution will give rise to a stable configuration. In fact, it is not at all implausible that, at sufficiently low density, the system will evolve into a non-uniform phase, *a soliton crystal*, that will be characterized by the clustering of quarks into local regions of high-density. How to *dynamically* generate the correct number of (3) quarks per cluster, independent of their (spin, flavor and color) degeneracy, is still an open problem. In fact, most if not all of the soliton crystal (or multi-bag) calculations consider nuclear matter as a collection of three-quark bags.[6,7,8,9] At low-density, then, the system does indeed resembles a collection of weakly interacting nucleons. Although it might be physically appealing to consider a non-uniform state with three quarks per site, it is not at all clear that this configuration will actually lead to a minimum in the energy density of the system.

The idea that, in the presence of an attractive interaction, the ground state of the system is spatially non-uniform was first proposed by Overhauser in the context of nuclear matter as early as 1960.[10] He showed that in one spatial dimension the wave number of these oscillations was controlled by the density (or equivalently the Fermi momentum k_F) and given by $q = 2k_F$. His findings suggest that, in the present case, while the periodic solution might indeed be energetically favorable, the one-dimensional ground state should contain, six (3×2 color-flavor degeneracy), and not three, quarks per bag.

We have investigated the structure of the mean-field ground state in two different, although equivalent, ways. In one of them, we have solved the mean-field equations for the one-dimensional soliton model by direct matrix diagonalization. A strength of this approach lies in the fact that no biases concerning the structure of the ground state are introduced into the calculation. In the second approach, we have solved the mean-field equations but only in the *uniform* phase. The stability of the uniform mean-field ground

state was then investigated by calculating the linear response of the system in a random phase approximation (RPA).

This work has appeared in Physical Review **C45**, 2963 (1992). Here we present a summary of our findings; those interested in a more detailed account are referred to the published article.

The dynamics will be prescribed by a Lagrangian density obtained from a simplified version of the nontopological soliton model first suggested by Friedberg and Lee,[5]

$$\begin{aligned} \mathcal{L} &= \overline{\psi}(i\partial\!\!\!/ - g\sigma)\psi + \frac{1}{2}\partial^{\mu}\sigma\partial_{\mu}\sigma - U(\sigma)\,, \\ U(\sigma) &= \frac{\lambda}{4}(\sigma^2 - f^2)^2\,. \end{aligned} \tag{01}$$

Here g is the fermion-meson coupling constant, f is the vacuum expectation value of the sigma field and λ is a positive constant characterizing the strength of the meson self-interactions. For small fermion density, the scalar field assumes a non-vanishing expectation value; *i.e.*,

$$\langle\sigma\rangle = \pm f\,. \tag{02}$$

This effect spontaneously generates both fermion and scalar masses. By defining a new scalar field that is shifted by its classical vacuum expectation value,

$$\phi(x) \equiv \langle\sigma\rangle - \sigma(x) = +f - \sigma(x)\,. \tag{03}$$

the Euler-Lagrange equations associated with the resulting Lagrangian become

$$\begin{aligned} (\partial^2 + m_s^2)\phi + V'(\phi) &= g\overline{\psi}\psi\,, \\ (i\partial\!\!\!/ - M + g\phi)\psi &= 0\,. \end{aligned} \tag{04}$$

where the meson field operator and its scalar source have been replaced by their vacuum expectation values:

$$\begin{aligned} \phi &\rightarrow \langle\phi\rangle \equiv \phi_0\,, \\ \overline{\psi}\psi &\rightarrow \langle\overline{\psi}\psi\rangle \equiv \rho_s\,. \end{aligned} \tag{05}$$

Solution of these equations assuming a uniform ground state is straightforward. Two distinct situations arise. In one, the expectation value of the scalar field vanishes and in consequence fermion masses are zero, too. This solution is the grounsd state in the high density limit. The other solution which yields the ground state for a range of lower densities yields non-zero scalar fields and fermion masses. Below a certain critical density the equations of motion derived *assuming uniformity* have no solution. At these densities the effective scalar mass becomes imaginary, *i.e.*, the scalar field becomes tachyonic.

These low density pathologies indicate that the ground state of the system is in fact *non-uniform*. In this case we solve the mean-field equations (Eq.(04)) are solved exactly by direct matrix diagonalization. The equations are solved in a one-dimensional box assuming antiperiodic boundary conditions for the fermion spinors which then implies that the densities and the scalar field satisfy periodic boundary conditions. The method is discussed in detail in Ref. 11 and in Sections ??? in this report where details of the method can be found.

The issue of the stability of the uniform ground state can be studied in, at least, two different ways.[12] In one of them, one directly compares the energy of the uniform system with the energy obtained from exact solution of the mean-field equations. A second way of learning about the stability of the uniform state is via linear response theory.[13] The presence of an RPA excited state at zero excitation energy or, equivalently, a pole in the scalar meson propagator for spacelike ($q_\mu^2 < 0$) momenta, will signal the onset of instability for the uniform system and suggests that the uniform and non-uniform states are degenerate.

We now proceed to show one-dimensional results obtained in a mean-field approximation to the soliton model. In all the calculations we have used $\gamma = 6$ for the (3×2 color-flavor) degeneracy. In Fig. 1 we show the energy per fermion as a function of the inverse of the Fermi momentum, or equivalently the length of the one-dimensional box for fixed fermion number. The energy per fermion in the uniform massless phase is shown by the dotted line while the solid line gives the energy in the massive phase. The massive solution terminates at $(k_F/M)^{-1} = 0.913$ due to an instability generated by the tachyonic nature of the scalar meson. Nevertheless, for this small value of the coupling, the massive solution not only binds but, in addition, saturates. In contrast, the value of the coupling is still too small for the massless solution to give binding. Nevertheless, at high-enough density, where the mesonic contribution to the energy density is small, the system is guaranteed to behave as a massless free Fermi gas. The squares in Fig. 1 represent the exact mean-field energy obtained from solving the equations of motion by matrix diagonalization. It indicates that at high enough density the massless solution is, indeed, energetically favorable and that at a lower density, where the mesonic contribution to the energy becomes important, the system moves into the uniform massive phase. At even lower density, however, we expect loss of uniformity in the system as the fermions will tend to cluster into regions of high density in order to benefit from the attraction. This is, indeed, confirmed by the exact mean-field calculations which show, particularly clearly in the inset, deviations from the massive uniform results. This fact is further confirmed in Fig. 2 where the effective fermion mass $M^* = M - g\phi_0$ (solid line) and the vector density (dashed line) are plotted as a function of the spatial separation at $(k_F/M)^{-1} = 1.97$. The figure clearly indicates the clustering of fermions around regions of strong attraction or, equivalently, small effective mass. To gain some insight into the nature of the non-uniform solution we have plotted, in Fig. 3, the conserved vector density as a function of the dimensionless ratio $k_F r/\pi$ for three different values of the density. The main purpose of this plot is to confirm Overhauser's claim that the true ground state, *i.e.*, the non-uniform state, is characterized by a periodic behavior of the vector density with the wave number of the oscillations, $q = 2k_F$, controlled by the density. In particular, one can readily verify from examining the full spatial range of the density (figure not shown) that each cluster contains six (and not three) fermions as suggested by the fermion degeneracy. We stress that nowhere in the matrix calculation have we assumed a particular form (*e.g.*, uniform or periodic) for the solution.

In Fig. 4, we show the regions of instability of the massive uniform state as given by

zeroes of the dimesic function calculated in RPA. The momentum transfer q represents the external momentum at which the uniform system is being probed. The curve labeled by $q_{\rm min}/k_F$ indicates the lowest value of the momenta at which the instability sets in. Analogously, q_{max}/k_F represents the largest value of the momenta that can still drive the instability. At low-density the region of the instability is large due to the strong fermion clustering as seen, for example, in the large spatial variations of the density. As the density increases, however, the region of the instability shrinks until, finally, at $(k_F/M)^{-1} \sim 1.8$ the instability disappears. Note, that in agreement with Overhauser's claim, the instability of the uniform state is most strongly driven at a momentum of $q = 2k_F$. In fact, in the limit of an infinitely large box, where the gap at the Fermi energy disappears, there is a costless ($\omega = 0$) excitation in the system of momentum $q = 2k_F$ (a particle from just below the Fermi level gets promoted to a state just above the Fermi level). This is the reason for the logarithmic singularity in the scalar polarization at $q = 2k_F$. The RPA study of the stability of the uniform state is, nevertheless, still meaningful as long the momentum is not too close to $q = 2k_F$. This behavior of the polarization, however, is particular to one spatial dimension. In three dimension, the singularity is integrable and the RPA analysis can be carried out even at $q = 2k_F$. In the inset of Fig. 4, we have also plotted the ratio ρ_1/ρ_0 of the non-uniform to the uniform component of the density,

$$\rho_v(r) = \rho_0 + \rho_1 \cos(2k_F r) \,. \tag{66}$$

In addition of showing the transition from the uniform to the non-uniform system, the picture establishes the consistency between the exact solution of the mean-field equations and the stability study of the uniform system by means of an RPA analysis.

In Fig. 5 we show the energy per fermion as a function of the inverse Fermi momentum for a coupling of $C_s^2 = 0.25$. In this case the results are *qualitatively* different from before. A simple consequence of the stronger coupling is that the system is now bound in the massless phase but no longer saturates in the massive phase. More interesting, perhaps, the uniform massive solution is now unstable for *all* values of the density. We have already established that at very high density the system is guaranteed to be in the uniform massless phase. As the density decreases, but still for large values ($k_F/M \sim 1$), the fermions start to cluster well before the uniform massive solution can become stable. The fact that the uniform massive solution is unstable for all values of the density can be confirmed by means of the RPA stability analysis. Figure 6 indicates that even though the uniform solution leads to a minimum in the energy density of the system for ($k_F/M > 2.288$), the minimum is only local. Perhaps the most interesting consequences of the strong coupling are seen in Fig. 7. Here, the effective fermion mass (solid line) and the vector density (dashed line) are plotted as a function of the spatial separation at a density of $(k_F/M)^{-1} = 1.36$. As in the previous case, and as suggested by Overhauser, the effective mass oscillates with a wave number given by $q = 2k_F$. The vector density, on the other hand, appears to oscillates at *twice* that rate. The answer to this apparent contradiction can be found in the shell-like (kink) solution discussed extensively by Campbell and Liao and by the SLAC bag collaboration.[14,15] In the previous sections we have discussed the fact that the dynamics of the problem involves a delicate balance between a fermionic contribution to the energy that, at least for the uniform system, is minimized for $M^* = 0$, and a mesonic contribution that is minimized for $M^* = M$. In fact, due to the discrete chiral symmetry of the underlying Lagrangian the mesonic contribution to the energy is minimized for $M^* = \pm M$. Consequently, a non-uniform field configuration of low energy could be achieved by allowing the scalar field to interpolate between its two vacuum values while concentrating

the fermion density in a shell around the transition region. In this way the mesonic contribution to the energy is minimized everywhere except in the transition region while the fermions are concentrated in a small region where they are effectively massless. Figure 7 shows a manifestation of this non-uniform configuration. The fermions are, indeed, concentrated in regions of space where they are effectively massless. Furthermore, since the energy of a free Fermi gas is an even function of the mass, it is equally costly to have a *local* fermion mass of $M^* = -M$ as it is to have $M^* = +M$. Consequently, the density oscillates twice as fast because the fermions are not only excluded from regions where the potential is shallow (with M^* large and positive) but also from regions where the potential is very deep (M^* also large but negative)! In particular, fermions no longer cluster into groups of six (as suggested by the degeneracy) but, instead, into groups of three. Although this behavior is, perhaps, suggestive of a fundamental QCD result (three quarks confined in a hadron) the simplicity of the one-dimensional model precludes us from attaching any real significance to it. Nevertheless, we stress that this behavior, namely, three fermions per cluster, was never imposed at any stage in the calculation but was, instead, a consequence of the dynamics of strong fields.

To summarize, we have calculated ground-state properties of hadronic matter in a mean-field approximation to the soliton model in one spatial dimension. The model incorporates fundamental physical principles like Lorentz invariance and (discrete) chiral symmetry from the outset. The symmetry, however, can be spontaneously broken in the ground state leading, in particular, to a dynamical generation of fermion mass. We have studied three possible phases of the model. A uniform massless phase in which chiral symmetry is restored and the system behaves like a free Fermi gas. A uniform massive phase that can be viewed as the finite-density limit of the broken-symmetry vacuum ground state and finally, a non-uniform, actually periodic, phase in which fermions cluster into local regions of high-density to benefit form the scalar attraction. In the "weak coupling" case, the non-uniform phase contained six (as opposed to three) fermions per cluster. However, in the "strong coupling" case, each cluster contains *three* fermions. Due to the simplicity of our one-dimensional model we do not attach profound significance to this result. We stress, however, that in contrast to some approaches that impose the three-quark-bag condition from the outset, the present result is a direct consequence of the strong relativistic dynamics.

1. M. Gell-Mann and M. Levy, Nuovo Cimiento **16** (1960) 705.
2. T. Matsui and B.D. Serot, Ann. Phys. **144** (1982) 107.
3. B.D. Serot and J.D. Walecka, Adv. in Nucl. Phys. **16**, J.W. Negele and E. Vogt, eds. (Plenum, N.Y. 1986).
4. T.D. Lee and G.C. Wick, Phys. Rev. **D 9** (1974) 2291.
5. R. Friedberg and T.D. Lee, Phys. Rev. **D 15** (1977) 1694; Phys. Rev. **D 16** (1977) 1096; Phys. Rev. **D 18** (1978) 2623.
6. L. Wilets, *Nontopological Solitons* (World Scientific, Singapore, 1989).
7. M.C. Birse, J.J. Rehr and L. Wilets, Phys. Rev. **C 38** (1988) 359.
8. L.R. Dodd, Aust. J. Phys. **44** (1991) 161.
9. L.R. Dodd and M.A. Lohe, J. Math. Phys. **32** (1991) 1368.
10. A.W. Overhauser, Phys. Rev. Lett. **4** (1960) 415.

11. T. C. Ferrée, Ph.D. Thesis, University of Colorado, 1992 (unpublished); T. C. Ferrée, C. E. Price and J. R. Shepard, to be published.

12. C.E. Price, J.R. Shepard and J.A. McNeil, Phys. Rev. **C 41** (1990) 1234.

13. A.L. Fetter and J.D. Walecka, *Quantum theory of many-particle systems* (McGraw-Hill, New York, 1971).

14. D.K. Campbell and Yao-Tang Liao, Phys. Rev. **D 14** (1976) 2093.

15. W.A. Bardeen, M.S. Chanowitz, S.D. Drell, M. Weinstein and T.-M. Yan, Phys. Rev. **D 11** (1975) 1094.

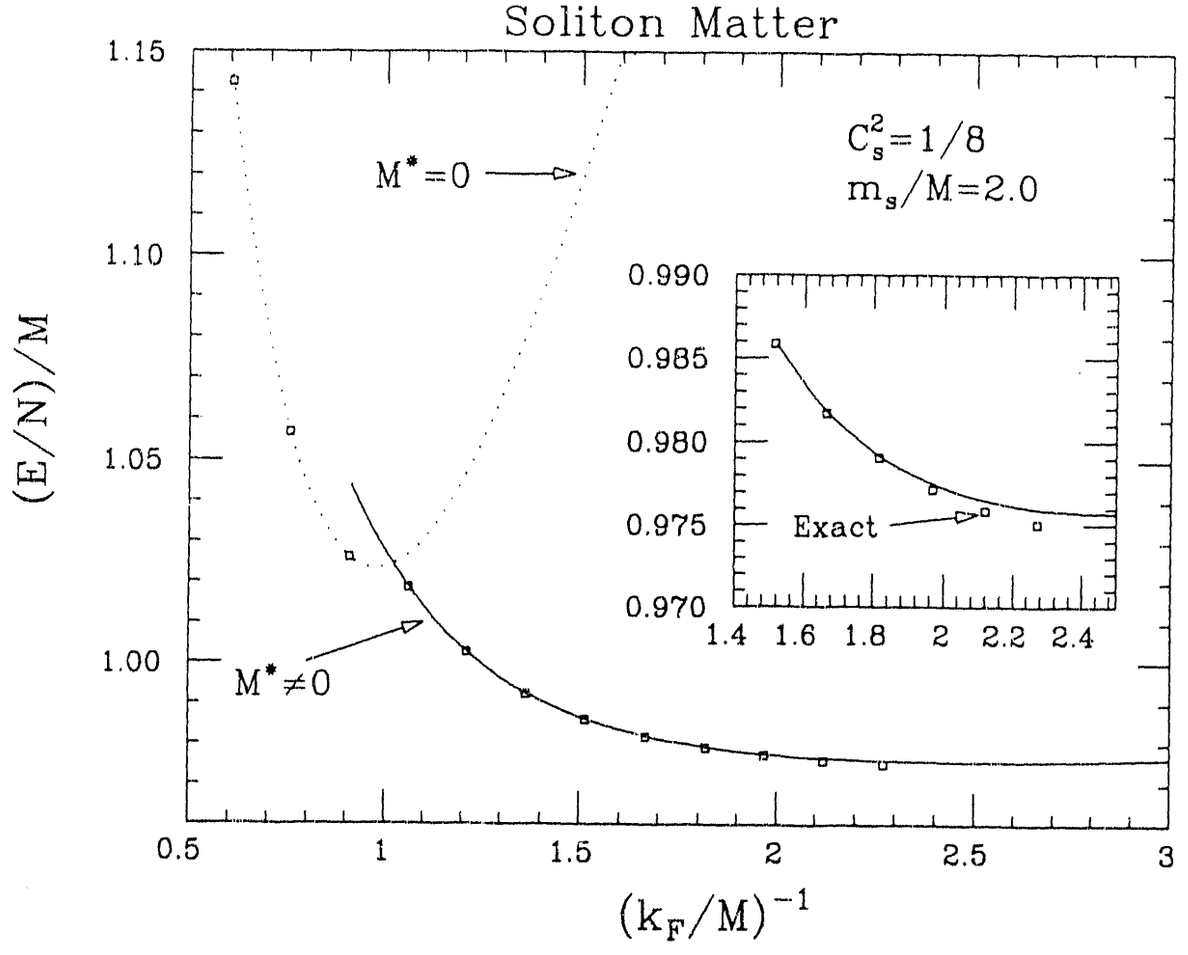

Figure 1. Energy per fermion as a function of the inverse Fermi momentum for $C_s^2 = 1/8$. The uniform massless (massive) solution is given by the dotted (solid) line. The squares indicate the results obtained by direct matrix diagonalization.

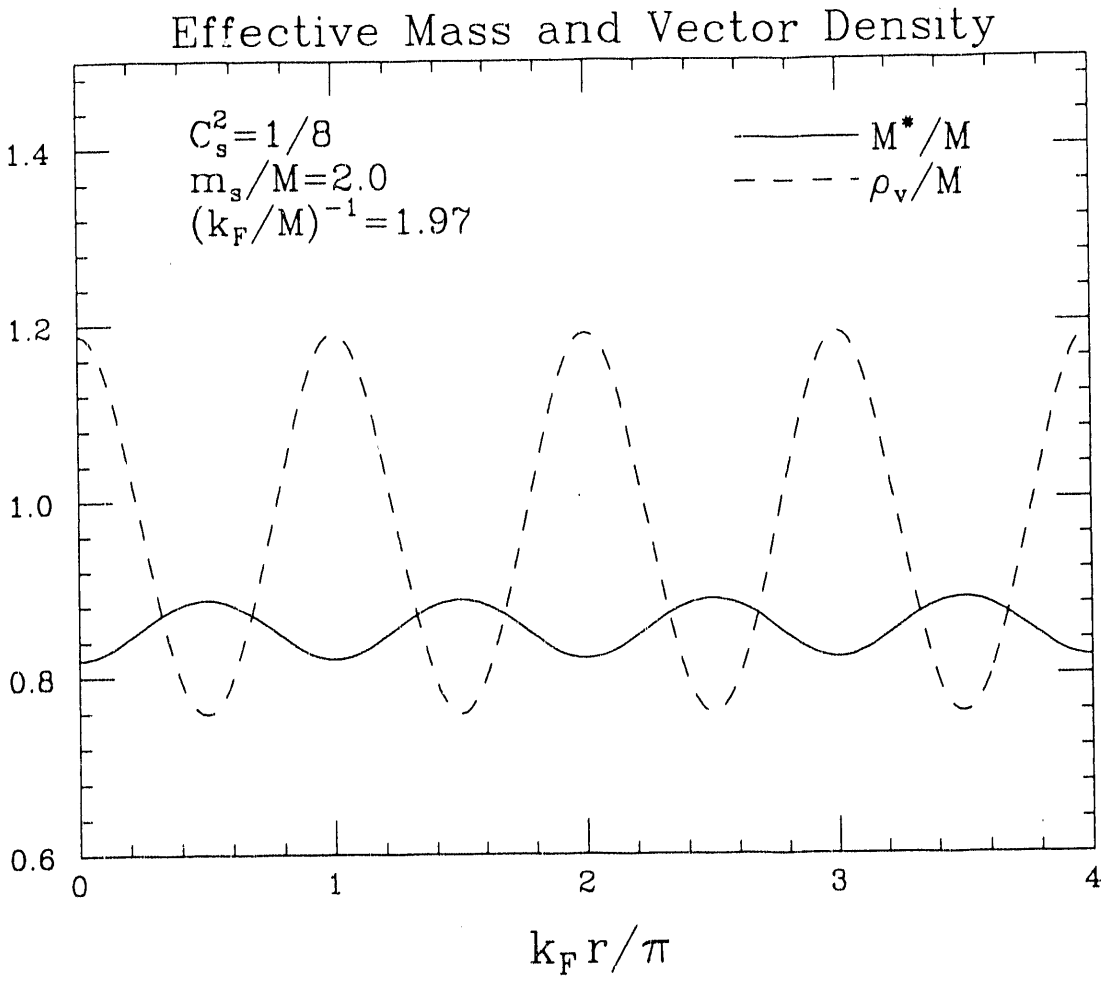

Figure 2. Effective fermion mass and vector density in the non-uniform phase as a function of position for $C_s^2 = 1/8$.

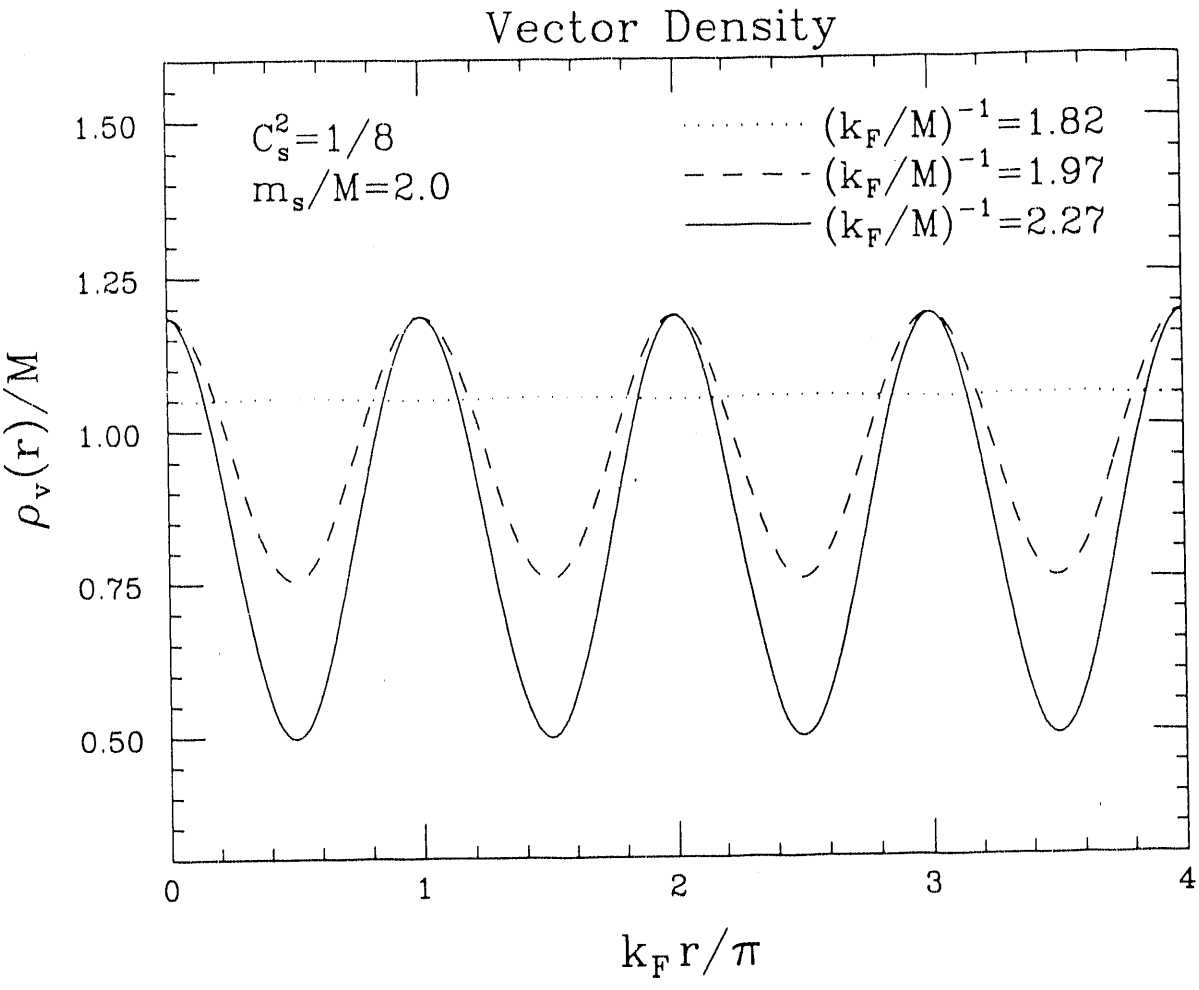

Figure 3. Vector density as a function of position in units of π/k_F for three different values of the Fermi-momentum.

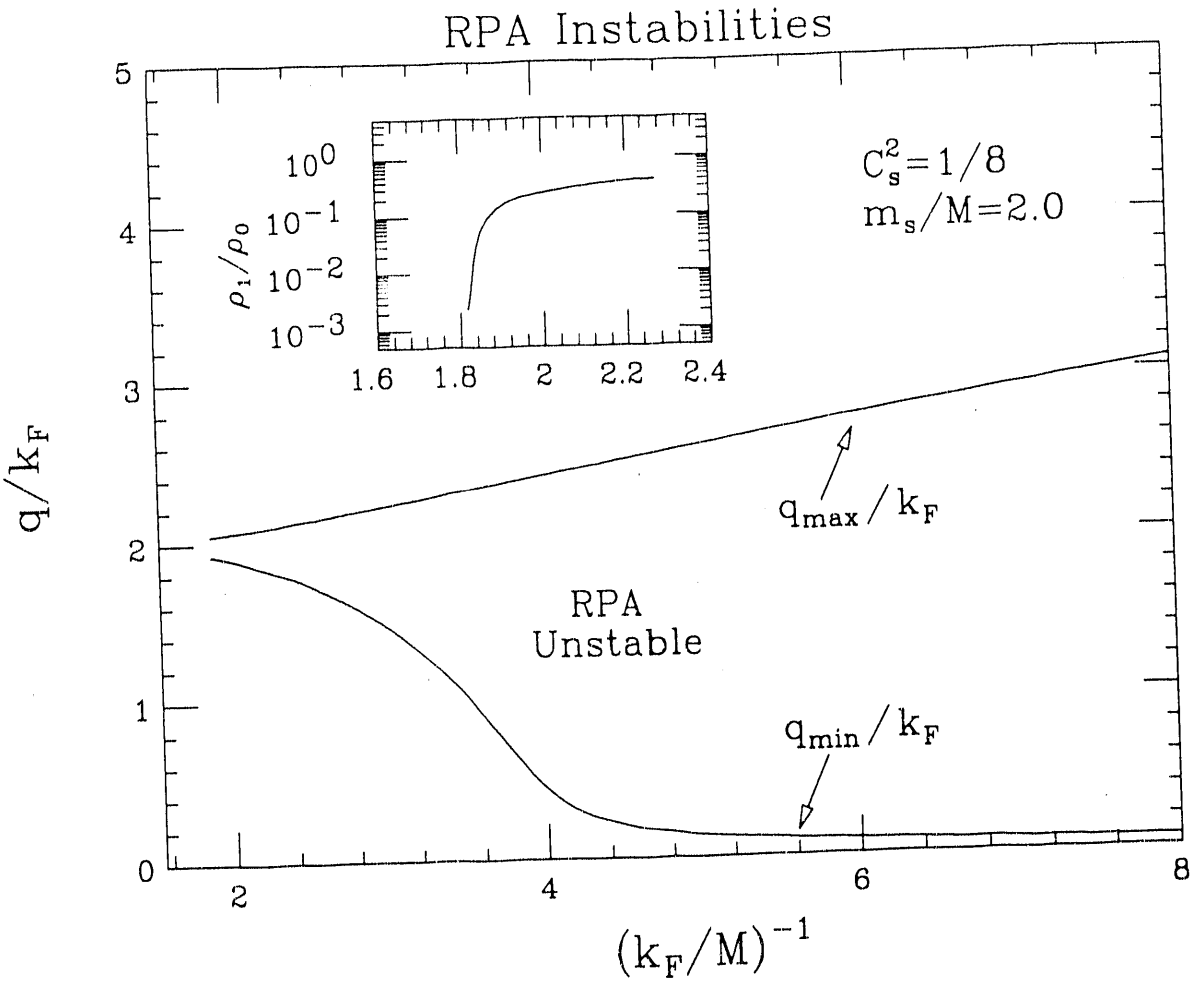

Figure 4. Ground-state instabilities of the uniform massive solutions as a function of the inverse Fermi momentum for $C_s^2 = 1/8$. The inset shows the ratio of the periodic to the uniform component of the vector density.

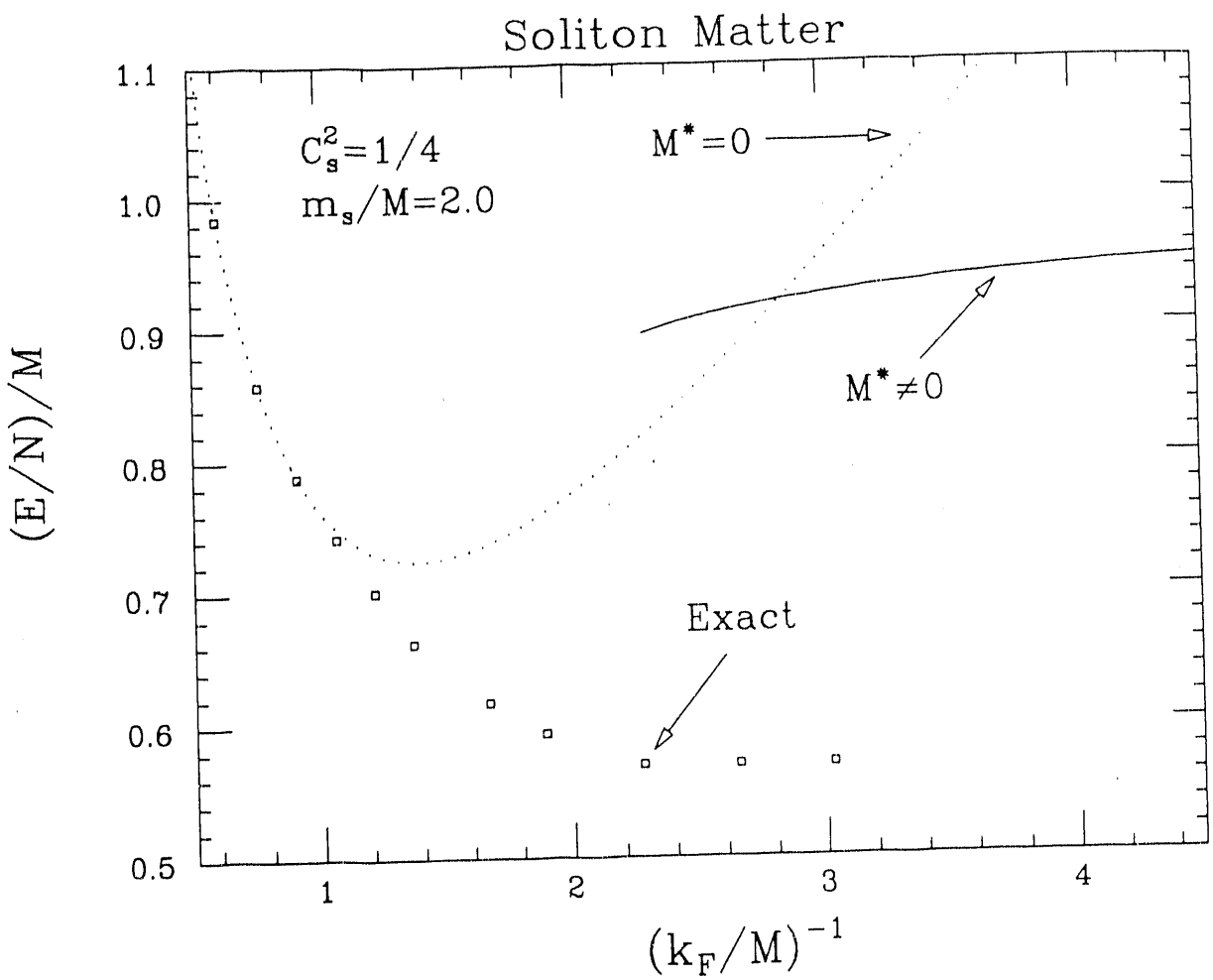

Figure 5. Energy per fermion as a function of the inverse Fermi momentum for $C_s^2 = 1/4$. The uniform massless (massive) solution is given by the dotted (solid) line. The squares indicate the results obtained by direct matrix diagonalization.

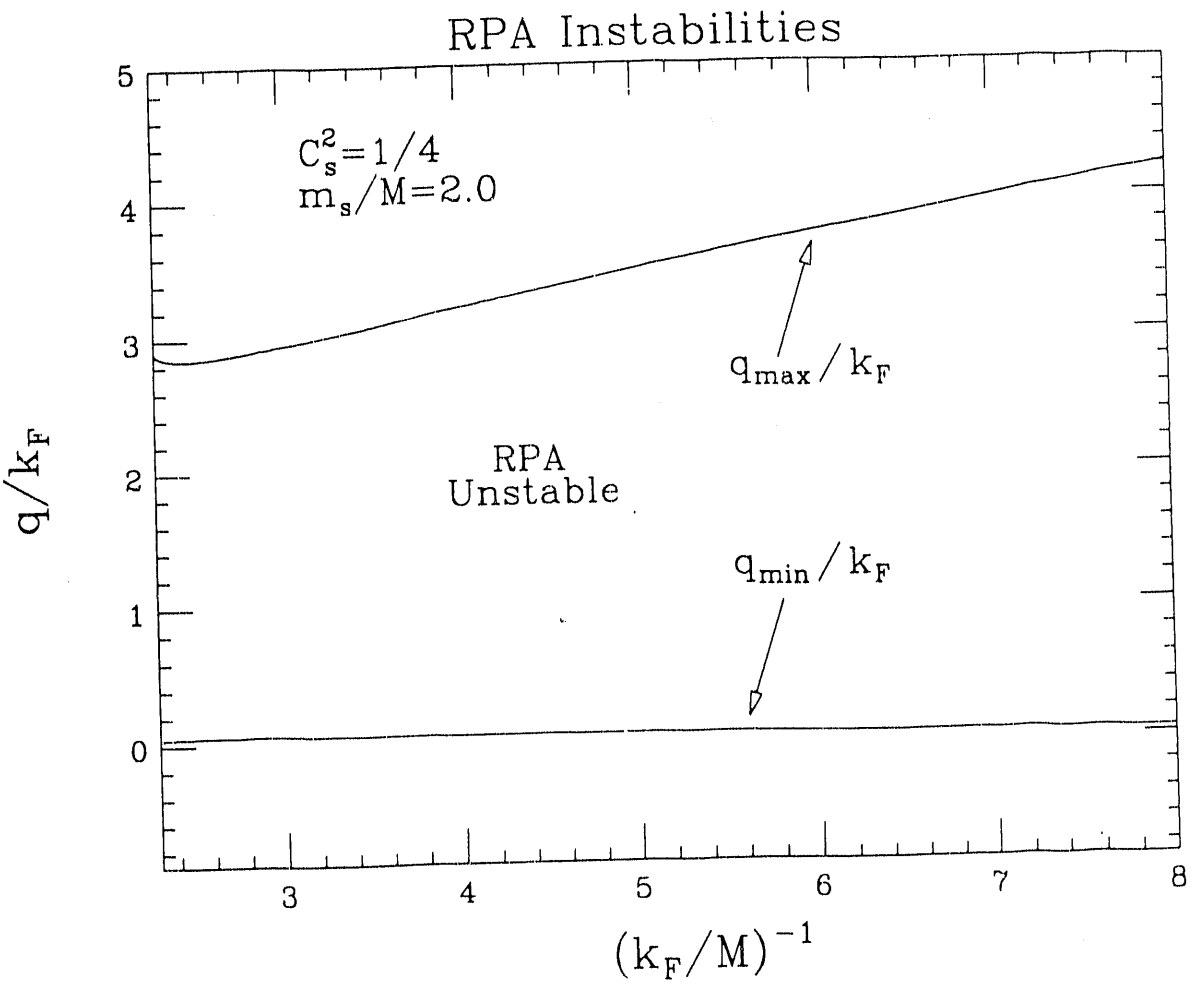

Figure 6. Ground-state instabilities of the uniform massive solutions as a function of the inverse Fermi momentum for $C_s^2 = 1/4$.

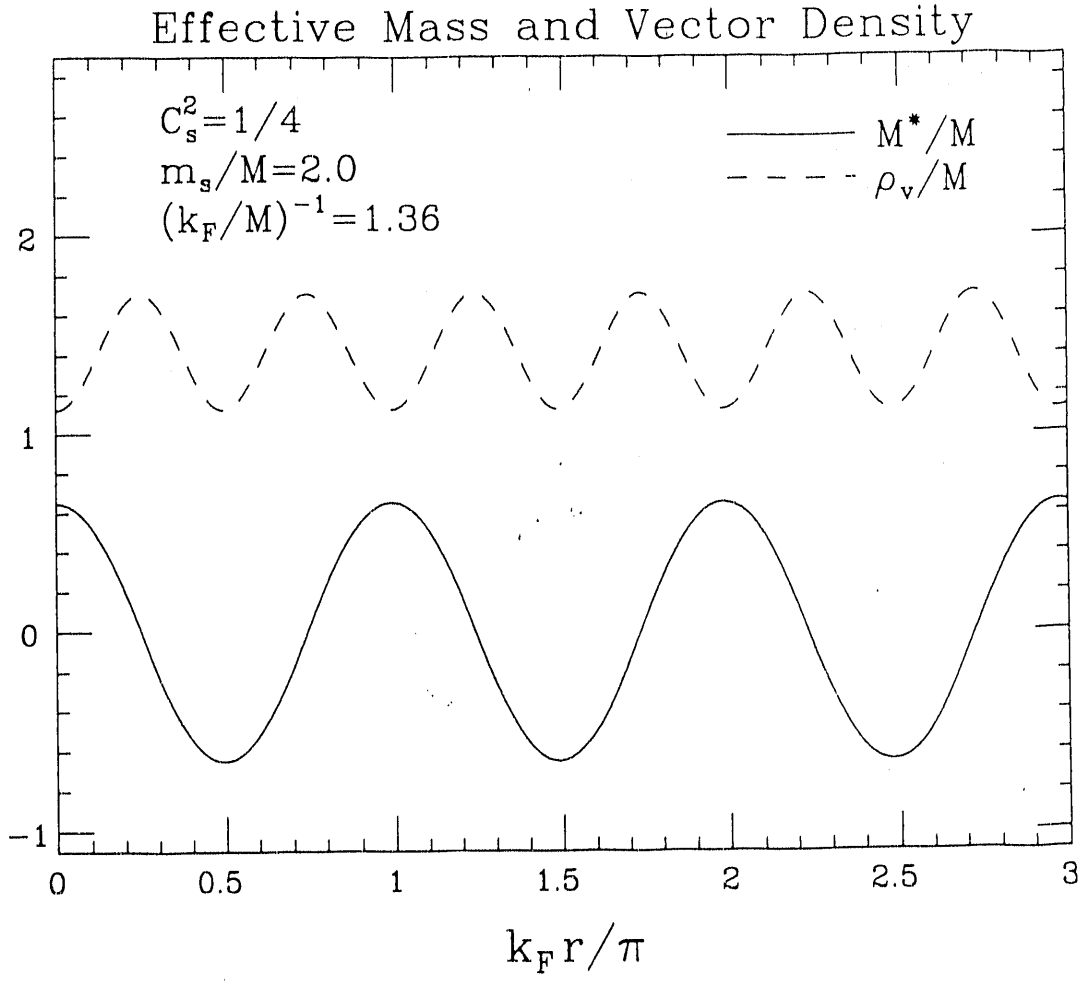

Figure 7. Effective fermion mass and vector density in the non-uniform phase as a function of position for $C_s^2 = 1/4$.

9. **Scalar and Vector contributions to $\bar{p}p \to \bar{\Lambda}\Lambda$ Reaction** P.D. Kunz and University of Washington Collaboration (M.A. Alberg, E.M. Henley and L. Wilets)

The reaction $\bar{p}p \to \bar{\Lambda}\Lambda$ has been described in two complementary models: meson exchange[1-5] or quark annihilation.[3,6-10,11] Both approaches provide reasonable fits to the data[12] as long as the effects of initial and final state interactions are included. Because meson exchange occurs at short distances one may expect quark degrees of freedom to be important. In this work we present here a calculation based on constituent quark dynamics. We describe our reaction mechanism, the initial and final state interactions, and a comparison of our results with the experimental data.

We have proposed a reaction mechanism which includes both scalar and vector contributions to the annihilation and subsequent creation of quark-antiquark pairs. The simplest graphs for these terms are shown in Fig. 1. The $^3P_0$ term represents the confining scalar force and the $^3S_1$ term describes a vector quantum exchange (e.g. of one or more gluons).

In our model, the operator for vector exchange is

$$I_v = g_v \overleftarrow{\sigma_3'} \cdot \overrightarrow{\sigma_3}$$

and that for scalar exchange is

$$I_s = g_s \overleftarrow{\sigma_3'} \cdot \left(\frac{\overleftarrow{\nabla}_{3'} - \overleftarrow{\nabla}_{6'}}{2m_s} \right) \overrightarrow{\sigma}_3 \cdot \left(\frac{\overrightarrow{\nabla}_3 - \overrightarrow{\nabla}_6}{2m} \right) ,$$

where m_s and m are the strange and up quark masses respectively. Our matrix element for the reaction is

$$\mathcal{M}_{\bar{p}p \to \bar{\Lambda}\Lambda} \sim \langle \chi_{\bar{\Lambda}\Lambda}(1'2'3';4'5'6')\phi(1'2'3')\phi(4'5'6')|(I_v + I_s) \times |\phi(123)\phi(456)\chi_{\bar{N}N}(123;456)\rangle ,$$

in which $\chi_{\bar{\Lambda}\Lambda}$ and $\chi_{\bar{N}N}$ are distorted waves in the relative coordinate between the initial and final particles, respectively, and ϕ is a harmonic oscillator wavefunction of the internal motion of the quarks. The quark wave function is parameterized in the form

$$\phi \sim \prod_{i<j} exp(-(r_{ij}/r_0)^2).$$

In our previous work[13] we used the same distorting potentials for $\bar{N}N$ as Kohno and Weise.[3] The real part of the $\bar{N}N$ potential is determined by a G-parity transformation of the long-range part of a realistic one-boson exchange potential, with a smooth extrapolation to the origin. An imaginary term, added to take into account annihilation processes, is of

Wood-Saxon form with a radius R = 0.55 fm and diffuseness parameter a = 0.2 fm. The strength of this potential was adjusted to produce good fits to $\bar{p}p$ elastic scattering data. For the real part of the $\bar{\Lambda}\Lambda$ interaction Kohno and Weise use the isoscalar boson exchanges of the real part of the $\bar{N}N$ potential. The annihilation term is taken to be of the same form as that for the $\bar{N}N$. Since the $\bar{\Lambda}\Lambda$ potential can not be verified by fitting of elastic scattering data, we adjust the strengths to fit $\bar{p}p \rightarrow \bar{\Lambda}\Lambda$ cross section, polarization and spin correlation data.

Our previous results fit only the data at momenta of 1508, 1546 and 1695 MeV/c separately. However, the recent acquisition of an IBM RS6000 computer system has given us a high speed computing facility which allows a more extensive search capability for fitting the data. The searches now include data sets at momenta of 1436, 1437, 1495, and 1477 MeV/c besides the three higher momenta. In addition we now have the computing power necessary to perform global searches on all data sets simultaneously. The searches varied the $\bar{\Lambda}\Lambda$ potential parameters, the strengths of the vector and scalar interactions along with the radius r_0 of of the quark bag and also the radius and diffuseness of the imaginary potential for the $\bar{\Lambda}\Lambda$ system. These two additional parameters particularly the diffuseness cause a markedly lower chi square for the searches. Thus we have nine parameters for 256 data points in the seven data sets.

Our procedure was to search first on only one of the two interaction strengths. These results are labeled vector only and scalar only in Table 1. Then, using these two parameter sets as starting points we continued the search for all nine parameters. The results seem to fall into two classes, labeled vector dominant and scalar dominant respectively and are shown in Table 1. The first result starts from the vector only case and remains dominantly vector while the second starts from the scalar only case and remains dominantly scalar with the lowest chi square for the scalar dominant case.

The parameters for the scalar dominant case are used to calculate the differential cross sections which are shown in Fig. 2 and the polarizations and spin correlation coefficients which are shown in Fig. 3 and Fig. 4 respectively. The strengths of the potential parameters in the table are the scaling factors for the Kohno-Weise potentials needed to obtain the fits. It seems clear the best fits included non-zero contributions from both scalar and vector terms, and strengths of terms in the hyperon-antihyperon potential that differ from those predicted by SU3..

Our searches find the oscillator parameter for the quark bag to be about 0.54 fm for the scalar dominant result and 0.86 fm for the scalar dominant result compared to the value of 0.64 fm required to describe the constituent quark radius in the nucleons and lambdas. The vector dominant case shows a destructive interference between the vector and scalar contributions but a low absorptive potential strength nearer to the value used by Kohno and Weise. The scalar dominant case, on the other hand, shows a constructive interference between the vector and scalar contributions but with the strength of the imaginary part of the potential that is a factor of two larger that used by Kohno and Weise and is thus more peripheral.

One further feature of the searches is that the real part of the central potential V is small for the vector dominant case and is of opposite sign to that predicted by the SU3 extension of the $\bar{p}p$ interaction for the scalar dominant case. Although the dependence of the fits on the tensor and spin orbit potentials is rather weak both results require a large modification to the tensor potential in the scalar results and to the spin orbit potential in the vector results. These changes may reflect the need for a more sophisticated model to take into account the annihilation region at short distances. Other workers[12,14] have found that a real part and spin dependent terms must be added to the model in order to achieve

fits superior to those using a simple absorptive term. Also our fits require an absorptive potential with a markedly sharper edge than that used by Khono and Weise.

Recently data has become available for the momenta at 1642 MeV/c. We have used our parameters for the scalar dominant case to fit these data without any adjustment. The resulting fits to the cross section, polarization and spin correlations are shown in Fig. 5.

In summary we have shown that a quark model which includes both scalar and vector contributions can provide good fits to experimental data for the $\bar{p}p \rightarrow \bar{\Lambda}\Lambda$ reaction. The sensitivity of the results to the parameters of the hyperon-antihyperon potentials may provide information about the hyperon-antihyperon interaction, but a more extensive model for the annihilation region needs to be added. Also, The sensitivity of the fits to other forms of the one boson exchange potentials for the $\bar{p}p$ system needs to be investigated before any definitive statements concerning the properties of the $\bar{\Lambda}\Lambda$ interaction can be made.

1. F. Tabakin and R.A. Eisenstein, Phys. Rev. C**31**, 1857 (1985)
2. J.A. Niskanen, Helsinki preprint HU-TFT-85-28
3. M. Kohno and W. Weise, Phys. Lett. B**179**, 15 (1986); Phys. Lett. B**206**, 584 (1988); Nucl. Phys. A**479**, 433c (1988)
4. R.G.E. Timmermans, T.A. Rijken and J.J. deSwart, Nucl. Phys. A**479**, 383c (1988)
5. P. LaFrance, B. Loiseau, and R. Vinh Mau, Phys. Lett. B**214**, 317 (1988)
6. M.A. Alberg, E.M. Henley, and L. Wilets, Z. Phys. A**331**, 207 (1988)
7. C.B. Dover and P.M. Fishbane, Nucl. Phys. B**244**, 349 (1984)
8. G. Brix, H. Genz and S. Tatur, Phys. Rev. D**39**, 20545 (1989)
9. P. Kroll, B. Quadder and W. Schweiger, Nucl. Phys. B**316**, 373 (1989)
10. S. Furui and A. Faessler, Nucl. Phys. A**468**, 669 (1987)
11. J. Haidenbauer *et al.*, Phys. Rev. C**45**, 931 (1992)
12. P.D. Barnes *et al.*, Phys. Lett. B**189**, 249 (1987); B**229**, 432 (1989); B**246**, 273 (1990); W. Dutty, Dissertation, University of Freiburg (1988); G. Sehl, Dissertation, University of Bonn, Jül-Spez-535 (1989)
13. M.A. Alberg, E.M. Henley, L. Wilets and P.D. Kunz, AIP Conference Proceedings **243**, Intersections Between Particle and Nuclear Physics, Tucson, AZ, ed. Willem T.H. Van Oers (1991)
14. R.G.E. Timmermans, "Antiproton-proton scattering at LEAR Energies", thesis, de Katholieke Universiteit Nijmegen, (unpublished, 1991)
15. R. Machleidt, K. Holinde and Ch. Elster, Phys. Rep. **149**, 1, (1987)

Global Search	g_v	g_s	r_0	W	V	V_T	V_{LS}	r_w	a_w	χ^2/df
Vector only	1.41	0.00	0.864	1.41	-1.23	5.43	-0.42	0.93	0.67	4.44
Scalar only	0.00	4.26	0.571	2.06	0.41	1.38	1.85	1.18	0.13	3.86
Vector dominant	1.31	0.29	0.856	1.04	-1.06	4.75	-0.85	1.13	0.50	4.20
Scalar dominant	-2.40	4.44	0.537	2.36	0.05	0.97	3.98	1.10	0.08	2.76

Table 1. Parameters of best fits to experimental data.

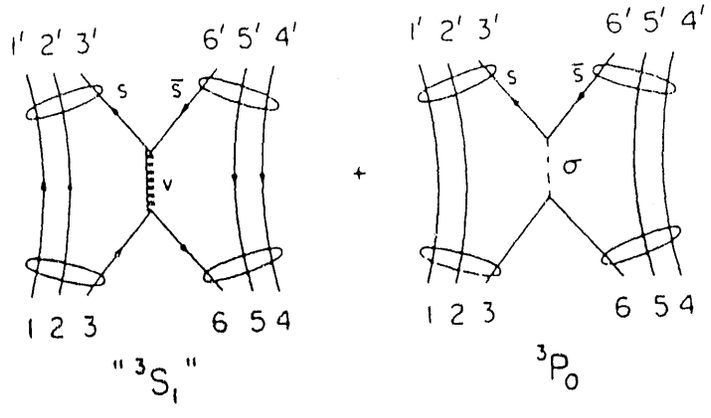

Figure 1. Lowest order diagrams for $\bar{p}p \to \bar{\Lambda}\Lambda$

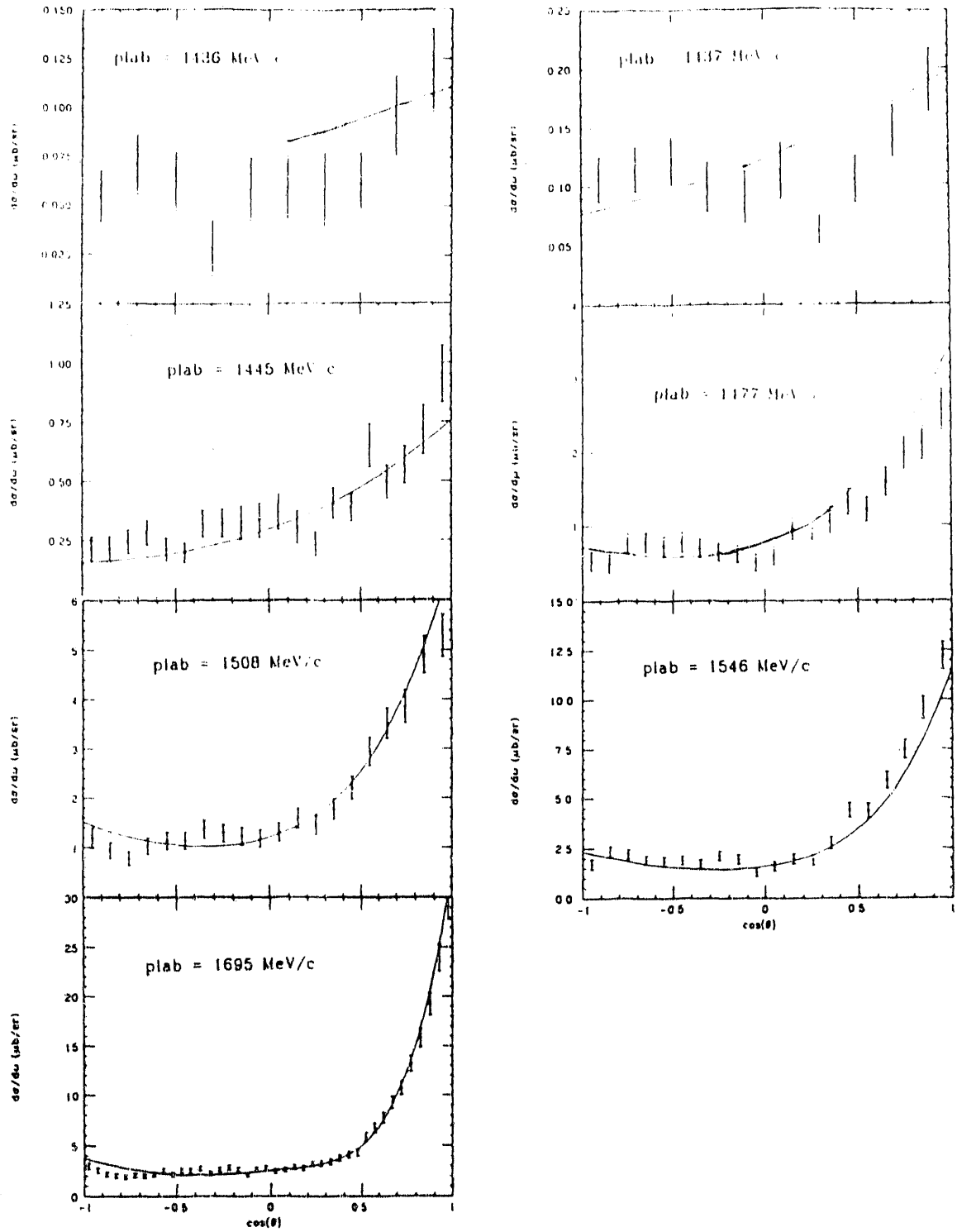

Figure 2. Comparison of calculations with the scalar dominant parameters of Table I with experimental data for the cross section[11].

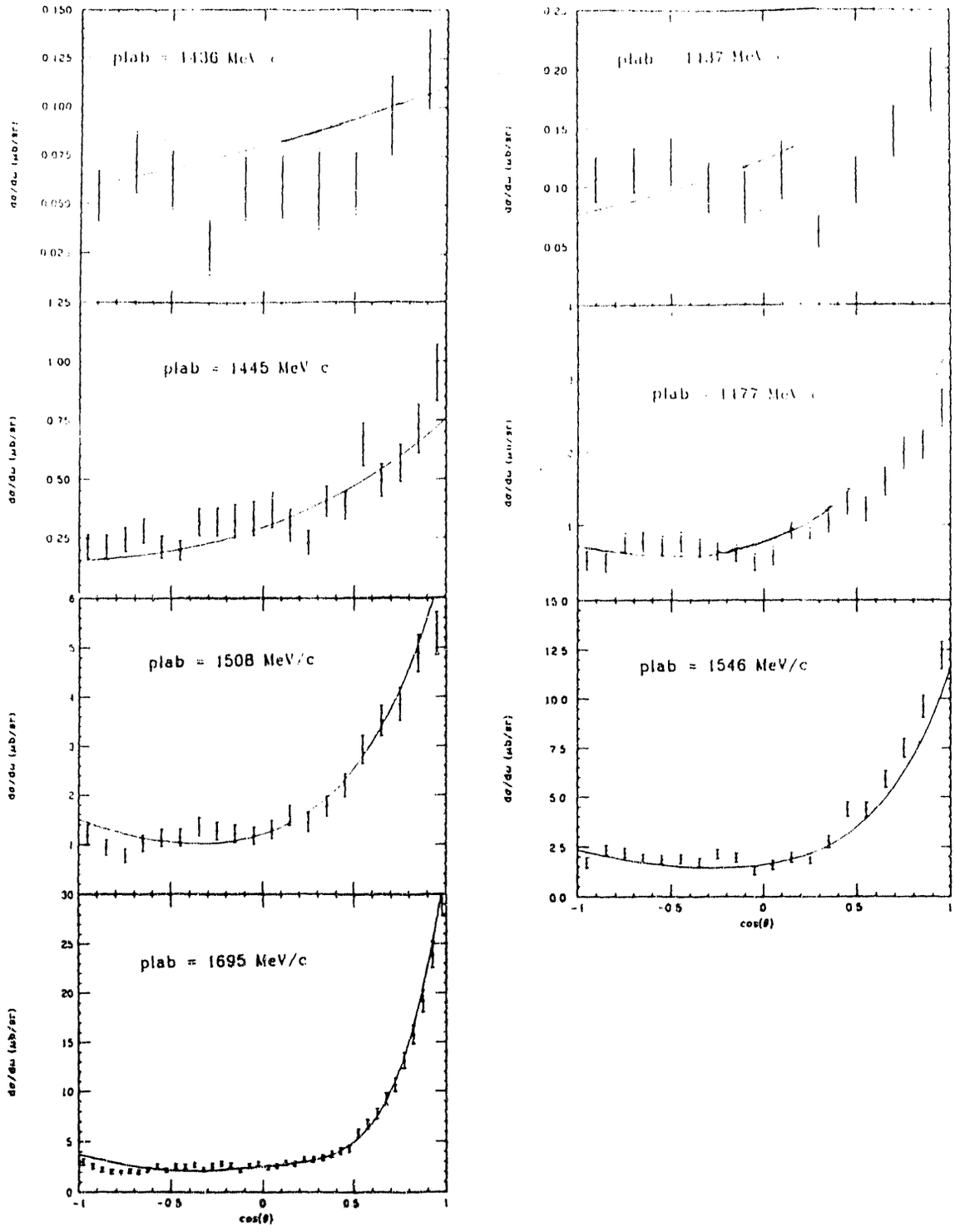

Figure 3. Comparison of calculations with the scalar dominant parameters of Table I with experimental data for the polarization[11].

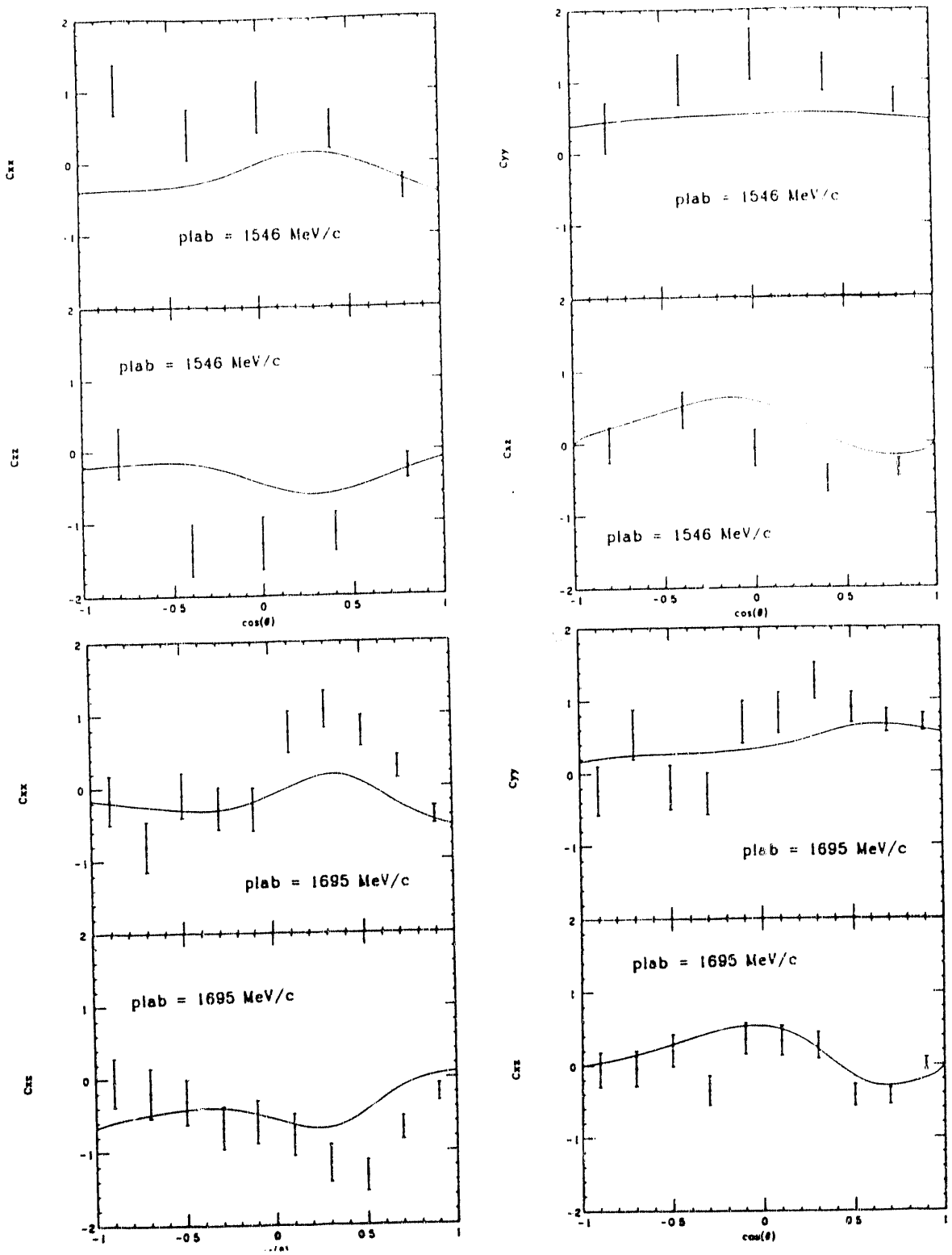

Figure 4. Comparison of calculations with the scalar dominant parameters of Table I with experimental data for the spin correlation coefficients[11].

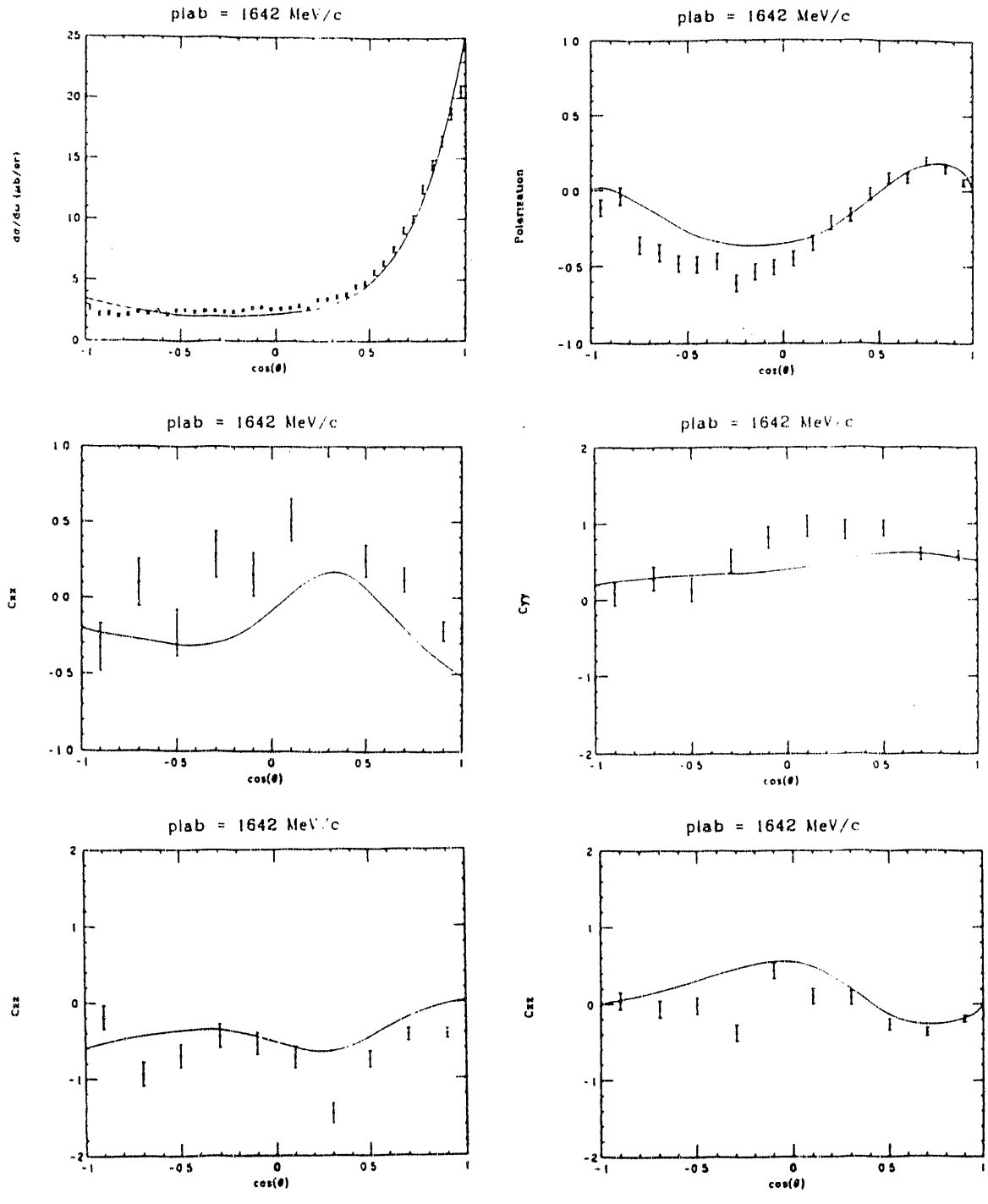

Figure 5. Comparison of calculations with the scalar dominant parameters of Table I with experimental data[16] at 1642 MeV/c.

10. 0^+ and 2^+ Strengths in Pion Double-Charge Exchange to Double Giant-Dipole Resonances

E. Rost, J. M. O'Donnell(LANL) and H. T. Fortune (Univ. Pennsylvania)

Although multi-phonon resonances have been considered in nuclear physics for a long time[1], it is only recently that such resonances have been unambiguously observed[2]. The observability of the two-phonon giant-dipole resonance (or double dipole, DD) in pion double-charge exchange (DCX) has been attributed to a number of features of such reactions. These include a reduced background due to the absence of isoscalar and isovector components in isotensor DCX reactions, and also the suppression of spin-flip excitations at forward angles.

The initial success in applying sequential-model calculations to describe DCX reactions to the double isobaric analog state[3] and the clear signal of the giant-dipole resonance (GDR) in pion single charge exchange (SCX)[4] suggest that similar calculations may be appropriate for double resonances involving the GDR. We have explored the details of a simple reaction model which is expected to describe the strongly populated DD paying special attention to the two-phonon nature of the DD. We use standard optical model parameters and fit to magnitudes of SCX data to obtain transition matrix elements to the GDR. The phonon model is then used to evaluate the matrix elements to the DD. The DCX cross sections are then calculated as a two-step sequential reaction process with no further free parameters.

The strength for a decay, $B(E\lambda)$ with multipolarity λ, from an n phonon state to one with $n-1$ phonons, is proportional to the $B(E\lambda)$ for the decay of the one-phonon state,

$$B(E\lambda; n \rightarrow n-1) = nB(E\lambda; 1 \rightarrow 0). \tag{1}$$

We obtain a similar relation for the reverse transition

$$B(E\lambda; [n-1, J_\ell] \rightarrow [n, J_u]) = n\frac{2J_u+1}{2J_\ell+1}\frac{1}{2\lambda+1}B(E\lambda; [0,0] \rightarrow [1,\lambda]). \tag{2}$$

Either of these expressions may be used to relate the reduced matrix element $\mathcal{M}(n \rightarrow n-1)$ to the one-photon reduced matrix element, $\mathcal{M}(1 \rightarrow 0)$, viz.

$$\mathcal{M}^2(n \rightarrow n-1) = n\frac{2J_u+1}{2\lambda+1}\mathcal{M}^2(1 \rightarrow 0). \tag{3}$$

We note from this equation that the reduced matrix element from the $J_{tran} = 2$ component of the DD is larger than for the $J_{tran} = 0$ component by a factor $\sqrt{5}$, where J_{tran} is the total angular momentum transfer in the two-step reaction.

Equations (1) and (2) may be applied for cases in which the phonons are built on a state with angular momentum j; in this case J_ℓ and J_u are then the J transfers associated with populating $n-1$ and n phonons, respectively. The total strength for a given J_{tran} is split

into several components with total angular momentum I, where $|J_{tran} - j| \leq I \leq J_{tran} + j$. In the weak-coupling limit, the strength to each component is given by[1]

$$B(E\lambda; [nJ_{tran}jI] \rightarrow [n \pm 1 J'_{tran} j I']) = (2I'+1)(2J_{tran}+1) \left\{ \begin{array}{ccc} J_{tran} & j & I \\ I' & \lambda & J'_{tran} \end{array} \right\}, \quad (4)$$
$$\times B(E\lambda; [nJ_{tran}] \rightarrow [n \pm 1 J'_{tran}])$$

where the curly brackets represent a 3-j symbol.

We have performed coupled-channel, distorted-wave calculations for the ^{40}Ca$(\pi^+, \pi^-)^{40}$Ti reaction to the DD. We chose this case because (1) sufficient single-charge-exchange data exist for us to make a reliable estimate of the strength of the transition matrix elements, (2) ^{40}Ca is a spherical nucleus, (3) the forward-angle DCX data show a slight rise[2] suggestive of a $J_{tran} = 0$ component in the DD and (4) previous calculations[2] for this nucleus had to be arbitrarily renormalized by different factors for the $J_{tran} = 0$ and $J_{tran} = 2$ components.

The pion optical potential employed nuclear densities[5] obtained from by electron scattering and used the Kisslinger optical model prescription[6] with phase shifts taken from ref. 7. Isovector transition matrix elements are proportional to β_1. We have extracted values of β_1 from the analysis of the GDR excitation in the $A = 40$ system at several energies and have found an average value $\beta_1 = 0.147 \pm 0.032$.

The double giant-dipole resonance (DD) cross sections are now obtained using the above formalism and a standard coupled channel calculation. The results are shown as the solid curve together with the data[2] in Fig. 1. The $J_{tran} = 0$ and $J_{tran} = 2$ components are shown as dotted and dashed curves. The main features (the location of the first minimum and the maximum around 22°) are reproduced by the calculations. The 5° datum is overpredicted although is is known that the forward rise in the $J_{tran} = 2$ component is very sensitive to effects such as pion absorption. Alternatively it may be that the $J_{tran} = 0$ component is overpredicted. However we do seem to have identified for the first time the $J_{tran} = 0$ component to the DD in DCX reactions.

In summary, we have performed coupled-channel, impulse-approximation calculations for the DD observed in DCX reactions and have interpreted the results as an indication that these reactions proceed via the GDR as an intermediate state. The main features of the cross section magnitude and shape were reproduced and are comparable to the better understood double isobaric analog state (π^+, π^-) transitions at this energy. We believe that the current calculations support the observation of a $J_{tran} = 0$ component of the DD.

A paper describing this work has been published in Physical Review C.

1. A. Bohr and B. Mottelson, *Nuclear Structure* (Benjamin, New York, 1975), Vol.2
2. S. Mordechai *et al.*, Phys. Rev. **C41** (1990) 202
3. P.A. Seidl *et al.*, Phys. Rev. **C30** (1984) 973
4. R. Loveman *et al.*, Phys. Rev. **C40** (1989) 2710
5. H. deVries, C.W. deJager and C. deVries, Atomic and Nucl Data Tables **36** (1987) 495

6. L.S. Kisslinger, Phys. Rev. **98** (1955) 761
7. G. Rowe, M. Salomon and R.H. Landau, Phys. Rev. **C18** (1978) 584

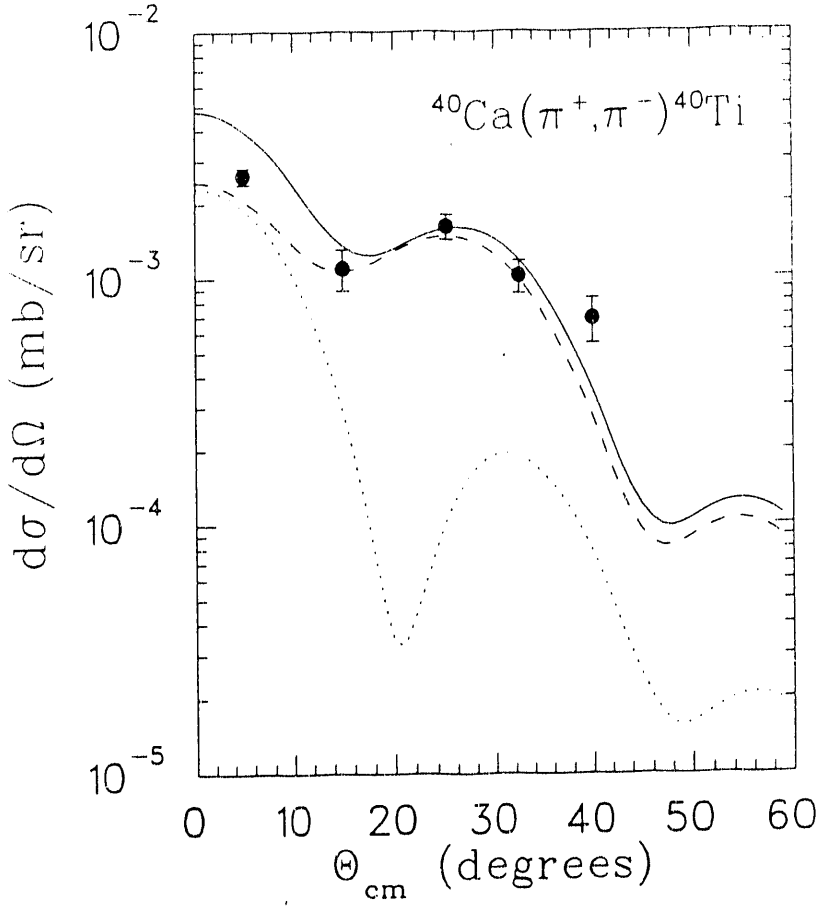

Figure 1. Angular distributions for the double giant-dipole (DD) resonance in the $^{40}Ca(\pi^+,\pi^-)^{40}Ti$ reaction at 295 MeV. The data were taken from Ref. 2. The curves are coupled-channel, impulse- approximation calculation with $J_{tran} = 0$ (dotted), $J_{tran} = 2$ (dashed), and the sum of the two (solid).

11. Nucleons in a Hybrid Sigma Model Including a Quantized Pion Field

C. E. Price and J. A. McNeil

The fundamental field theory of the strong interaction, QCD, has not yet evolved to a form which makes possible quantitative, first-principle calculations of low-energy hadronic properties. Nevertheless, there is general agreement that, when such calculations are done, they will be consistent with the ideas of quark confinement and hidden chiral symmetry. Much effort has been expended to develop phenomenological field theories which are at once calculationally tractable and also to some degree compatible with QCD. A familiar example is that of the Skyrme model[1] which can be interpreted as the large N_c limit of low-energy QCD[2] and whose topological solitons possess both the properties of absolute confinement and hidden chiral symmetry. It is both the strength and weakness of the Skyrme models that they make no explicit reference to quarks. Non-topological soliton (or hybrid) models[3] have been put forward as alternatives which include quark degrees of freedom throughout. These models still possess hidden chiral symmetry but the quarks are not absolutely confined. This latter shortcoming, it may be argued, should not be distressing provided the binding energy of the quarks in hadrons is large on the scale set by our definition of the "low-energy" hadronic properties we seek to describe. In any case, such hybrid models, typically based on elaborations of the Lagrangian of the σ-model,[4] can provide very economical descriptions of, *e.g.*, the N-Δ system. For example, the calculations of Birse and Banerjee[3] and reproduce with reasonable accuracy nucleon properties such as rest mass, magnetic moments, rms radii, g_A and $g_{\pi NN}$ with essentially two free parameters, namely the coupling constant g for the interaction between the quarks and the chiral field (or equivalently, the effective quark mass) and m_σ, the mass of the scalar meson. These and virtually all other hybrid model calculations employ the "hedgehog" ansatz. This amounts to assuming that the pion field has the form $\vec{\pi} = \pi\hat{r}$ and then calculating an intrinsic state in which isospin $\vec{I}$ and angular momentum $\vec{J}$ are coupled to yield a state for which the "grand spin" $\vec{K} = \vec{I} + \vec{J}$ is a good quantum number. Since the matrix elements of the quark spin and isospin operators are readily evaluated for such states, significant calculational simplifications are achieved. More significantly, it has been shown that the hedgehog is a local minimum of energy at least with respect to some restricted variation.[5] However, it is also true that the hedgehog is an unphysical object and physical states with well defined $\vec{I}$ and $\vec{J}$ must be projected from it much as, in the standard treatment of deformed nuclei, states of "good" angular momentum must be projected from a deformed intrinsic state.

With these difficulties in mind, we developed an alternative to the hedgehog model which utilized techniques employed in calculations of deformed nuclear ground states[6] in the framework of quantum hadrodynamics (QHD).[7] We found that we could obtain predictions for the nucleon mass, magnetic moments, rms radii and coupling constants that were in good agreement with experiment (perhaps even better than the values obtained in the hedgehog approach) and that our solutions had the 'correct' angular momentum and isospin projections (z-components). There are two important limitations of these earlier calculations; 1) lack of total angular momentum and total isospin quantum numbers (because of the deformation our states are mixtures of various total angular momentum and total isospin states having the same z-components), and 2) no contributions from

charged pions (only the neutral pion contributed).

These two problems may be addressed simultaneously by treating only the sigma field in the mean field approximation and insisting that the 3 quarks and whatever pions are present couple to the correct spin and isospin (namely $J = 1/2$, $I = 1/2$). As a first step, we have assumed that the nucleon is made up of three quarks and at most one pion. Therefore our nucleon state is written as:

$$|g.s.\rangle = \left\{ A \left[b^\dagger_{\frac{1}{2},\frac{1}{2}} b^\dagger_{\frac{1}{2},\frac{1}{2}} b^\dagger_{\frac{1}{2},\frac{1}{2}} \right]_{\frac{1}{2}m,\frac{1}{2}t} + B \left[\left[b^\dagger_{\frac{1}{2},\frac{1}{2}} b^\dagger_{\frac{1}{2},\frac{1}{2}} b^\dagger_{\frac{1}{2},\frac{1}{2}} \right]_{j,\tau} a^\dagger_{1,1} \right]_{\frac{1}{2}m,\frac{1}{2}t} \right\} |0\rangle \, |\sigma\rangle_c$$

where $b^\dagger_{\frac{1}{2}m,\frac{1}{2}t}$ creates a quark with angular momentum $\frac{1}{2}m$ and isospin $\frac{1}{2}t$, $a^\dagger_{1m,1t}$ creates a pion with angular momentum $\frac{1}{2}m$ and isospin $\frac{1}{2}t$ and $|\sigma\rangle_c$ is a sigma coherent state.[10] This ground state ensures that the nucleon has the correct spin *and* isospin quantum numbers and explicitly includes the lowest order effects of both neutral and charged pions. Numerical calculations are in progress.

Ultimately, we must recognize that the pions will have significant contributions beyond this lowest order. These effects will be included in two ways: first we will investigate the possibility of including higher numbers of pions (more than one) by adding terms to the ground state given above (this should demonstrate the convergence properties of such a series), and second, we will attempt to include the pion via a coherent state (as we have done for the sigma). A meson coherent state is defined by the relations:

$$\hat{a} \, |z\rangle_c = z \, |z\rangle_c \qquad \hat{a}^\dagger = \frac{\partial}{\partial z} |z\rangle_c$$

$$\langle z|_c \, \hat{a}^\dagger = \langle z|_c \, z^* \qquad \langle z|_c \, \hat{a} = \frac{\partial}{\partial z^*} \langle z|_c$$

where $|z\rangle_c$ is the coherent state characterized by the c-number z and $\hat{a}$ ($\hat{a}^\dagger$) is a meson destruction (creation) operator. For our sigma meson such a state can be written as:

$$|z\rangle_c = \sum_n \frac{(z\hat{a}^\dagger)^n}{n!} |0\rangle = \exp(z\hat{a}^\dagger) \, |0\rangle = \sum_n \frac{z^n}{\sqrt{n!}} |n\rangle$$

where $|n\rangle$ is the usual n-meson state. One advantage of a coherent state for the mesons is that it provides a justification of the usual mean-field substitution:

$$\langle z| \, \hat{\sigma} \, |z\rangle_c = \sigma(\vec{r})$$

where the c-number z is simply related to the mean-field $\sigma(\vec{r})$. Since $|z\rangle_c$ contains components with all possible numbers of mesons, the expectation value of a single meson operator need not be zero.

For the pion field, which is an isovector, the coherent state is more complicated. Since the nucleon has a definite isospin, it is inappropriate to think of it as involving a state with an arbitrary number of uncorrelated pions. It is, therefore, necessary to form the coherent state for the pion by including the proper coupling to the quarks so that the final nucleon state has the desired quantum numbers. We will approach this problem by writing two pion states, one involving only even numbers of pions and one involving only odd numbers of pions. In each of these states the pions are coupled pair-wise to zero total isospin. In other words the even state involves all possible numbers of di-pions (two pions coupled to isospin zero), and the odd state involves all possible numbers of di-pions and one unpaired pion whose quantum numbers determine the quantum numbers of the odd pion state. Then each of these states is coupled to the three quarks to form a nucleon. A state defined in this way will be very similar to the state used above and the calculational procedure should be virtually identical.

1. T.H.R. Skyrme, Proc. R. Soc. London **A260** 127 (1961); Nuclear Physics **31** 556 (1962); J. Math. Phys. **12** 1735 (1971)
2. E. Witten, Nuclear Physics **B223** 422 (1983); Nuclear Physics **B223** 433 (1983); G. Holzwarth and B. Schwesinger, Reports on Progress in Physics **49** 825 (1986)
3. M.C. Birse and M.K. Banerjee, Physics Letters **136B** 284 (1984); Physical Review **D31** 118 (1985)
4. M. Gell-Mann and M. Levy, Nuovo Cimento **16** 705 (1960)
5. K. Goeke, J.N. Urbano, M. Fiolhais and M. Harvey, Physics Letters **164B** 249 (1985)
6. R.J. Furnstahl and C.E. Price, Physical Review **C40** 1398 (1989)
7. B.D. Serot and J.D. Walecka, in *Advances in Nuclear Physics, Vol. 16, J.W. Negele and E. Vogt, eds.*, Plenum, N.Y. (1986)
10. P. Ring and P. Schuck, 'The Nuclear Many-Body Problem', Springer-Verlag, New York (1980)

B PUBLICATIONS AND REPORTS—October 1, 1991 to August 1, 1992

1. Published Articles

1. Charge Density Differences Near ^{208}Pb in Quantum Hadro-Dynamics, R. J. Furnstahl and C. E. Price, Phys. Rev. **C44** 895 (1991)
2. Excitation of the 10.957 MeV 0^-;T=0 State in ^{16}O by 400 MeV Protons, J.D. King, D. Frekers, R. Abegg, R.E. Azuma, L. Buchmann, C. Chan, T.E. Drake, R. Helmer, K.P. Jackson, L. Lee, C.A. Miller, E. Rost, R. Sawafta, R. Schubank, S.S.M. Wong, S. Yen and X. Zhu, Phys. Rev. **C44** 1077 (1991)
3. Complete Spin Transfer Measurements for Inelastic Polarized Proton Scattering from ^{12}C, X.Y. Chen, J.R. Shepard, M.R. Braunstein, T.A. Carey, K.W. Jones, J.B. McClelland, L. Rees, T.N. Tadeucci and N. Tanaka, Phys. Rev. **C44** 2041 (1991)
4. 0^+ and 2^+ Strengths in Pion Double Charge Exchange to Double Giant Dipole Resonances, J. M. O'Donnell, H. T. Fortune and E. Rost, Phys. Rev. **C 44** 2426 (1991)
5. Toward a Consistent Random Phase Approximation based on the Relativistic Hartree Approximation, C. E. Price, E. Rost, J. R. Shepard, and J. A. McNeil, Phys. Rev. **C45** 1089 (1992)
6. Nuclear Compressibility and the Isoscalar Monopole Response in a Relativistic Continuum RPA, N. Auerbach, D. S. Oakley, and J. R. Shepard, Phys. Rev. **C45** 2254 (1992)
7. Hadronic Matter in a Nontopological Soliton Model, J. Piekarewicz and J. R. Shepard, Phys. Rev. **C45** 2963 (1992)

2. Articles Accepted or Submitted for Publication

1. Transverse Response Functions in the Δ-Resonance Region, E. Rost, C. E. Price, and J. R. Shepard, submitted to Nucl. Phys. **A**
2. Relativistic Nuclear Matter with Self-Consistent Correlation Energy, J. A. McNeil, C. E. Price and J. R. Shepard, submitted to Phys. Rev. **C**
3. Exact 1-Fermion Loop Contributions in 1+1 Dimensional Solitons, J. R. Shepard, C. E. Price, and T. C. Ferrée, submitted to Phys. Rev. **D**
4. Distorted Wave Born Approximation, P.D. Kunz and E. Rost, in *Computational Nuclear Physics*, J.A. Maruhn ed., Springer Verlag, Heidelberg, to be published 1992.
5. Exact Vacuum Polarization in 1+1 Dimensional Finite Nuclei, T. C. Ferrée, C. E. Price, and J. R. Shepard, submitted to Phys. Rev. **C**

3. Invited and Contributed Papers

1. Vacuum Renormalization via a Single Particle Basis on a Hyper-Sphere, C. E. Price, J. F. Garten and J. R. Shepard, B.A.P.S. **37** 1040 (1992)
2. Exact Vacuum Polarization in 1+1 Dimensional Finite Nuclei, T. C. Ferrée, J. R. Shepard and C. E. Price , B.A.P.S. **37** 1040 (1992)
3. Relativistic $e^+ - e^-$ Resonances in the Fermi-Yang Approximation, B. Wallin, J. A. McNeil and C. E. Price, B.A.P.S. **37** 931 (1992)

C. PERSONNEL

1. Academic and Scientific

P.D. Kunz	Professor
E. Rost	Professor
J.R. Shepard	Professor
C.E. Price	Research Associate
J.A. McNeil	Colo. School of Mines (separate funding)

2. Research Assistants

T. C. Ferrée

J. F. Garten

END

DATE
FILMED
10/1/92